Low-Cost Phase Change Material for Building Envelopes

Syntroleum Corporation

Final Report

for

U.S. Department of Energy

Contract: DE-EE00003924

March 2013

Acknowledgment: This material is based upon work supported by the Department of Energy under Award Number DE-EE00003924.

Table of Contents

List of Tables

List of Figures

Executive Summary

A low-cost PCM process consisting of conversion of fats and oils to PCM-range paraffins, and subsequent “encapsulation” of the paraffin using conventional plastic compounding/pelletizing equipment was demonstrated. The PCM pellets produced were field-tested in a building envelope application. This involved combining the PCM pellets with cellulose insulation, whereby 33% reduction in peak heat flux and 12% reduction in heat gain was observed (average summertime performance).

The selling price of the PCM pellets produced according to this low-cost process is expected to be in the $1.50-$3.00/lb range, compared to current encapsulated PCM price of about $7.00/lb. Whole-building simulations using corresponding PCM thermal analysis data suggest a payback time of 8 to 16 years (at current energy prices) for an attic insulation retrofit project in the Phoenix climate area.

1. Introduction

Products referred to as Phase Change Material (PCM) contain an encapsulated substance with (1) relatively high heat of fusion (latent heat), and (2) melting point near a desired "control" temperature. In systems displaying cyclical temperature variability, PCMs can be used to reduce the temperature swings, or the amount of cooling/heating needed to control the temperature within the desired range. A building undergoing diurnal temperature fluctuation is an example of such a cyclical system, and thus a good candidate for PCM deployment. In general, PCMs can be used to store heat (e.g. the solar energy), store cold (e.g. the nighttime cold, wind, or "off peak" air-conditioning), and control temperature (during melting/freezing).

PCMs are particularly effective in reducing peak cooling loads. By storing the heat during the day and releasing it at night through natural cooling or "off-peak" air-conditioning (when electric grid power supply exceeds demand), the potential reduction in greenhouse gas emissions provided by PCMs disproportionally exceeds their net energy savings.

The potential of PCMs in energy-efficient buildings has been recognized for decades—at least since the 1970's (*1*). The PCM research and development up to about 2008 has been summarized in a number of good reviews (*2-4*). In theory, any substance with a melting point within the indoor comfort temperature range (i.e. 20-26 ºC or 68-79 ºF), and having a relatively high heat of fusion, is a good candidate for use in PCM applications. Indeed, many different substances have been used—salt hydrates, fatty acids/esters, fatty alcohols, sugar alcohols, and paraffins. However, most demonstrated PCM building prototypes (*5*), and the major products advanced to early commercial stage (*6*), have been paraffin-based. These paraffin compositions include n-octadecane, and blends of n-hexadecane with n-octadecane.

Paraffins offer a number of advantages that have likely contributed to these becoming the PCM material of choice: they are non-toxic, non-corrosive, odorless, self-nucleating, water repellant, and have high thermo-oxidative stability. The main disadvantage of paraffins is their fire properties.

Paraffin-based PCM products have been successfully show-cased in a number of commercial buildings—mainly in Europe (*7*). However, despite reported energy savings, high price and limited availability have so far inhibited use of PCMs by the building and construction industry.

Two factors impact current cost of PCM production: paraffin price and micro-encapsulation expenses. The active ingredient in PCMs is a paraffin composition rich in n-octadecane. Clearly, the fact that octadecane is sold as a small volume specialty chemical limits the production volumes and final price of products using it. Furthermore, the process for paraffin micro-encapsulation is a specialty small batch operation involving an energy-intensive drying step which adds to the final cost of PCM. The combination of high paraffin price and encapsulation costs makes the PCM too expensive for the commoditized construction products market.

While working on synthetic paraffinic diesel technologies in 2006-2009, Syntroleum developed a selective process for conversion of fats and oils to PCM paraffins (i.e. n-octadecane and n-hexadecane) (*8, 9*). In July 2010, the company was awarded DOE Contract DE-EE00003924 to develop a low-cost process for production of PCMs, combining its paraffin production process with a proposed “encapsulation” method using conventional thermoplastic compounding/pelletizing equipment. The proposed work sought to demonstrate all steps of the

low-cost PCM manufacturing process, to field-test the product in a building envelope application, and test the fire properties of the envelope system evaluated. An economic analysis, including determination of the likely "payback period" for various markets, was also included in the project scope.

The contractual work began in August 2010 and continued through December 2012. This report documents the project and its key findings.

2. Manufacture and Product Properties

2.1. Paraffin Production: Production of PCM paraffin for the project was conducted at the hydrogenation pilot plant of the Southwest Research Institute (San Antonio, TX). Most of this work was performed during the Sept.-Dec. 2010 period.

2.1.1. Feed stocks – Three feeds were used for paraffin production: soybean oil, canola oil, and beef tallow. All three are common domestically produced biorenewable commodities. Table I provides the fatty acid profile of each lipid, and the expected paraffin composition according to Eq. 1 type hydrodeoxygenation reaction (shown for a typical triglyceride and described in next subsection).

As observed in Table I, the biorenewable feedstocks are virtually all comprised of even carbon number fatty acids (e.g. oleic acid and palmitic acid), resulting in a corresponding hydrodeoxygenation product that is a mainly even carbon number paraffin composition (e.g. n-hexadecane and n-octadecane). Since even carbon number n-paraffins have a higher heat of fusion than the odd carbon numbered homologues within the same melting point range (ΔH_{C15} = 207 J/g; ΔH_{C16} = 238 J/g; ΔH_{C17} = 215 J/g; ΔH_{C18} = 245 J/g), the process is particularly well-suited for production of PCMs where a high heat of fusion is sought.

2.1.2. Hydrodeoxygenation – The conversion of fats and oils to n-paraffins was conducted using a hydrogenation catalyst with both hydrogenolysis and olefin saturation activity. An example of hydrodeoxygenation (HDO) is given by Eq 1. In this illustrative equation, a typical triglyceride molecule containing three common C18 fatty acids is shown. The reaction converts the fatty acids to n-paraffins of same carbon number. The glycerol backbone is converted to propane (a fuel co-product of the process).

Table I. Fatty Acid Composition of Lipid Feeds Used for PCM Paraffin Production, and Corresponding Theoretical Paraffin Composition (wt %)

			Canola Oil	Soybean Oil	Beef Tallow
Feed Composition (Typical)					
	Lauric acid	C12:0			0.2
	Myristic acid	C14:0			2.9
	Palmetic acid	C16:0	3.8	9.4	24.3
	Palmeloic acid	C16:1	0.3		2.1
	Stearic acid	C18:0	1.9	4.1	22.8
	Oleic acid	C18:1	63.9	22	40.2
	Linoleic acid	C18:2	19	55.3	3.3
	Linolenic acid	C18:3	9.7	8.9	0.7
	Arachidic acid	C20:0	0.6		0.2
	Eicosenoic acid	C20:1			0.6
	Eicosedienoic acid	C20:2			
	Behenic acid	C22:0	0.4	0.3	
	Erucic acid	C22:1			
	Lignoceric acid	C24:0	0.2		
	Tetracesenoic acid	C24:1	0.2		
	Unknowns		0	0	2.7
Derived Paraffin Composition (Theoretical)					
	n-Dodecane	n-C12			0.2
	n-Tetradecane	n-C14			2.9
	n-Hexadecane	n-C16	4.1	9.4	26.4
	n-Octadecane	n-C18	94.5	90.3	67
	n-Eicosane	n-C20	0.6		
	n-Docosane	n-C22	0.4	0.3	
	n-Tetracosane	n-C24	0.2		

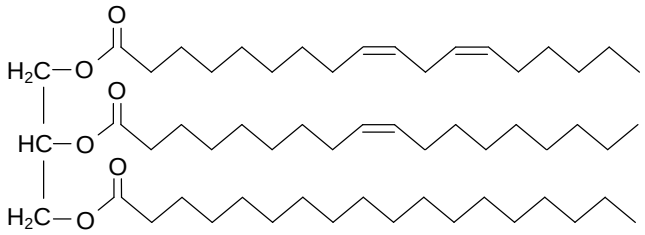

+ 15 H_2

(typical triglyceride with linoleic, oleic, and stearic acids)

NiMo cat

3 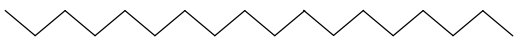

+ 6 H_2O + C_3H_8 (1)

(n-octadecane)

A continuous fixed-bed hydrogenation reactor system was operated according to the conditions specified in Ref. 8. The fat/oil throughput was about 12-16 gal/d. The volumetric yield of paraffin from fat/oil feeds was about 100% (gal paraffin/gal oil). This is about 84% by mass, which is close to the stoichiometric paraffin yield (Eq 1).

Photos of the paraffin in solid/wax and melt form are presented in Figure 1. Table II provides a summary of the bio-based paraffins produced. The phase transition properties were measured by Differential Scanning Calorimetry (DSC) and the paraffin composition by Gas Chromatography (GC).

Table II. Composition and Thermal Properties of Vegetable Oil HDO Paraffins

Drum ID[(a)]	Amount (lbs)	Visual Inspection		Phase Transition Properties by DSC		Density (g/mL @ 15.6 °C)	Paraffin Composition by GC (wt %)				
		>28 °C (liquid)	<20 °C (solid)	Melt Range[(b)] (°C)	Heat of Fusion[(c)] (J/g)		C_{15}^-	C_{16}	C_{17}	C_{18}	C_{23}^+
1	356	Slightly cloudy	White wax	19-22	179	0.7915	0.51	5.40	3.34	95.12	1.03
20	329	Clear, bright	White wax	19-22	190	0.7920	1.18	4.73	3.38	82.67	0.47
21	330	Clear, bright	White wax	19-22	177	0.7928	1.34	5.05	3.34	88.71	1.71
22	330	Clear, bright	White wax	19-22	163	0.7929	0.42	2.29	2.08	89.07	0.62
23	330	Clear, bright	White wax	18-22	171	0.7932	0.83	4.47	3.57	87.20	1.02
24	330	Clear, bright	White wax	19-23	173	0.7928	0.96	5.28	6.67	84.35	0.69
27	99	Clear, bright	White wax	18-22	176	0.7928	0.85	4.89	4.97	86.87	0.77

Notes:
(a) Drums were numbered in order of production as feedstock transitioned from canola oil, to soybean oil and tallow
(b) melt range is indicated as onset of melting (first number in range) and crystallization/freezing (second number in the range)
(c) DSC heat of fusion data measured at Southwest Research Institute

As observed in Table II, over 2,100 lb of PCM-range paraffin was produced having a weighted average octadecane concentration of 88 %. The presence of low concentrations of odd carbon number paraffins (mainly pentadecane and heptadecane), indicates occurrence of decarboxylation side reactions. During decarboxylation, the oxygen atoms are removed as CO and CO_2 instead of water, resulting in loss of a carbon from the even carbon number fatty acid chains. Nevertheless the selectivity toward the desired octadecane and hexadecane components was high (93-97%), confirming that HDO is an elegant process for production of PCM-range paraffins.

To make a higher purity octadecane product, the tallow-based HDO paraffin was subjected to vacuum distillation. The distillation involved separation of the "C17 minus" fraction of the HDO product as a distillate to yield a "bottoms" fraction with an octadecane concentration greater than 90 wt %. Additionally, technical grade octadecane was purchased from the only domestic producer of the product, ChevronPhillips Chemical, through their distributor ChemPoint. The paraffin analysis results for these are summarized in Table III.

Table III. Thermal Properties of Octadecane from Vacuum Distillation of Tallow HDO Product and from Petrochemical Process

Drum ID	Amount (lbs)	Visual Inspection		Phase Transition Properties by DSC		Paraffin Composition by GC (wt %)				
		>28 °C (liquid)	<20 °C (solid)	Melt Point (°C)	Heat of Fusion (J/g)	C_{15}^-	C_{16}	C_{17}	C_{18}	C_{23}^+
Tallow-based Octadecane	156	Clear	Wax	23	214[(a)], 191[(b)]	0.51	0.0	4.3	91.2	4.0
Petrochem Octadecane[(d)]	320	Clear, bright	White wax	22-24	209[(b)]	n.m.[(c)]	n.m.	n.m.	90.9	n.m.

Notes:
(a) Southwest Research Institute DSC
(b) University of Tulsa DSC; average of three measurement scans
(c) n.m. = not measured
(d) Produced by hydrogenation of linear alpha-olefin (1-octadecene)

As observed in Table III, the properties of octadecane obtained by distillation of HDO product are very similar to the product obtained from the petrochemical process.

2.2. PCM Pelletizing: The lab work validating the concept of shape-stable paraffin/HDPE composites was summarized in the interim report for this project (*10*). This was followed by a series of pelletizing trials at the Polymer Center of Excellence (Charlotte, NC), using conventional plastic processing equipment. In these runs, high density polyethylene (HDPE product PE161 from PolyOne Corporation) was used in both powder and pellet form. (The powder was prepared by grinding some of the PE161 pellets.) Production of shape-stable PCM pellets containing 65-70% paraffin was demonstrated on a twin-screw extruder and two types of pelletizer. The results of the compounding/pelletizing runs are summarized in Table IV.

Table IV. Summary of PCM Compounding and Pelletizing Trials

Pelletizing Run Number/ Date	PCM paraffin source	HDPE form	Paraffin/ HDPE ratio	Pelletizer Type	PCM Pellet Properties		
					DSC Phase Change Range (ºC)	DSC Heat of Fusion (J/g)	Paraffin seepage [(a)]
1. June 2011	Table II	Powder	70/30	Strand	19-22 ºC	103	3%
2. Sept. 2011	Table II	Powder	65/35	Underwater	17-22 ºC	103	1%
3. June 2012	Table III	Pellet	70/30	Underwater	25-28 ºC	126	0.14%
4. June 2012	Table III	Pellet	65/35	Underwater	24-25 ºC	120	~2%
5. Dec. 2012	Table III	Pellet	65/35	Underwater + Dusting [(b)]	23-25 ºC	120	-

Notes:
(a) Ultimate paraffin seepage estimated by extrapolation of weight loss (pellet basis) after 10 heating/cooling cycles
(b) Dusting refers to powder coating with calcium silicate; see Section 3

The PCM compounding line with the underwater pelletizer is shown in Figure 2. Photographs of the PCM pellets produced are presented in Figures 3 and 4. The nominal pellet

size is 2 mm, but can be varied within the 1 mm to 5 mm range by adjusting the pelletizer cutter speed, die hole size, and a few other variables.

In addition to PCM thermal properties, Table IV quantifies the observed paraffin seepage from the pellets. Although the pellets maintain their solid form above the PCM melt point, they become oily. GC analysis of the oil confirmed that this was the paraffin exuding/seeping out of the plastic PCM composite. An explanation for the seepage is volumetric expansion of the paraffin as it changes from solid to liquid.

The rate of paraffin seepage for a typical PCM pellet is shown in Figure 5. As observed, the rate of paraffin seepage drops with repeated heating/cooling cycles. The paraffin seepage value indicated in Table IV is the total paraffin seepage as extrapolated from such multi-cycle weight loss curves.

3. PCM Pellet Coating

Encapsulative coating was determined to be the most cost-effective option to address the issue of paraffin seepage. Two coating technologies were explored: (1) polymer coating, and (2) powder coating. Both approaches were successful, resulting in two coating options depending on the building energy efficiency application. All the coating R&D for this project was conducted at Southwest Research Institute's Encapsulation Labs.

3.1. Polymer Coating: Polyvinylidene chloride (PVDC) was selected as the leading candidate for the polymer coating studies because of its reported barrier and flame retardant properties. The properties of PVDC that makes it a good barrier coating for the paraffin/HDPE composite, namely its polarity and insolubility in paraffin, also made it difficult to adhere to that non-polar substrate. Hence much of the research was focused on identifying a proper pre-coat.

The effectiveness of the coating system was assessed by two methods: (1) SEM analysis of the sliced pellet cross-section, and (2) measuring pellet weight loss from repeated heating/washing cycles. The coating system that resulted in the best performance used an ethyl cellulose pre-coat (2-7% of final coated pellet) and a DARAN® SL112 PVDC latex coating (10-20% of coated pellet). A fluidized bed spray coater/dryer was used for this work. The coating conditions involved heating the fluidizing air to 20-30 ºC in stages to dry the latex and form a good PVDC film. The fluid-bed coating process was successfully scaled up from the 100 g lab unit to 5 kg scale at Coating Place Inc. (Verona, WI). Figure 6 shows the fluid-bed spray-coater.

The PVDC-coated pellets remained dry to touch (i.e. no oily feel), even at temperatures above paraffin melting point. The weight loss curves based on multi-cycle heating/washing treatment for pellets from both lab and 5 kg coating scales are presented in Figure 7 (each cycle included heating for 120 min. at 60 ºC, followed by washing with hexane solvent). The polymer

coating reduced the latent heat of the PCM pellet from 120-126 J/g to 82-88 J/g range (Tables IV and V respectively).

The quality of the coating was also analyzed with SEM microscopy. Figure 8 provides the SEM image of a sliced pellet cross-section, confirming the good coverage obtained by the coating system.

Table V. Summary of Large-Scale (>5 kg) PCM Pellet Coating Results

Type of Coating	Amount of Coating (wt % coated pellet)	Method/ Equipment	Coated PCM Pellet Properties				
			DSC Phase Change Temp (ºC)	DSC Heat of Fusion (J/g)	Hexane solvent resistance	Paraffin seepage	Dry to touch (non-oily)
Powder [(a)]	6%	Tumbler	24	113	No	<1%	Yes
Powder	6%	V-blender	24	112	No	<1 %	Yes
Polymer [(b)]	10%	Fluid-bed Coater	22-23 ºC	88.2	Yes	none	Yes
Polymer	18%	Fluid-bed Coater	22-23 ºC	82.3	Yes	none	Yes

Notes:
(a) Calcium silicate powder ~ 6 micron average size (Akrochem Corporation)
(b) DARAN® SL112 (Owensboro Specialty Polymers) with 6.6% ETHOCELL® 20 (Dow Chemical) pre-coat

3.2. Powder Coating: An oil absorbing calcium silicate powder was identified as a low cost alternative that is effective in preventing paraffin seepage from the pellet. However, unlike the PVDC polymer coating, calcium silicate is not solvent resistant. The 1-10 micron powder created a permanent coating on the pellet by forming an intermediate layer bound to the paraffin/HDPE composite substrate. This intermediate layer, clearly observed via SEM analysis (Figure 9), is believed to be lamella of paraffin-saturated calcium silicate.

A good coating, providing a non-blocking pellet with virtually no paraffin seepage, is obtained by tumbling about 6% calcium silicate powder with the pellets. The lab preparation

was done by rolling a bottle of pellets and powder. This was successfully scaled up using conventional solid blending equipment: a tumbler (like a cement mixer) and a twin-shell dry blender ("V-blender"); the latter is shown in Figure 10. The powder-coated pellets are also referred to as "dusted pellets" in this report. The thermal and physical properties of some of the coated pellets are summarized in Table V.

3.3. Comparison to Microencapsulated PCM: The coating on the pellet may be regarded as an encapsulating film, retaining the paraffin within the plastic composite. The performance attributes of the low-cost PCM product thus produced compare favorably with the more costly microencapsulated products. Table VI provides a thermal property summary.

Table VI. Comparison of Low-Cost PCMs to Microencapsulated PCM

Product Description	Melting point (°C)	Latent heat capacity (kJ/kg)	Overall storage capacity in 10-30 °C operating range (kJ/kg)	Reference
PVDC-Coated Pellet	22-23	88.2	NM [b]	Table V
Powder-Coated Pellet	24	112-113	183	Table V
Microencapsulate DS 5001[a]	26	110	145	6
Microencapsulate DS 5008[a]	23	100	135	6
Microecapsulate DS 5029[a]	21	90	125	6

Notes:
(a) BASF MICRONAL® PCM product grade
(b) n.m. = not measured

4. Field Tests

The pellets produced in Pelletizing Runs 2-4 (Table IV) were shipped to Oak Ridge National Laboratory for field testing. The tests were conducted at the ORNL Natural Exposure Test Facility in Hollywood, SC (near Charleston). The building envelope that was the focus of the study was PCM-modified cellulose insulation.

A 30% blend of PCM pellets in cellulose insulation was prepared and added to test wall for installation and natural exposure. The loading and test details are described in the ORNL report, provided as Appendix A1. Figure 11 is a photograph taken during installation of the test wall.

Several weeks into the first field test, the decision was made to test a condensed PCM configuration in one of the test wall cavities. When the wall was opened to install the new test insulation systems, it was observed that some of the test insulations had settled within the cavities. For the second installation, modifications were made to use equally sized test cavities, and care was taken to achieve uniform cellulose density in each cavity. This phase of the tests ("Phase 2") started at the beginning of the summer (late June 2012), and lasted until end of the project in Dec. 2012. The two PCM-modified insulation configurations tested were (1) 30% PCM pellets dispersed in cellulose insulation (5.5 inch thickness), and (2) condensed PCM (0.75 inch layer) within two layers of insulation (3.75 inch layer external; 1 inch layer internal). These were coded as "cellulose+PCM" and "cell/PCM/cell" (or "PCM sandwich"), respectively.

The weekly datasets were plotted and analyzed. A typical weekly dataset is shown in Figure 12. (See the Appendix A4 for a complete set of weekly data plots.) As observed in Figure 12, both PCM modifications resulted in significant reduction in peak heat flux (rate of heat transfer into the building per unit wall area). Furthermore, based on the observed pattern of

daily reduction in heat flux and cavity temperatures with the PCM-containing envelopes, both PCM configurations seem to have resulted in daily phase change (i.e. refreezing every night during the summer). Note that the PCM melt range (23-25 ºC) exceeded the diurnal low temperatures and the thermostat set point (21 ºC), providing two directions for PCM discharge.

Since some of the heat stored in the PCM during the day was released inside at night, the net heat gain (the area under the heat flux curve) was not reduced by as high a percentage as the peak heat flux value. In the case of the PCM sandwich configuration ("cell/PCM/cell"), perhaps because the total thickness of the insulation was reduced by 0.75 inch, the net heat gain was in fact higher than the control ("cell"). Table VII provides an overview of the summer performance results, highlighting the effect of PCM dispersion ("cell+PCM") on insulation performance.

Table VII. Field Test Results: Summer Performance Summary

Date	Max T deg C	Min T deg C	Max Heat Flux cell W/m2	Max HF cell+PCM W/m2	Max HF cell/PCM/cell W/m2	Total Heat cell kJ/m2	Total Heat cell+PCM kJ/m2	Total Heat cell/PCM/cell kJ/m2	% Reduction with Cell+PCM	
									Peak Heat Flux	Heat Gain
7/4/2012	33.6	21.9	5.35	3.58	3.57	213.2	190.7	271.9	33.0%	10.6%
7/5/2012	34.3	25.3	5.81	4.13	3.56	258.1	220.9	280.3	28.9%	14.4%
7/6/2012	34.0	22.9	5.84	4.02	3.86	246.1	220.5	296.6	31.2%	10.4%
7/7/2012	35.0	23.0	6.17	4.30	3.86	252.9	219.1	293.6	30.3%	13.4%
7/8/2012	34.4	25.8	6.19	4.43	3.97	279.3	240.6	311.3	28.3%	13.8%
7/9/2012	34.7	26.8	6.34	4.58	4.20	284.5	247.2	328.3	27.8%	13.1%
7/10/2012	33.1	22.8	6.24	4.45	4.36	222.7	203.7	291.5	28.7%	8.5%
7/11/2012	32.2	22.3	5.23	3.58	3.71	185.8	174.6	277.0	31.5%	6.0%
7/12/2012	32.4	22.6	5.16	3.57	3.46	216.6	189.4	270.4	30.9%	12.6%
7/13/2012	32.0	23.4	5.56	3.76	3.48	226.9	199.5	271.7	32.3%	12.1%
7/14/2012	32.7	23.0	5.59	3.83	3.48	219.0	194.2	268.6	31.6%	11.3%
7/15/2012	31.5	22.1	5.59	3.54	3.44	186.0	171.1	258.6	36.7%	8.1%
7/16/2012	32.6	21.6	6.45	4.15	3.39	221.2	188.3	252.8	35.7%	14.9%
7/17/2012	32.6	23.3	5.31	3.46	3.27	211.5	186.9	262.7	34.9%	11.6%
7/18/2012	31.5	22.4	5.50	3.50	3.22	206.1	180.3	257.8	36.2%	12.5%
7/19/2012	32.1	24.5	5.58	3.95	3.46	240.4	207.6	274.7	29.2%	13.7%
7/20/2012	32.1	25.0	5.73	3.89	3.63	238.2	209.1	283.9	32.1%	12.2%
7/21/2012	32.5	24.7	5.10	3.52	3.36	227.3	198.3	274.0	30.9%	12.7%
7/22/2012	33.5	25.1	5.48	3.97	3.49	236.2	207.0	279.5	27.5%	12.4%
7/23/2012	32.8	23.2	6.59	4.43	3.71	250.9	216.1	284.0	32.7%	13.9%
7/24/2012	34.8	22.2	6.44	4.45	3.84	273.0	231.8	298.3	30.9%	15.1%
7/25/2012	34.9	22.4	5.91	4.02	3.74	242.6	213.6	299.1	32.0%	12.0%
7/26/2012	35.5	25.0	7.08	4.80	4.01	283.0	238.6	311.7	32.1%	15.7%

Table VII. continued

Date	Max T deg C	Min T deg C	Max HF cell W/m2	Max HF cell+PCM W/m2	Max HF cell/PCM/cell W/m2	Total Heat cell kJ/m2	Total Heat cell+PCM kJ/m2	Total Heat cell/PCM/cell kJ/m2	% Reduction with Cell+PCM	
									Peak Heat Flux	Heat Gain
7/27/2012	34.7	23.0	5.61	4.16	3.99	253.1	225.7	318.9	25.9%	10.8%
7/28/2012	32.6	24.5	6.36	4.19	3.88	250.4	214.8	299.9	34.0%	14.2%
7/29/2012	34.1	23.7	6.57	4.60	3.82	234.3	205.0	292.0	30.0%	12.5%
7/30/2012	29.2	20.6	3.32	2.38	3.14	147.3	149.2	245.7	28.1%	-1.3%
7/31/2012	31.2	19.9	5.35	3.49	3.07	177.9	151.4	225.2	34.8%	14.9%
8/1/2012	31.6	23.5	4.83	3.23	3.05	208.5	179.3	238.7	33.1%	14.0%
8/2/2012	34.6	21.4	6.98	4.46	3.46	218.7	197.4	264.0	36.0%	9.8%
8/3/2012	32.5	20.8	5.73	3.68	3.22	202.9	170.6	243.0	35.7%	15.9%
8/4/2012	32.2	23.5	6.34	4.02	3.48	224.1	193.4	265.6	36.6%	13.7%
8/5/2012	31.7	23.6	5.89	3.85	3.40	198.2	180.3	264.1	34.6%	9.1%
8/6/2012	32.2	23.0	6.47	4.16	3.37	219.0	188.5	256.9	35.7%	14.0%
8/7/2012	26.5	23.7	2.21	1.89	2.93	143.4	140.6	232.9	14.5%	2.0%
8/8/2012	30.1	22.6	3.23	2.16	2.45	139.5	129.1	197.1	33.2%	7.5%
8/9/2012	32.5	21.7	7.20	4.38	3.20	215.6	177.3	222.9	39.1%	17.8%
8/10/2012	30.2	22.4	4.85	3.15	3.12	193.0	168.3	244.9	35.0%	12.8%
8/11/2012	31.6	22.1	5.89	3.94	3.42	192.6	174.0	251.3	33.2%	9.6%
8/12/2012	30.9	23.9	5.59	3.67	3.23	211.8	175.9	242.5	34.5%	17.0%
8/13/2012	31.8	22.2	5.91	3.84	3.29	209.1	182.7	252.8	34.9%	12.6%
8/14/2012	32.9	22.8	6.39	4.13	3.51	232.2	194.3	262.0	35.3%	16.3%
8/15/2012	32.2	24.1	5.59	3.79	3.52	235.1	201.4	276.3	32.2%	14.3%
8/16/2012	32.1	22.1	4.87	3.12	3.14	173.2	163.7	251.7	35.9%	5.5%
8/17/2012	32.5	20.8	6.55	4.13	3.17	195.1	171.8	238.8	36.9%	11.9%
8/18/2012	31.7	22.2	5.36	3.31	3.00	189.4	162.3	230.9	38.2%	14.3%
8/19/2012	29.4	23.3	3.96	2.72	3.00	168.6	155.1	236.8	31.3%	8.0%
8/20/2012	28.9	23.2	4.11	2.81	2.85	163.3	150.3	222.0	31.5%	8.0%
8/21/2012	28.6	22.3	4.24	2.75	2.78	158.7	144.1	210.9	35.1%	9.2%
8/22/2012	29.4	21.1	4.21	2.88	2.75	150.9	136.0	202.7	31.6%	9.9%
8/23/2012	27.7	21.3	3.38	2.19	2.50	116.4	113.4	184.2	35.1%	2.5%
8/24/2012	27.6	20.2	4.08	2.45	2.50	128.8	119.2	175.6	39.9%	7.5%
8/25/2012	29.9	17.8	4.72	3.01	2.53	110.8	100.9	162.0	36.2%	8.9%
8/26/2012	30.9	18.6	4.97	3.09	2.62	134.3	110.3	162.6	37.8%	17.9%
8/27/2012	30.3	23.0	4.32	2.87	2.74	174.2	146.9	201.2	33.7%	15.7%
8/28/2012	25.2	23.7	1.74	1.60	2.62	124.5	123.7	197.5	7.6%	0.7%
8/29/2012	30.7	21.8	5.00	3.12	2.78	184.1	158.6	205.1	37.6%	13.8%
8/30/2012	28.2	22.1	2.71	2.05	2.57	132.0	122.0	197.7	24.2%	7.6%
8/31/2012	32.1	22.2	7.26	4.21	3.25	214.5	174.4	221.3	42.0%	18.7%
9/1/2012	33.0	22.4	7.03	4.46	3.49	226.6	186.5	251.1	36.5%	17.7%
9/2/2012	33.2	24.0	7.31	4.80	3.81	247.7	204.9	274.3	34.3%	17.3%
9/3/2012	31.3	24.1	6.55	4.30	3.72	223.5	193.5	275.7	34.3%	13.4%
9/4/2012	30.7	23.2	5.10	3.52	3.25	199.0	175.8	253.0	30.9%	11.7%
Average									**32.6%**	**11.7%**

The 33% average reduction in peak heat flux (HF) is consistent with the performance reported for more costly micro-encapsulated PCMs in similar wall insulation systems (*11*). Assuming this is representative of the whole building's envelope, we would expect a 33% reduction in peak cooling load (e.g. air-conditioner duty) and 12% decrease in net energy

consumption during the summer. The annualized reduction is affected by climate, but is generally expected to be less. The whole-building modeling study (next section) considered various variables to estimate total annual energy savings.

The thermal conductivity of cellulose insulation holding 30% dispersed PCM was found to bed 6 to 7% higher than cellulose insulation alone. (Test details and results may be found in reports by ORNL and Fraunhofer in Appendices A1 and A2 of this report.) Although a small increase, and perhaps within the variability of the cellulose insulation loading density, this needs to be considered when evaluating alternative PCM-modified envelope systems (e.g. “condensed” vs. “dispersed” PCM systems having the same total insulation thickness). Aging the cellulose insulation with 30% dispersed PCM pellets at conditions simulating a summertime attic was found to have no effect on its thermal conductivity.

5. Whole-Building Model and Market Analysis

The whole-building simulation studies for low-cost PCM pellets were performed at Fraunhofer CSE (Cambridge, MA). Fraunhofer used the field test data from ORNL, plus their own analytical test results from evaluation of the PCM and PCM/cellulose insulation system, to model the performance of the PCM-modified attic insulation system. A key goal of the study was to estimate the energy savings obtained by adding the PCM pellets to attic insulation as part of a building retrofit project. Four different climates were considered: Phoenix, Houston, San Francisco, and Miami. Fraunhofer's report, providing model development details and results for various simulation cases, is included as Appendix A3.

The conclusion of configuration modeling was that the optimum arrangement places a "condensed" layer of the PCM pellets at the bottom of the attic insulation. Since the PCM pellets have a much higher density than cellulose insulation, pellets added to existing attic insulation (or blown along with additional insulation), naturally settle to the bottom to form a condensed layer there.

The results suggest that addition of PCM to the attic insulation can reduce electricity usage for cooling by 750 kW-h in Phoenix—a 4.2% annual saving. Savings in Houston and Miami were found to be in the 390-420 kW-h range.

A reduction in natural gas consumption during winter is also expected for San Francisco, Houston, and Phoenix. The annual reduction in natural gas for heating was 10.4 therm for San Francisco—a 17% annual saving.

For this type of attic insulation retrofit project, the cost of PCM pellets for the consumer is expected to be in the $900-$1,800 range (assuming a PCM selling price of $1.5-$3.0/lb).

Based on current U.S. electricity and natural gas prices (10-13 cents/kW-h; $1.5-$2.2/therm), the payback period for a house in Phoenix climate is expected to be in the 8 to 16 year timeframe.

Another approach to quantifying the economic benefit of PCM to the consumer is as a substitute for extra air-conditioning capacity. To provide a boost in cooling load equivalent to the 30+% reduction observed with PCM, an additional small A/C unit would be required. The price of such units typically exceeds the projected PCM cost range.

6. Fire Tests

The burn properties of the coated PCM pellets were tested by placing a table spoon of the pellets on an aluminum foil covered table. A lit match was then placed on the pellets until these were ignited. The burn behavior of the PCM pellets was then observed.

For the PVDC polymer-coated and the calcium silicate powder-coated PCM pellets, the fire self-extinguished after about 6 and 7 minutes respectively. Without coating, the pellets did not self-extinguish and continued to burn until only a molten mass of HDPE remained. Figure 11 presents the sequence of pictures taken from a film-strip of this burn experiment.

Different fire standards govern building envelope components. For cellulose insulation, the governing standard in ASTM C739, "Standard Specification for Cellulosic Fiber Loose-Fill Thermal Insulation." Sections 10 and 14 of this document provide the description and specifications for two different flammability tests: Critical Radiant Flux (ASTM Test Method E970) and Smoldering Combustion.

These tests were conducted at the QC laboratories of Advanced Fiber Technologies (Bucyrus, OH), a manufacturer of cellulose insulation that certifies its products according to C739 standard. The fire tests were conducted on the powder-coated pellets, with 30% pellets based on final envelope weight. Further details about the test are summarized in the Fraunhofer test report, provided in the Appendix A2.

Two configurations of PCM-modified cellulose insulation envelope were tested: (1) PCM pellets uniformly dispersed in the envelope, and (2) PCM pellets concentrated 1 inch below top of the insulation (similar to the "condensed PCM" configuration that was found to provide the optimum energy savings in the modeling studies). Both configurations passed the smoldering combustion test, but only the configuration holding no pellets in the top 1 inch

passed the E970 test. As such, the preferred configuration ("condensed PCM" variations) fully conforms to the ASTM C739 flammability standard.

When a grade of cellulose insulation with extra flame retardant chemical was used for the test, the uniform dispersion of PCM pellets in the insulation system also passed the E970 fire test. These results are listed in Table VIII. Based on Table VIII, for a PCM-modified insulation system to conform to the C739 standard's fire specifications, either the PCM pellets need to be present as a "condensed layer" within the cellulose insulation, or a cellulose insulation with extra flame retardant (50% higher than standard) is to be employed.

Table VIII. Conformance of PCM-Modified Cellulose Insulation to ASTM C739 Standard Fire Specifications (30% powder-coated PCM pellets)

Cellulose Insulation Type	PCM Placement	Smoldering Combustion Test	Critical Radiant Flux Test	Conformance to ASTM C739 Fire Specifications
Standard	Uniform	Pass	Fail	No
Standard	Condensed (1" below top of insulation)	Pass	Pass	Yes
FIRE SHIELD™ (50% higher flame retardant concentration)	Uniform	Pass	Pass	Yes

7. Alternate PCM Forms and Energy-Efficient Building Applications

The low-cost process demonstrated as part of this project was also explored for production of different forms of PCM—mainly for building applications not requiring a "carrier" like cellulose insulation or gypsum wallboard. Since the Paraffin/HDPE composite is a homogeneous thermoplastic, it can be "converted" to forms other than pellets. To test the viability of conventional plastic processing equipment for this purpose, the low-cost PCM compound was injection-molded into plaques and extruded into sheets.

Injection molding can be used to make PCM floor/ceiling tiles, plates, or other molded objects of interest. Figure 14 is a photograph of a parallel-plate thermal storage device prototype model made of injection molded PCM plates. Such an object may be inserted in the air handling system/ducts of central air-conditioning units. By operating the A/C at night time, the PCM (e.g. having a melt point in the 19-22 ºC range as in Table II) can store cold at night as it freezes, maintaining the building below 23 ºC (73 F) during the day with just the fan running. Refrigerant compressors run more efficiently at cooler nighttime conditions, providing energy savings to the consumer. Furthermore, by reducing demand for peak load power generation (natural gas fired power plants), this type of "cold storage" offers the potential for a disproportionally higher reduction in greenhouse gas emissions.

Alternatively, the plastic compound can be extruded into sheets, providing a flexible PCM form for lamination to the exterior face of gypsum wallboards and ceiling boards. The photograph of a PCM sheet prototype is shown in Figure 15. The heat storage potential of the low-cost PCM sheet was computed from specific heat measurements (see Fraunhofer's PCM evaluation report in Appendix A2), and is presented in Figure 16 along with the same for

concrete and brick. This shows that the thermal mass of the PCM sheet in the building envelope exposure temperature range is about 16 times greater than concrete or brick. In other words, the use of the low-cost PCM plastic sheet would provide as much thermal mass as a brick or concrete wall having 16 times the thickness.

Figure 17 shows how these PCM products could be deployed in a building. With the combined use of PCM products, each installed to take advantage of a different PCM feature (e.g. cold storage at 20 ºC, temperature control at 22-23 ºC, and heat storage at 25 ºC), a more significant reduction in energy costs and a shorter payback time may be achieved.

8. Summary and Conclusions

This project demonstrated the concept of low-cost PCM manufacturing based on the combination of processes to (1) convert vegetable oils/fats into octadecane-rich PCM paraffins, and (2) "encapsulate" the paraffins using conventional plastic compounding equipment. Such a continuous process can be used for single-train PCM production plants, such as that shown in Figure 18.

Additionally, the project evaluated the performance of the low-cost PCM pellets produced from this process in cellulose insulation building envelopes. The results and main conclusions of the project are summarized below.

- Vegetable oils were converted into PCM-range paraffins at 100% volumetric yield
- PCM paraffins derived from vegetable oils and animal fats had melting points in the 18-25 ºC range, and heats of fusion in the 170-210 J/g range
- Shape-stable PCM pellets were formed by compounding with HDPE in a twin-screw extruder. The paraffin/HDPE ratios were in the 65/35 to 70/30 range. An underwater pelletizer and a strand pelletizer were successfully used at different stages in the project.
- Paraffin seepage from PCM pellets was eliminated by encapsulative coating. Two coating methods were developed: polymer-coating using a PVDC latex, and powder-coating with calcium silicate.
- The PVDC-coated pellets were solvent resistant, showing no loss in weight after multiple heat/wash cycles with hexane
- The coated PCM pellets had melt points of 22-24 ºC, and heats of fusion in the 82-113 J/g range. These thermal properties are similar to the more expensive micro-encapsulated PCMs.

- The PCM-modified cellulose insulation system was field-tested at ORNL Natural Exposure Test Facility; 33% reduction in peak heat flux, and 12% reduction in heat gain was observed (average summertime performance)
- Whole-building modeling indicated that the most effective use of PCM in cellulose attic insulation is as a condensed layer at the bottom. The simulation cases show that electricity consumption for cooling, and natural gas for heating, would both be reduced as a result of PCM addition to attic insulation. Such a retrofit was estimated to provide savings that would pay for the PCM in 8 to 16 years at current energy prices in a climate like Phoenix.
- Fire tests were conducted according to the cellulose insulation standard. The condensed PCM configuration conformed to the fire standard. For uniform dispersion of PCM in cellulose insulation, a cellulose grade with higher concentration of flame retardant was needed.
- Alternate forms of the PCM plastic composite, such as extruded sheets and injection molded tiles/plates, were also produced and evaluated as part of the project. These open up new deployment strategies for enhancing building energy efficiency, potentially shortening payback times.

References

1. Abhat, A. *Revue Phys. Appl*. **1980**, *15*, 477-501.

2. Mehling, H.; Cabeza, L. F. *Heat and Cold Storage with PCM*; Springer-Verlag: Berlin, 2008; Chapter 9.

3. Sharma, A.; Tyagi, V. V.; Chen, C. R.; Buddhi, D. *Renewable & Sustainable Energy Reviews*, **2009**, *13*, 318-345.

4. Sharma, S. D.; Sagara, K. *International Journal of Green Energy*, **2005**, *2*, 1-56.

5. "Kedl, R. J. "Wallboard with Latent Heat Storage for Passive Solar Applications"; Oak Ridge National Laboratory: Oak Ridge, TN; 1991, ORNL/TM-11541.

6. "Micronal® PCM: Intelligent Temperature Management for Buildings"; BASF: Ludwigshafen, Germany, 2008.

7. "News Release: BASF Products in Ravenscraig Innovation Park"; BASF: Ludwigshafen, Germany; Oct. 9, 2012.

8. Abhari, R.; Havlik, P. Z. "Hydrodeoxygenation Process"; U.S. Patent 8 026 401; 2011.

9. Abhari, R. "Even Carbon Number Paraffin Composition and Method of Manufacturing Same"; U.S. Patent 8 231 804; 2012.

10. "Production of Low Cost Phase Change Material for Building Envelopes"; interim report to the Department of Energy on Award DE-EE00003924; Syntroleum Corporation: Tulsa, OK, 2011.

11. Kosny, J.; Yarbrough, D. W.; Miller, W. A.; "Use of PCM Enhanced Insulation in the Building Envelope"; Oak Ridge National Laboratory: Oak Ridge, TN; 2007.

Figure 1. **Paraffin product of vegetable oil hydrodeoxygenation in melt (left) and solid/wax phase**

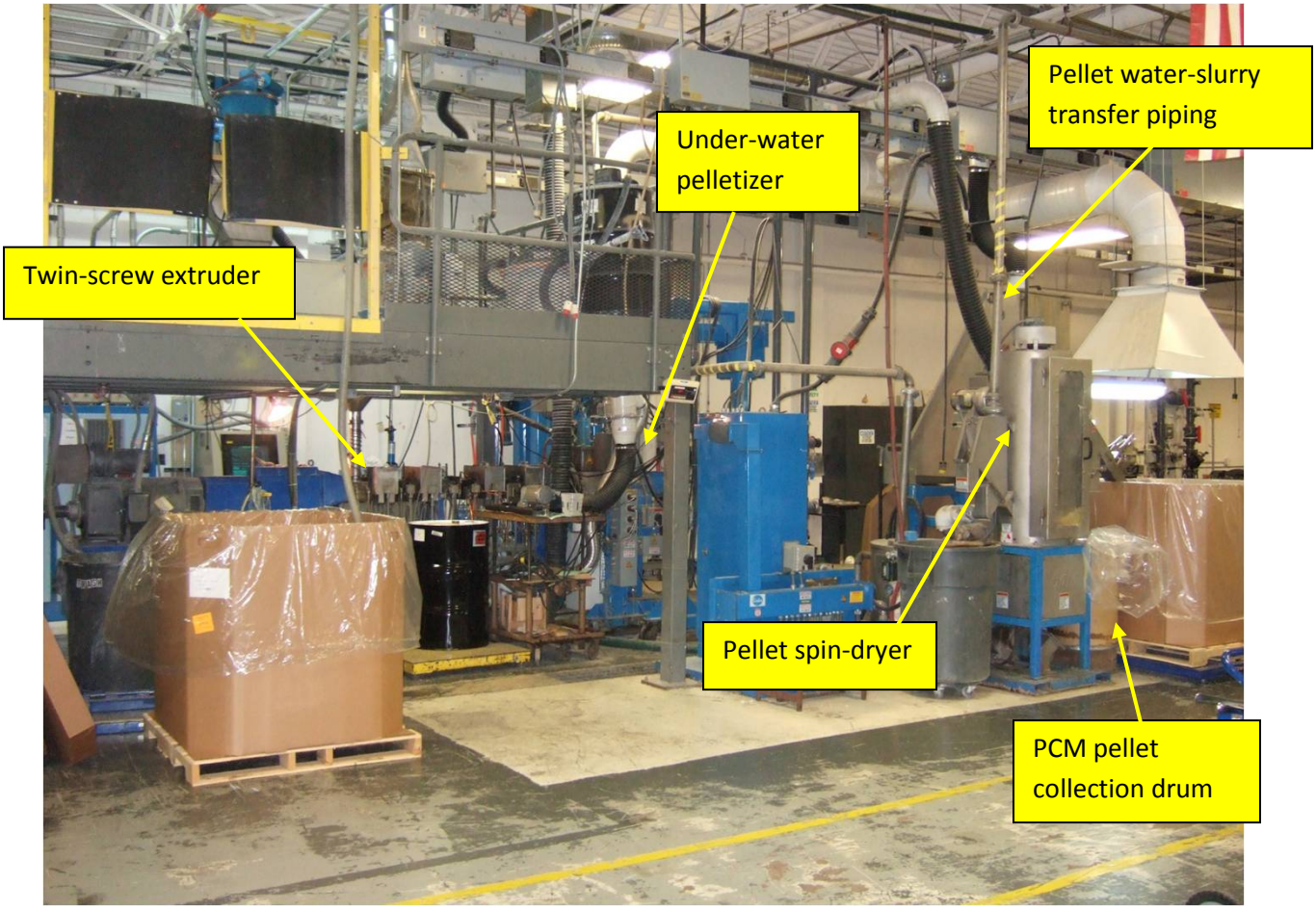

Figure 2. PCM compounding and pelletizing line

Figure 3. PCM pellets (~2 mm) coming off of the compounding/pelletizing line

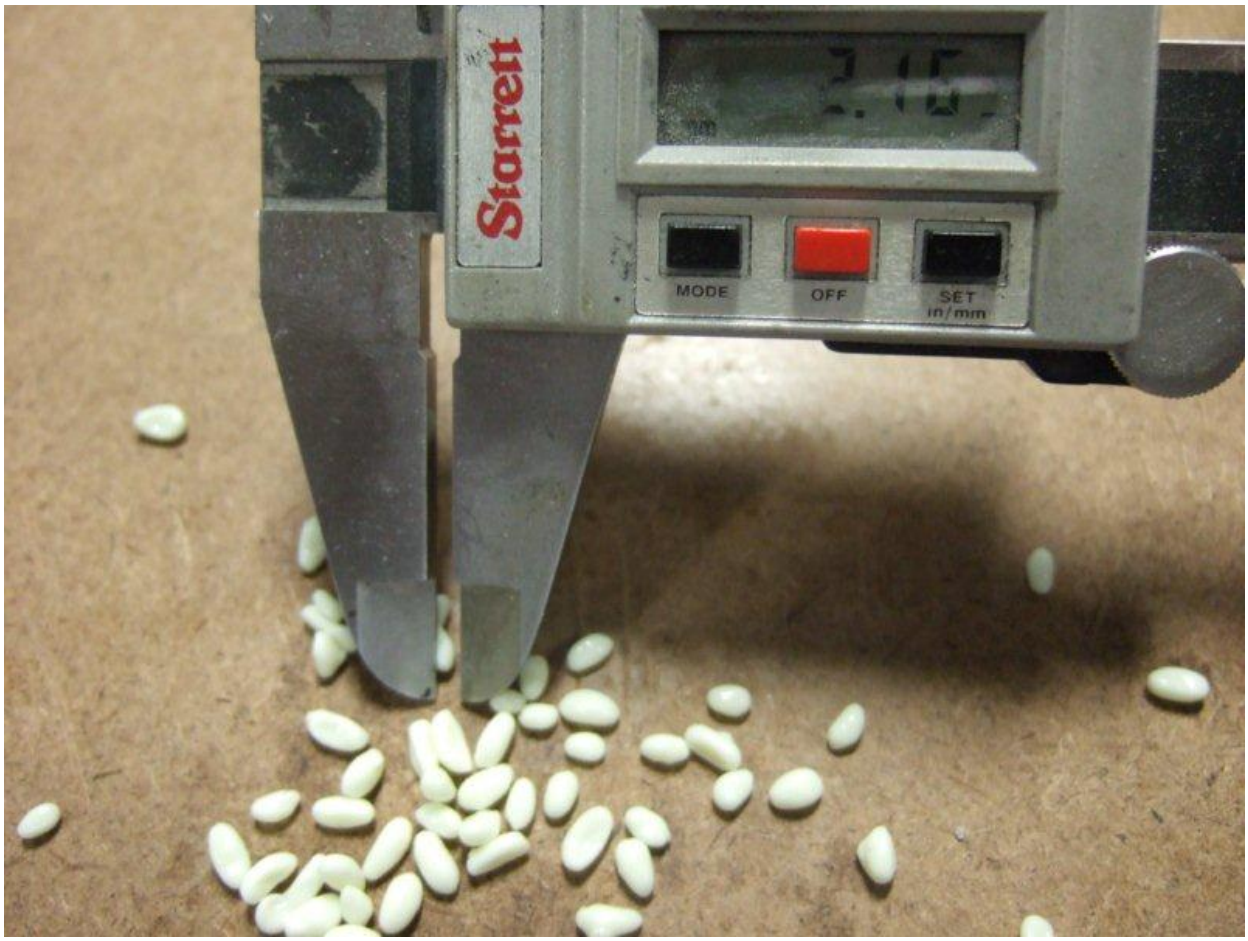

Figure 4. **PCM pellets measure about 2 mm**

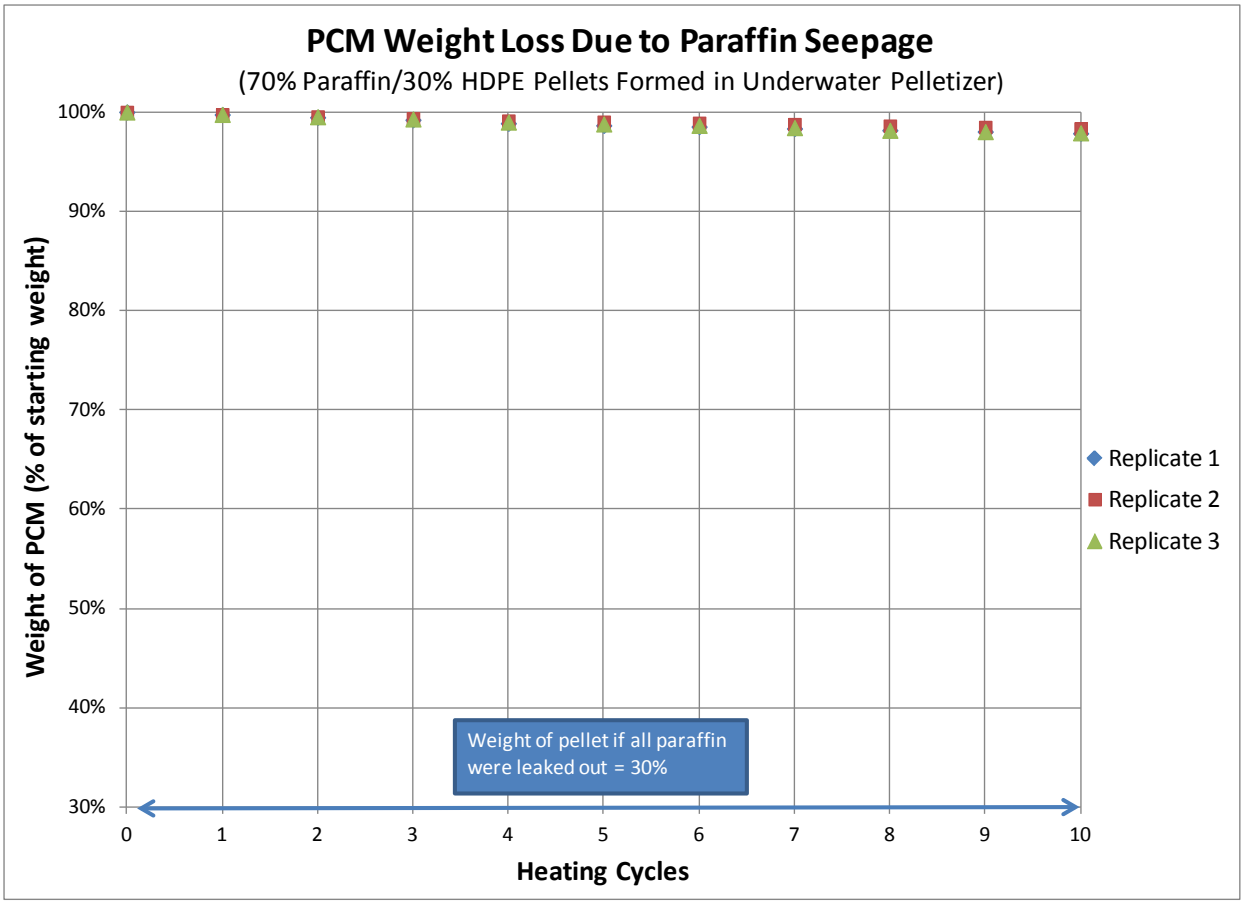

Figure 5. Paraffin seepage from PCM pellets (uncoated); each cycle includes weighing of pellets after two hours in 40 ºC oven

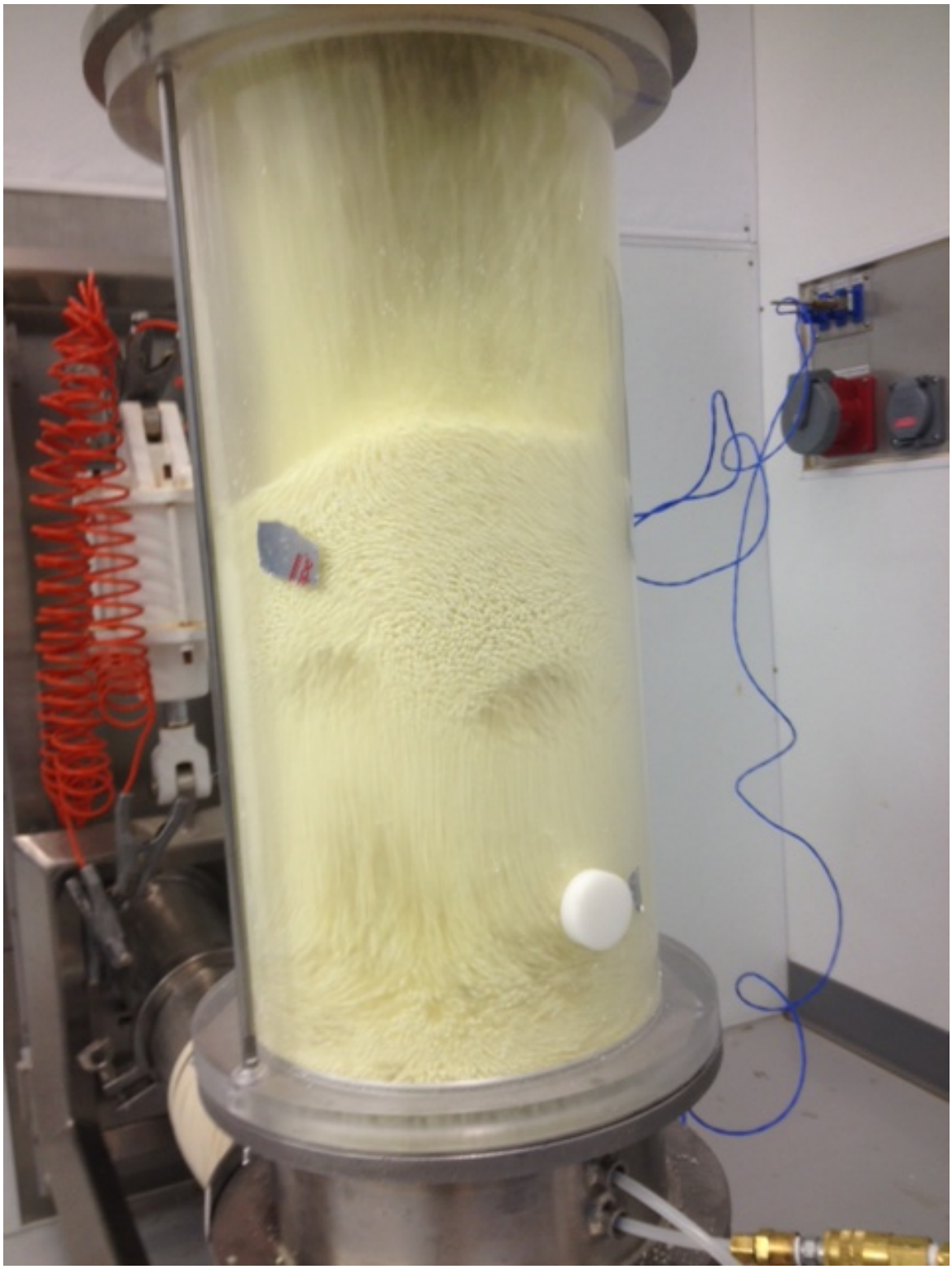

Figure 6. Fluidized-bed spray-coater used to apply polymer coating to the PCM pellet

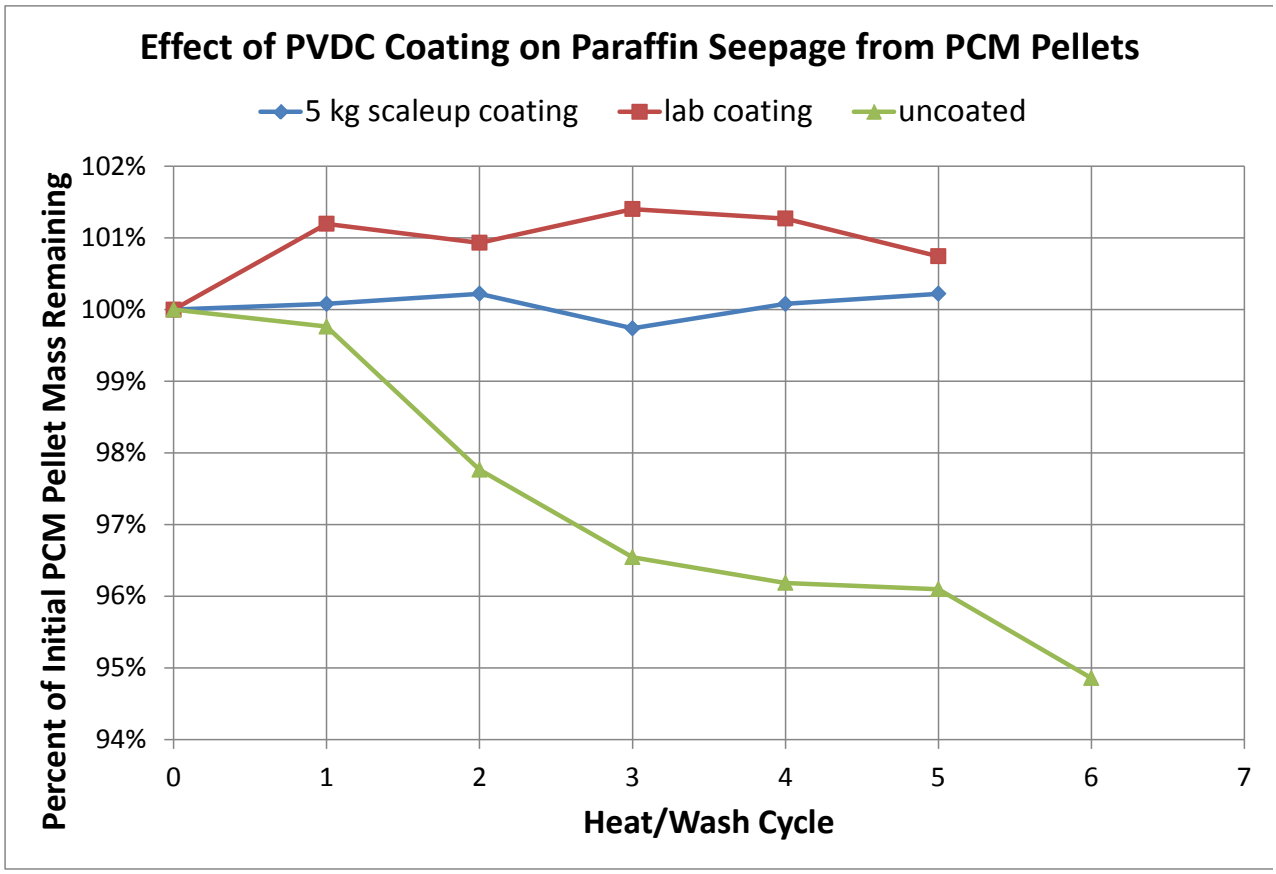

Figure 7. PVDC coating eliminates paraffin seepage from pellets; results show weight loss after heating/washing cycles involving two hours in 60 C over followed by hexane wash

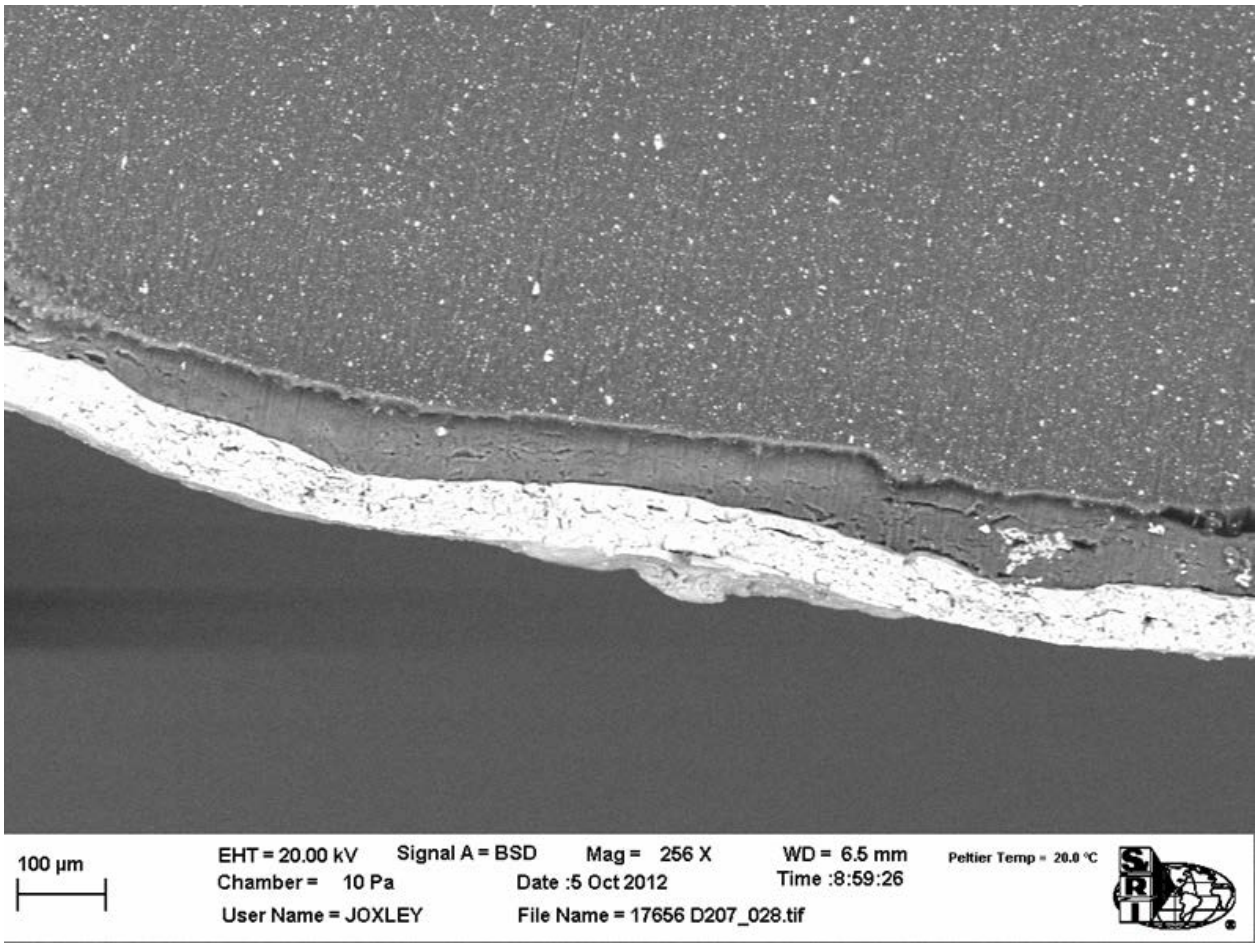

<u>Figure 8.</u> SEM image (256X magnification) of pellet cross-section, showing the good coverage obtained by use of ethyl cellulose pre-coat and PVDC latex coating

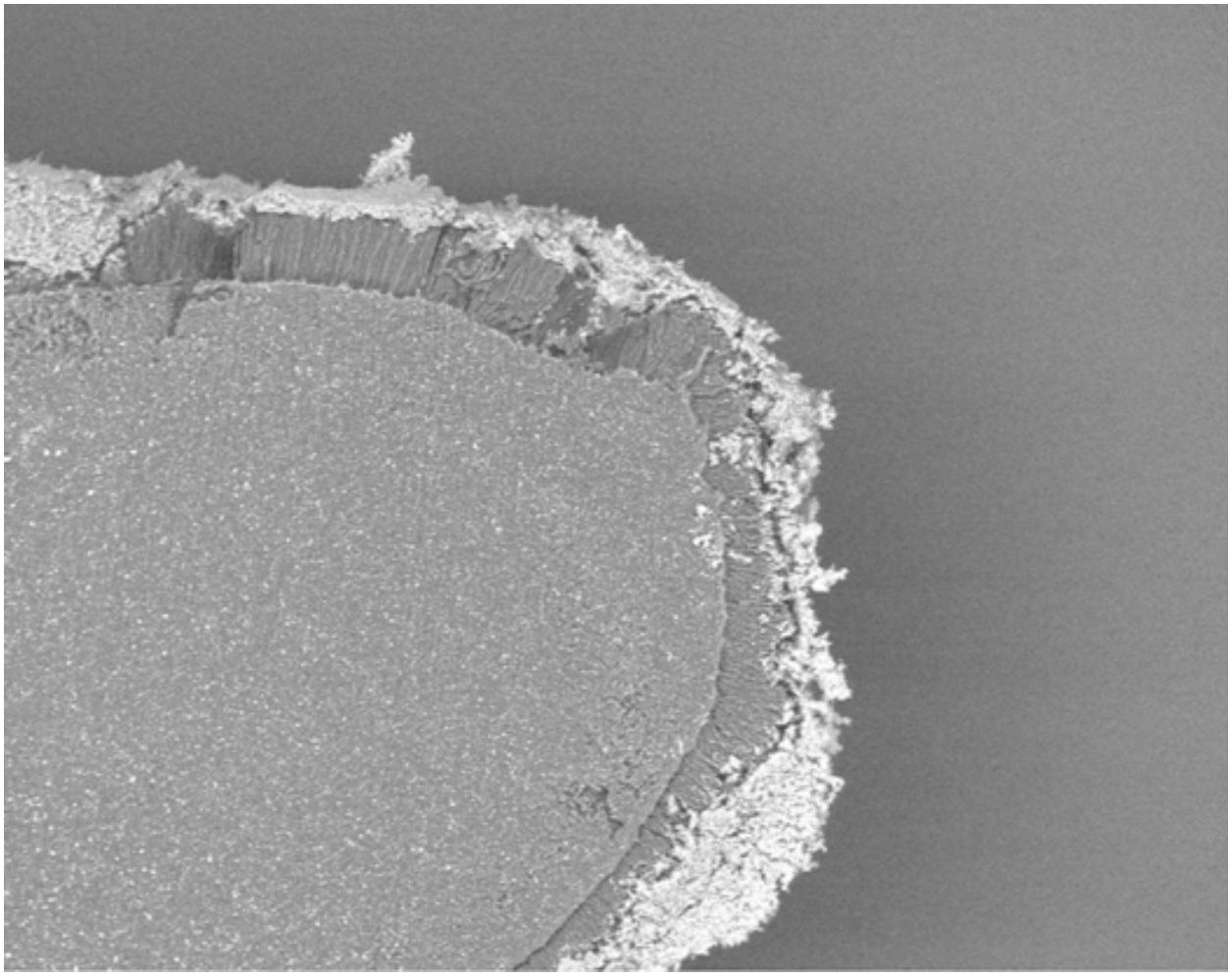

<u>Figure 9.</u> SEM image (100X magnification) of pellet cross-section, showing the good coverage obtained by use of calcium silicate powder; note the lamellar intermdiate layer binding the powder layer to pellet surface

<u>Figure 10.</u> The V-blender used to successfully scale up PCM powder coating

<u>Figure 11.</u> Installation of wall for field test. The wall cavities were filled with cellulose insulation, and two configurations of PCM-modified cellulose insulation.

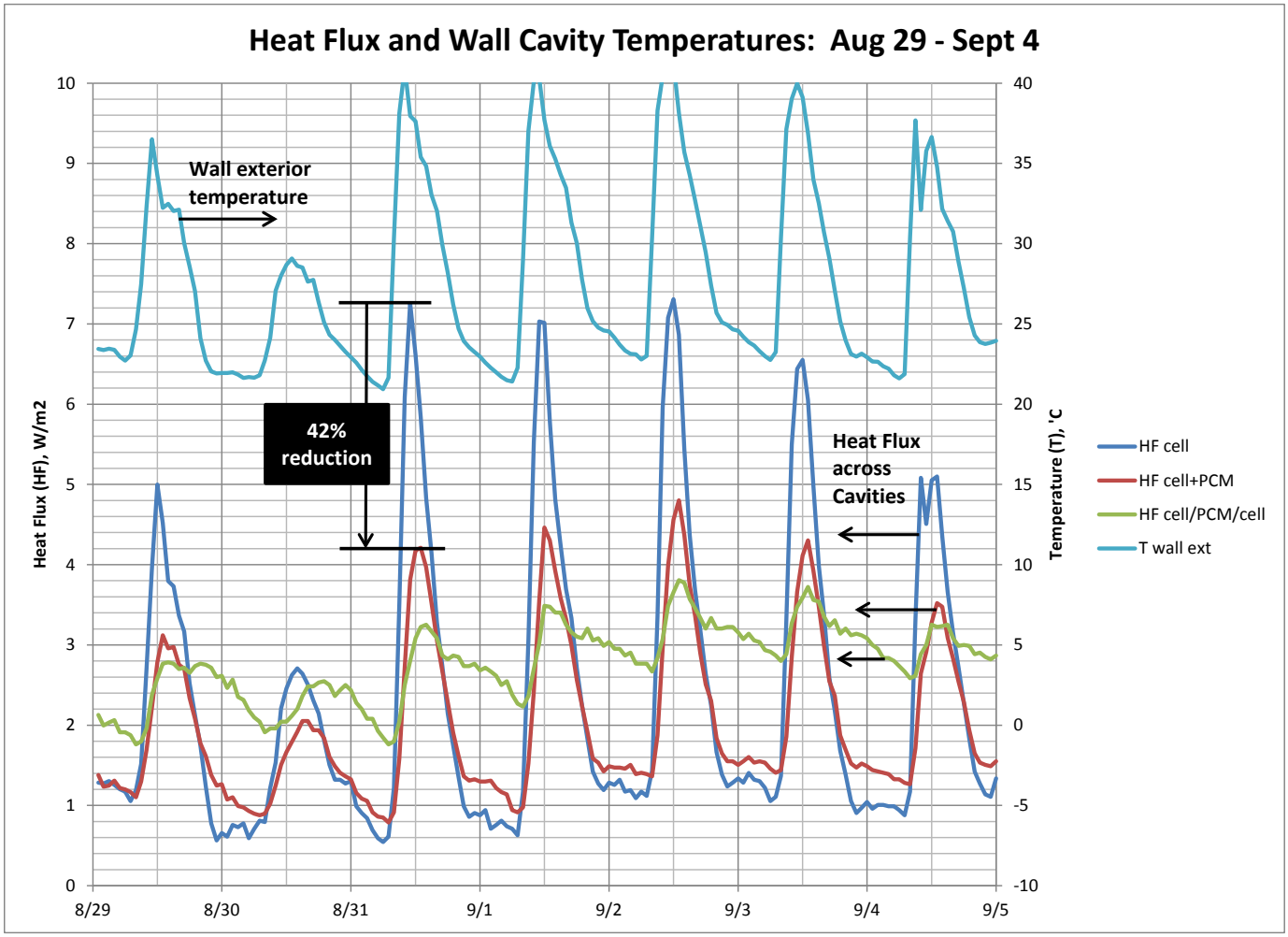

Figure 12. **Typical weekly dataset from field test. The reduction in peak heat flux with PCM-containing insulation on August 31 is marked.**

<u>Figure 13.</u> Sequence of images showing that the PVDC-coated PCM pellets self-extinguish after being set on fire. The time from start of fire until it extinguished was about six minutes.

<u>Figure 14.</u> Prototype of parallel-plate thermal storage device suitable for air handling systems. The plates are made by injection-molding the low-cost PCM composite.

<u>Figure 15.</u> Prototype of PCM sheet for lamination to wallboards and other building envelopes. The sheet was prepared by extrusion of the low-cost PCM composite.

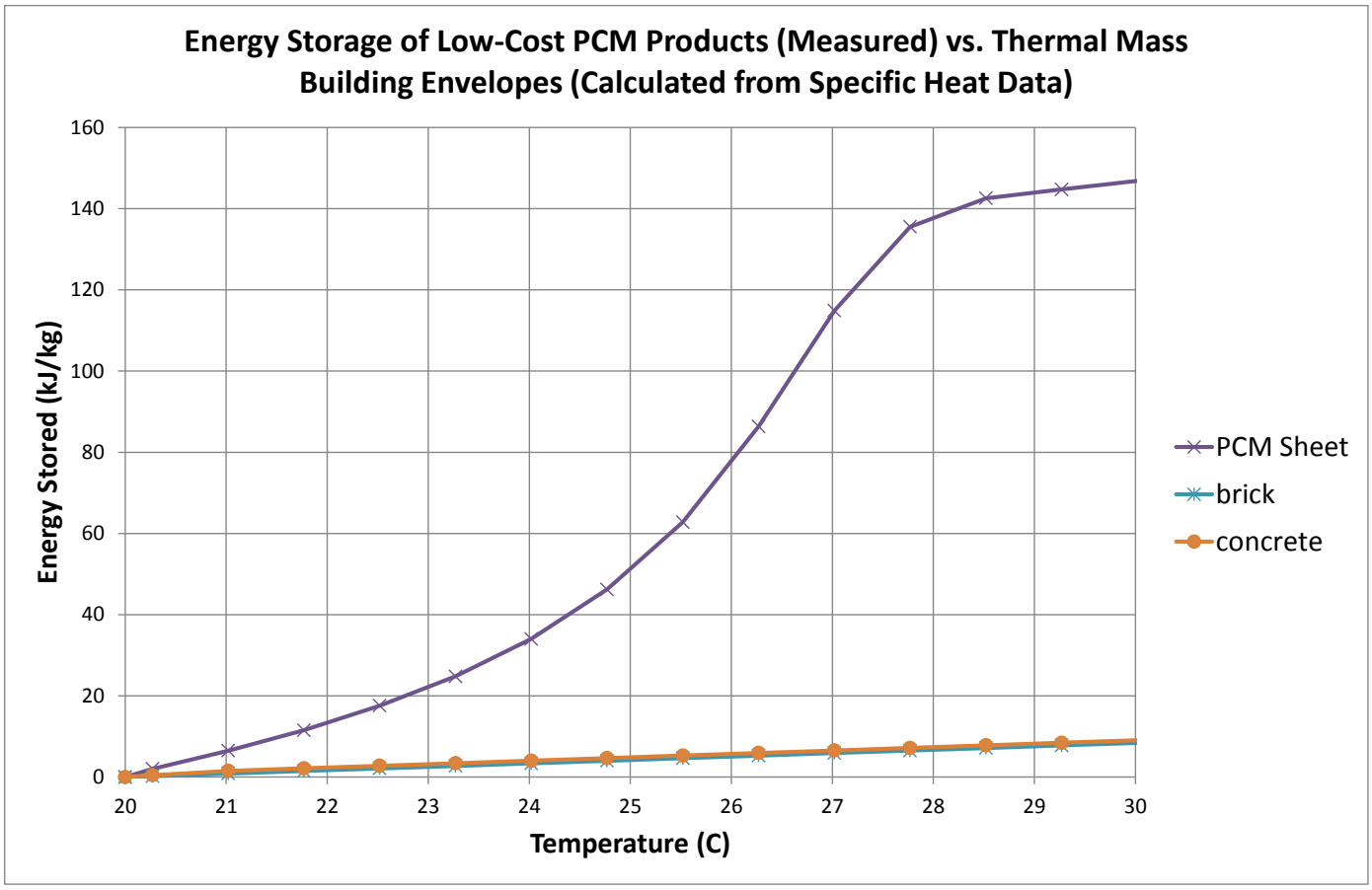

Figure 16. Stored energy vs. temperature curves (derived from specific heat data) for concrete, brick, and the low-cost PCM compound. The curve shows that the thermal mass of the low-cost PCM compound in the 20-30 ºC range is 16 times higher than common material of construction such as brick and concrete

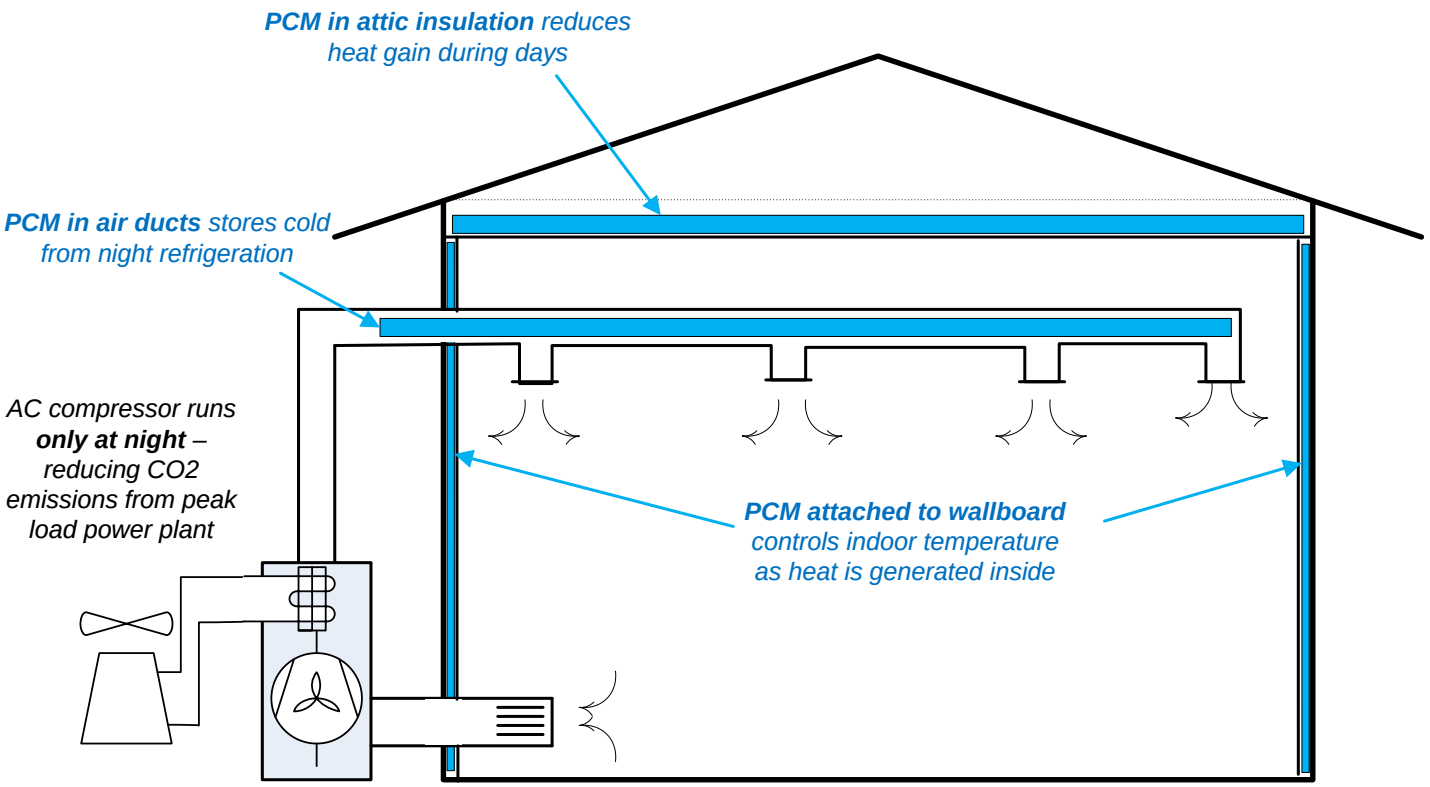

Figure 17. Concept for use of different forms of low-cost PCM in a building, working to reduce energy consumption by different mechanisms

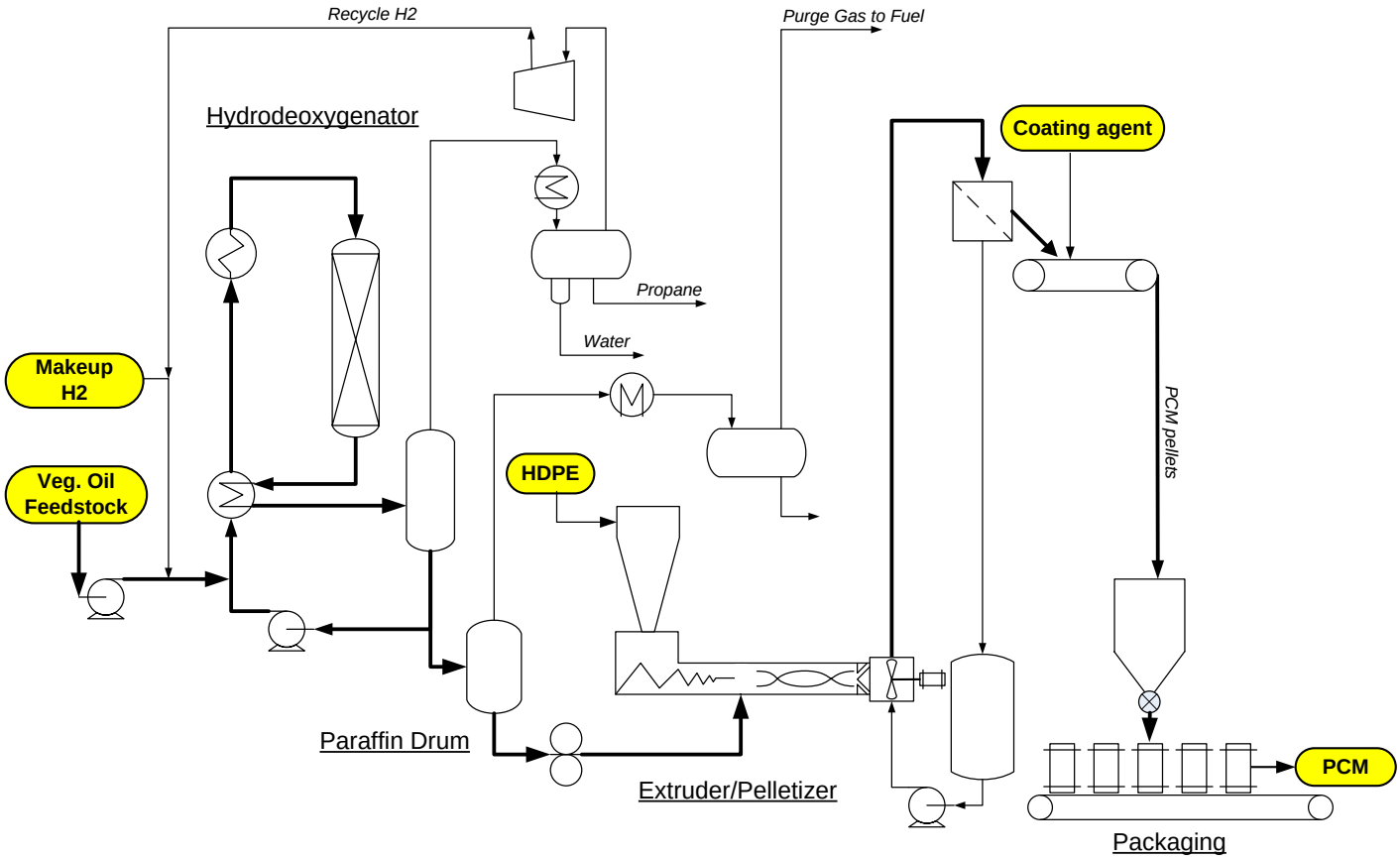

Figure 18. Single-train, low-cost process for manufacture of PCM pellets from biorenewable commodities. All three steps of the process, (1) production of paraffin, (2) shape-stable paraffin/HDPE pellets, and (3) encapsulative coating of the pellets, were demonstrated.

Appendices

A1. ORNL Report

ORNL/TM-2013/99

Field Testing of Low-Cost Bio-Based Phase Change Materials as Energy Storage Medium in Building Envelopes

March 2013

Prepared by
Kaushik Biswas, Ph.D.
Phillip Childs
Jerald Atchley

DOCUMENT AVAILABILITY

Reports produced after January 1, 1996, are generally available free via the U.S. Department of Energy (DOE) Information Bridge.

Web site http://www.osti.gov/bridge

Reports produced before January 1, 1996, may be purchased by members of the public from the following source.

National Technical Information Service
5285 Port Royal Road
Springfield, VA 22161
Telephone 703-605-6000 (1-800-553-6847)
TDD 703-487-4639
Fax 703-605-6900
E-mail info@ntis.gov
Web site http://www.ntis.gov/support/ordernowabout.htm

Reports are available to DOE employees, DOE contractors, Energy Technology Data Exchange (ETDE) representatives, and International Nuclear Information System (INIS) representatives from the following source.

Office of Scientific and Technical Information
P.O. Box 62
Oak Ridge, TN 37831
Telephone 865-576-8401
Fax 865-576-5728
E-mail reports@osti.gov
Web site http://www.osti.gov/contact.html

ORNL/TM-2013/99

Energy and Transportation Science Division

FIELD TESTING OF LOW-COST BIO-BASED PHASE CHANGE MATERIALS AS ENERGY STORAGE MEDIUM IN BUILDING ENVELOPES

Kaushik Biswas
Phillip Childs
Jerald Atchley

Date Published: March, 2013

Prepared by
OAK RIDGE NATIONAL LABORATORY
Oak Ridge, Tennessee 37831-6283
managed by
UT-BATTELLE, LLC
for the
U.S. DEPARTMENT OF ENERGY
under contract DE-AC05-00OR227

TABLE OF CONTENTS

ABSTRACT

A test wall built with phase change material (PCM)-enhanced loose-fill cavity insulation was monitored for a period of about a year in the warm-humid climate of Charleston, South Carolina. The test wall was divided into various sections, one of which contained only loose-fill insulation and served as a control for comparing and evaluating the wall sections with the PCM-enhanced insulation. This report summarizes the findings of the field test.

1. INTRODUCTION

This project was initiated in 2010 by Syntroleum Corporation, in response to a funding opportunity announcement by the U.S. Department of Energy. The major goal was to fundamentally change the manufacture of phase change material (PCM). The proposed low cost process involves a sustainable and more selective route to PCM paraffins and a low cost approach to converting the paraffins to form-stable PCM pellets. By significantly lowering the payback time for PCM-enhanced building material (e.g. wallboards and insulation), high market penetration and proportionally large environmental benefit is expected.

PCMs in building envelopes operate by changing phase from solid to liquid while absorbing heat from the outside and thus reducing the heat flow into the building, and releasing the absorbed heat when it gets cold outside reducing the heat loss through the building envelope. The energy saving potential of PCMs for buildings has been demonstrated [1], but the traditionally high PCM prices have precluded extensive application of PCMs in the building industry. Commercializing a low cost PCM platform was the main goal of this project. The low cost PCM production process involves two components: (1) on-purpose production of C_{16}-C_{18} paraffins from low cost bio-renewable feedstocks, and (2) low cost encapsulation using under-water pelletizers. Paraffins are straight chain saturated hydrocarbons with high latent heat. Hexadecane ($C_{16}H_{34}$), heptadecane ($C_{17}H_{36}$), and octadecane ($C_{18}H_{38}$) are three paraffins that melt/freeze between 18 ºC (64 ºF) and 28 ºC (82 ºF). This temperature range is considered the comfort zone for most people. The high latent heat and suitable phase change temperature range make these paraffins attractive as PCMs for building applications.

Animal fats and vegetable oils are 97% or higher C_{16} and C_{18} fatty acids, and can be converted to C_{16}-C_{18} paraffins using a reaction called hydrodeoxygenation. Further, studies have shown that paraffins can be trapped into high density polyethylene (HDPE) by co-crystallizing a paraffin/HDPE melt. Up to 70% paraffin can be trapped in the HDPE matrix such that molten paraffin does not seep out solid HDPE matrix. Under-water pelletizers have been successfully used to convert molten polymer systems to pellets of various sizes, including < 1 mm pellets. The combination of C_{16}-C_{18} paraffin production from low value fats and waste vegetable oils, combined with low cost encapsulation via under-water pelletizers, is expected to result in a step-change in PCM production costs.

Syntroleum collaborated with Oak Ridge National Laboratory to field-test their PCMs in one of ORNL's test facilities located in Charleston, SC. The test was initiated in January 2012 for a period of about 1 year. A test was built and installed with different combinations of cellulose and PCM containing HDPE pellets as cavity insulation. The wall was instrumented with temperature, humidity and heat flux sensors. The data were remotely monitored and downloaded on a weekly basis. All test data were periodically provided to Syntroleum and are being used for whole building modeling to determine the impact of PCM on annual building energy use. This report provides the test wall and sensor details and briefly summarizes the test data, with a description of key findings.

2. TEST FACILITY AND TEST WALL DETAILS

The Syntroleum wall test is ongoing in a Natural Exposure Test (NET) facility in Charleston, SC, shown in Figure 1. NET facilities expose side-by-side roof/attic and wall assemblies to natural weathering in four different humid US climates. The data help industry develop products to avoid adverse moisture-related impacts in buildings, and are essential in validating hygrothermal and energy models. NET structures are located at ORNL and at Charleston, SC; Tacoma, WA; and Syracuse, NY. Each is temperature and humidity controlled and instrumented to measure moisture content in materials, vapor pressure, temperature, heat flux, humidity, etc. Figure 1 shows the southeast wall of the Charleston NET facility, which houses multiple side-by-side test walls. Also shown is a weather station on the southwest gable end of the building.

Figure 1. Charleston, SC NET facility.

Originally, the test wall was constructed in January 2012, followed by a modification in June 2012. Figure 2 shows the test wall frame built for the January installation. It shows three wall cavities, with sensors installed in the center, and separated by wood studs and thin foam insulation strips, along with a retaining net for holding the insulation. The foam strips were added to minimize the thermal interactions between the cavities. The larger cavity was filled with the cellulose-PCM mixture, while one of the smaller cavities was filled with only cellulose insulation to serve as control for comparison and evaluation of the PCM-enhance insulation. The third cavity was filled with a mix of cellulose and HDPE pellets (without PCM), to try and further isolate the effects of PCM on the insulation properties.

The wall was built using 2 x 6 wood studs, resulting in a cavity depth of 14 cm (5.5 inch), with 1.2 cm (0.5 inch) oriented strand board (OSB) attached to the exterior side of the wall. The larger cavity dimensions were 2.2 x 0.4 m^2 (87.8 x 14.5 square inch) and smaller cavities were 1.1 x 0.4 m^2 (42.4 x 14.5 square inch). The nominal amount of PCM in the larger cavity was 20% by weight. The PCM-HDPE pellet design was such that the pellets contained 65% paraffin by weight. Thus, the PCM pellets and cellulose were mixed so that the mixture contained 31% of pellets, or 0.45 kg of pellets for each kg of

cellulose. For the cavity with cellulose mixed with the HDPE pellets without PCM, the same volume ratio as the cellulose-PCM pellet mixture was maintained.

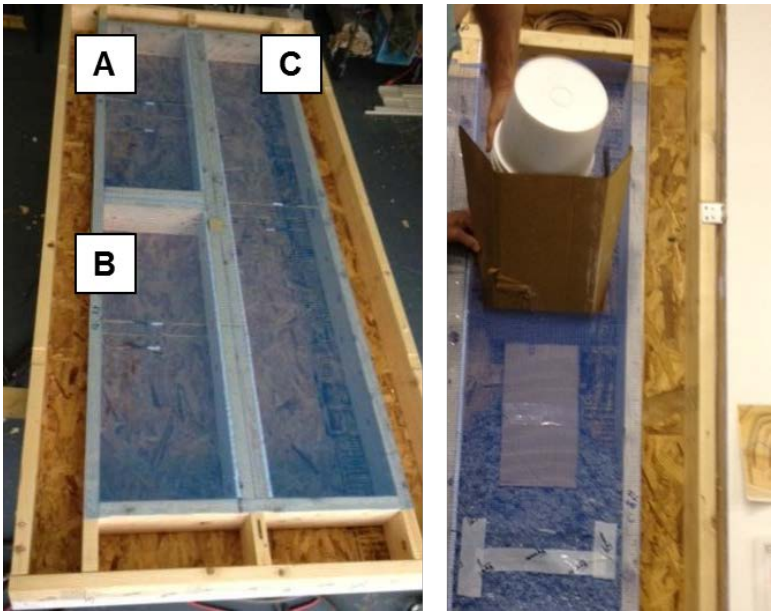

Figure 2. Original test wall frame (January 2012) (left) - (A) cellulose-only insulation, (B) cellulose-HDPE mix, (C) cellulose-PCM mix; Addition of PCM containing insulation to a wall cavity (right).

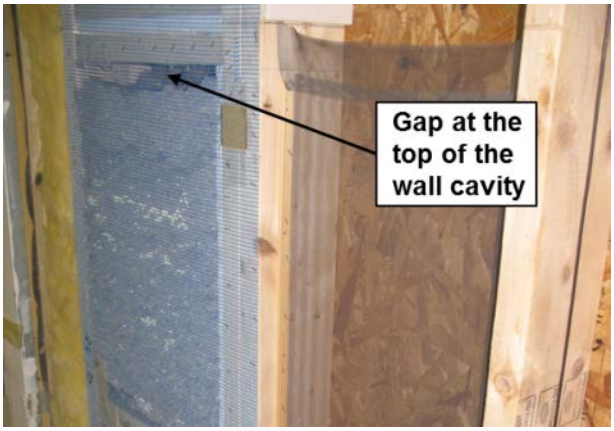

Figure 3. Gap at the top of a cavity.

The cellulose and PCM pellets, in the appropriate ratio, were mixed together in buckets. The wall cavities were loaded by filling insulation through slots cut in the retaining net, also shown in Figure 2, and allowing it to settle under gravity. It should be noted that, after filling, there was further settling of the cellulose insulation in the cavities, which resulted in about 2.5-3.8 cm (1- 1.5 inch) gaps at the top of the cavities with time. This phenomenon was noted when the wall was revisited in June 2012, as shown in Figure 3.

During June, the wall was modified by breaking the larger cavity into two smaller ones, so all the cavities had dimensions of 1.1 x 0.4 m^2 (42.4 x 14.5 square inch). Both the newer cavities contained PCM pellets;

however, in one cavity the pellets were mixed in the desired weight ratio with cellulose insulation, while the second one contained a sandwich structure. Figure 4 shows the cellulose-PCM-cellulose sandwich configuration used in one of the additional smaller wall cavities. The second new smaller cavity was filled with a cellulose-PCM mixture containing PCM with different phase change characteristics than the one used in the original cellulose-PCM mix used previously. The newer PCM pellets contained 66% paraffin by weight, which resulted in 30% pellets by weight in the cellulose-PCM mixture. The in-situ density of the newer cellulose-PCM mixture was 61.6 kg/m^3 (3.85 lb/ft^3). The density of the original cellulose-PCM used during the January installation is not available.

Once installed, the outer cavities of the test wall were filled with fiberglass insulation to thermally insulate the wall from the other neighboring test walls, as shown in Figure 5. Further, the gaps observed at the top of the cavities were filled with more cellulose insulation. Figure 6 shows the finished interior and exterior faces of the test wall. The interior side was covered with 1.3 cm (0.5 in) gypsum board and the exterior OSB was covered with a weather resistive barrier (0.15 mm thick high density polyethylene sheet) underneath vinyl siding. Also visible on the interior face are four (4) temperature sensors, one centered on each cavity, which are further described in the next section.

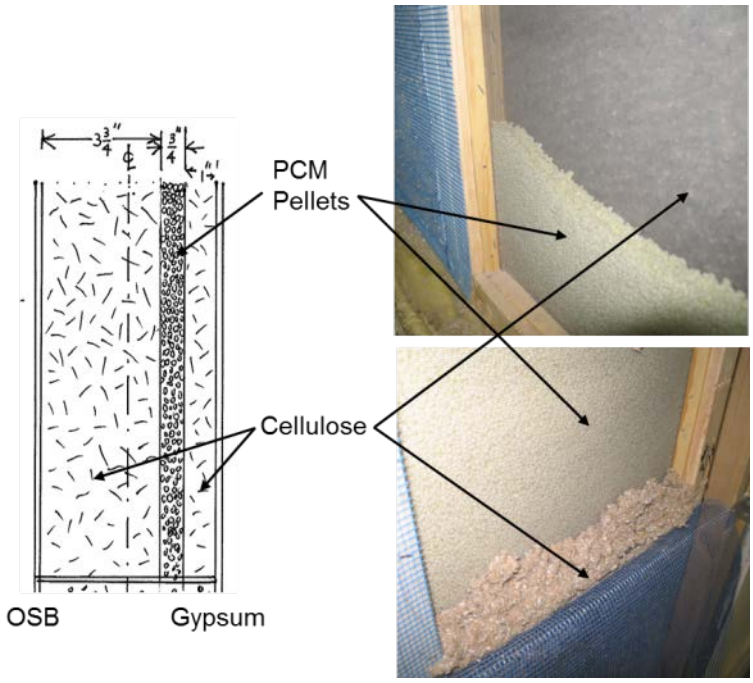

Figure 4. Cellulose-PCM sandwich structure.

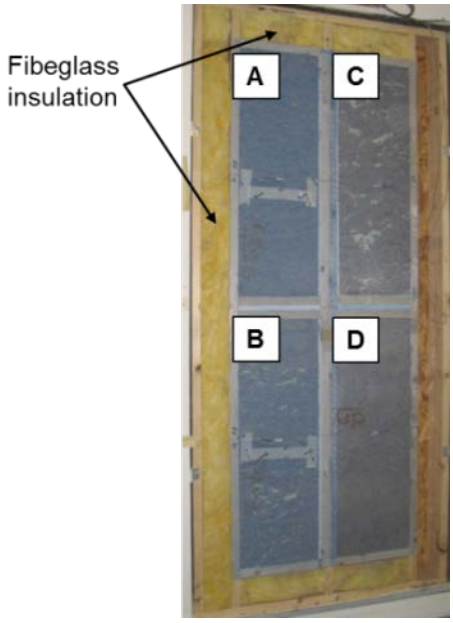

Figure 5. Modified test wall – (A) cellulose-only insulation, (B) cellulose-HDPE mix, (C) cellulose-PCM mix, and (D) cellulose-PCM-cellulose sandwich structure.

Figure 6. Finished interior (left) and exterior (right) sides of the test wall (June 2012).

3. DATA ACQUISITION SYSTEM AND INSTRUMENTATION

Figure 7 shows a typical instrumentation layout in the wall cavities. The wall contained vinyl siding and a weather barrier over OSB on the exterior side of the wall, which is exposed to the atmosphere (as seen on the south wall in Figure 1). The interior side is covered with a gypsum board. Each cavity contains a thermistor and RH sensor combination (T/RH sensor) on the OSB and gypsum surfaces facing the cavity, thermistor inside the cavity (mid-depth) and on the gypsum surface facing the room interior, and a heat flux transducers on the gypsum surface facing the cavity. Within each cavity, these sensors are located approximately in a line along both the vertical and horizontal midpoints of the cavity. In addition, a

single thermistor is attached to the wall exterior (interior face of the siding) and a T/RH sensor combination on the OSB surface facing the exterior, which are not shown in Figure 7. The T/RH sensor is indicated by the white packets seen in Figure 7.

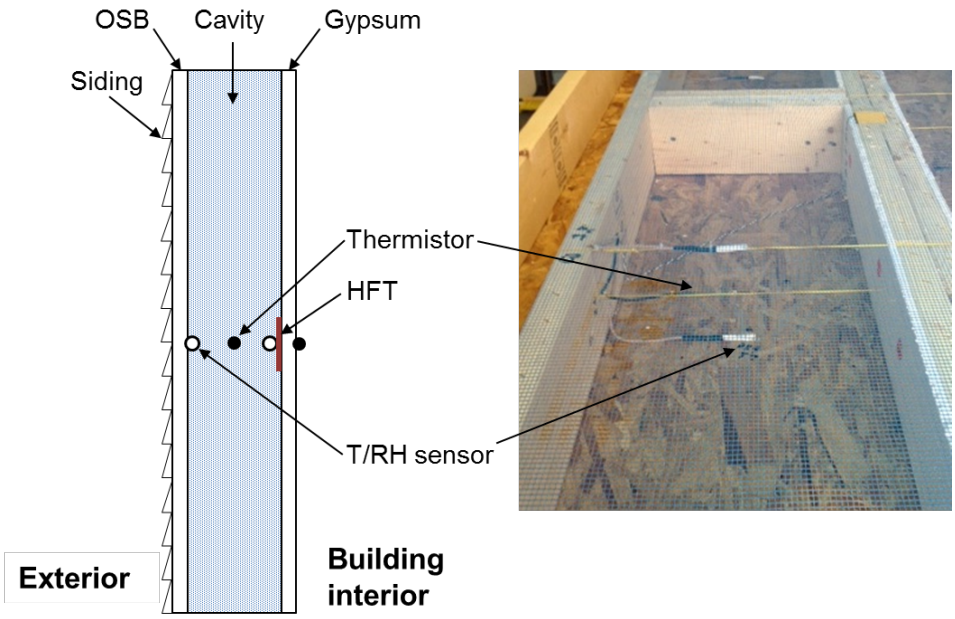

Figure 7. Sensor placement in test wall.

In addition to the sensors attached to the test wall, the NET facility includes sensors and instruments to monitor the local weather conditions, including temperature, humidity, solar irradiance, wind conditions, etc. These sensors are controlled and monitored by Campbell Scientific (CSI) CR10X dataloggers and multiplexers (http://www.campbellsci.com/cr10x). Each sensor is scanned at five minute intervals and the data are then averaged and stored at hourly intervals. The data are downloaded on a weekly basis at ORNL using a dedicated computer and modem. Table 1 provides the sensor list for the NET facility. Table 2 provides the sensor specifications.

Table 1. Charleston NET facility sensor list.

Sensor	Location	Number
Outdoor temperature	Top of building exterior	1
Outdoor RH	Top of building exterior	1
Solar horizontal	Top of building exterior	1
Solar vertical	South center building exterior	1
Wind speed	Top of building exterior	1
Wind direction	Top of building exterior	1

Rainfall horizontal	Top of building exterior	1
Rainfall vertical south 1	South wall center	1
Rainfall vertical south 2	South wall east	1
Rainfall vertical north	North wall east	1
Indoor temperature Rm. 1	Room 1 high and low	2
Indoor RH Rm. 1	Room 1 high and low	2
Indoor temperature Rm. 2	Room 2 high and low	2
Indoor RH Rm. 2	Room 2 high and low	2
Test wall panel thermistors	17 per wall, 18 walls	306
Test wall panel RH sensors	6 per wall, 18 walls	108
Test wall panel moisture pin sets	8 per wall, 18 walls	144

Table 2. Installed sensor accuracy.

Sensor	Accuracy	Sensitivity	Repeatability	Supply Voltage
Fenwall Uni-curve 10K ohm thermistor	± 0.2%	-	± 0.2%	2.5Vdc
Honeywell Hy-Cal Humidity Sensor *HIH-4000 Series*	± 3.5%	-	± 0.5%	5Vdc
Heat Flux Transducer (Concept Engineering Model F-002-4)	± 5%	$(5.7\ W/m^2)/mV$ / $[(1.8\ Btu/hr\text{-}ft^2)/mV]$	-	-
Outdoor RH (Vaisala CS500)	± 3%	-	-	12Vdc
Wind Speed (R. M. Young Model 05305 Wind Monitor)	± 0.4%	-	-	-
Wind Direction (R. M. Young Model 05305 Wind Monitor)	± 3°	-	-	12Vdc
Rainfall (Texas Electronics Model TE525)	± 1% @ 1"/hr	-	-	-
Solar pyranometer, vertical (LI-Cor LI200X	± 3%	$0.2 \cdot kW \cdot m^{-2} \cdot mV^{-1}$	-	-
Solar pyranometer, horizontal (Kipp & Zonen SP-Lite	± 3%	$10\mu V \cdot W^{-1} \cdot m^{-2}$	-	-
Campbell Sci CR10X w/32 Channel multiplexer	± 0.1% of FSR**	-	-	12Vdc

*MC – Moisture content, **FSR – Full scale reading

4. RESULTS AND DISCUSSION

4.1. Field Data Analysis

This section shows some sample temperature, humidity and heat flux data, with the focus on some key findings. As mentioned earlier, all sensor data have been provided to the sponsor for further detailed analysis and modeling. The intent of this report is not to investigate the overall energy savings, but to examine how the PCM impacts the test wall based on the field data. For the sake of analysis, the monitoring period has been divided into two phases. Phase 1 defines the period before the wall modification took place, from January to June 2012, and phase 2 is the period after June 2012. The data monitoring started around January 18, 2012, and since then they have been compiled into weekly files containing hourly data.

Temperature and Heat Flux

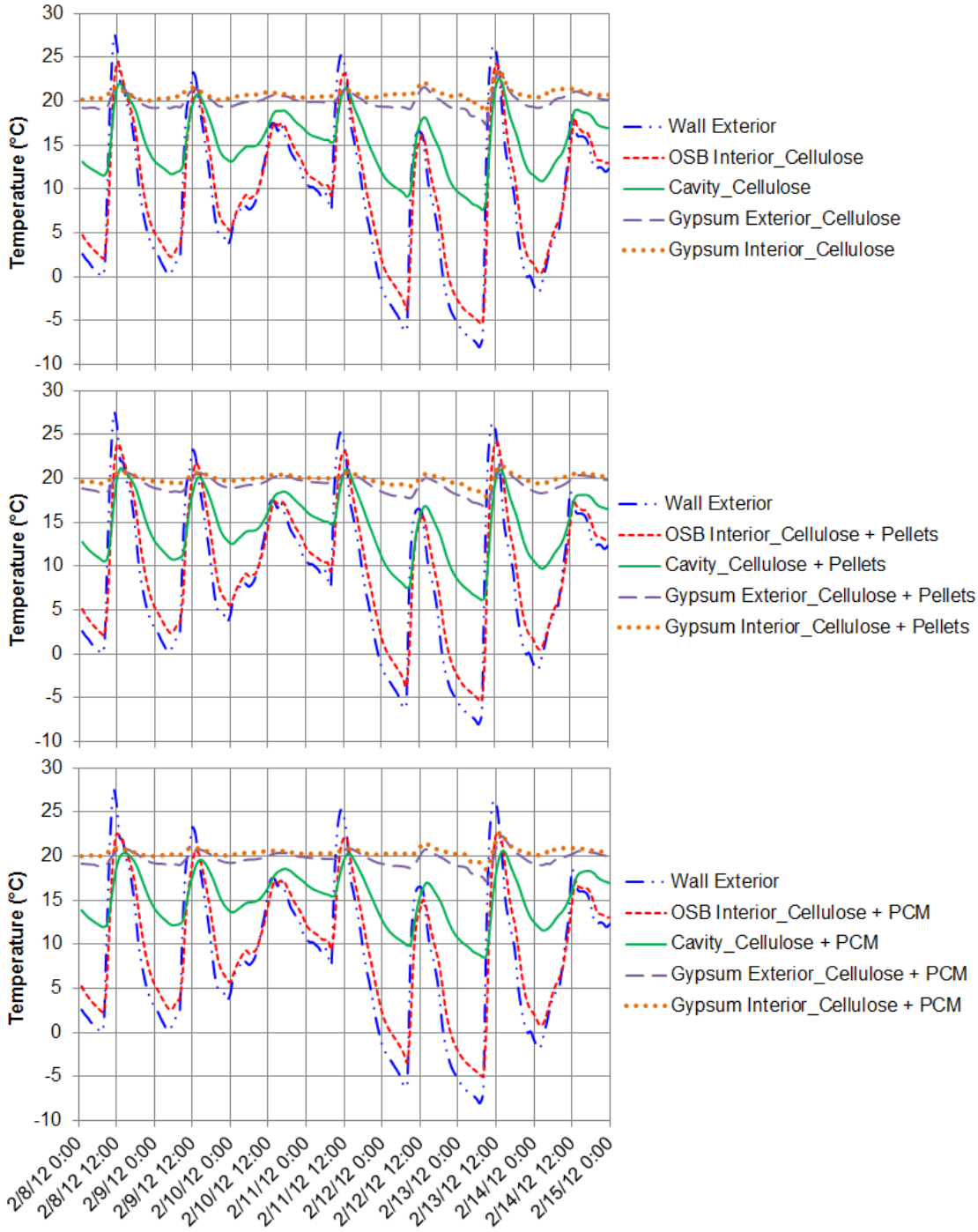

Figure 8. Temperature variations within different wall sections during a phase 1 winter week.

Figure 8 shows the temperature distribution across the wall depth or thickness within the different wall sections ('Cellulose', 'Cellulose + Pellets' and 'Cellulose + PCM') during a winter week in phase 1. This week was chosen since it saw the coldest outside air temperatures during the phase 1 evaluation period. The sensor descriptions are based on their locations within the test wall. 'Interior' refers to any surface faced towards the building interior and 'Exterior' indicates any surface facing outside to the building exterior. In Figure 8, the 'Wall Exterior' is the thermistor located under the outer vinyl siding, 'OSB

Interior' is the thermistor (T/RH combination) on the OSB surface facing the cavity, 'Cavity' is the thermistor installed in the cavity center along its depth, 'Gypsum Exterior' is the thermistor (T/RH combination) facing the cavity (or building exterior), and 'Gypsum Interior' is the thermistor facing the building interior.

As seen in Figure 8, the outer- and innermost surface temperatures were very similar for the different wall sections. Within the cavities, some differences were observed. To further illustrate these differences, the cavity center temperatures from all sections were plotted together and are shown in Figure 9. The data indicate that the cellulose-PCM section showed the least temperature fluctuations in the cavity center.

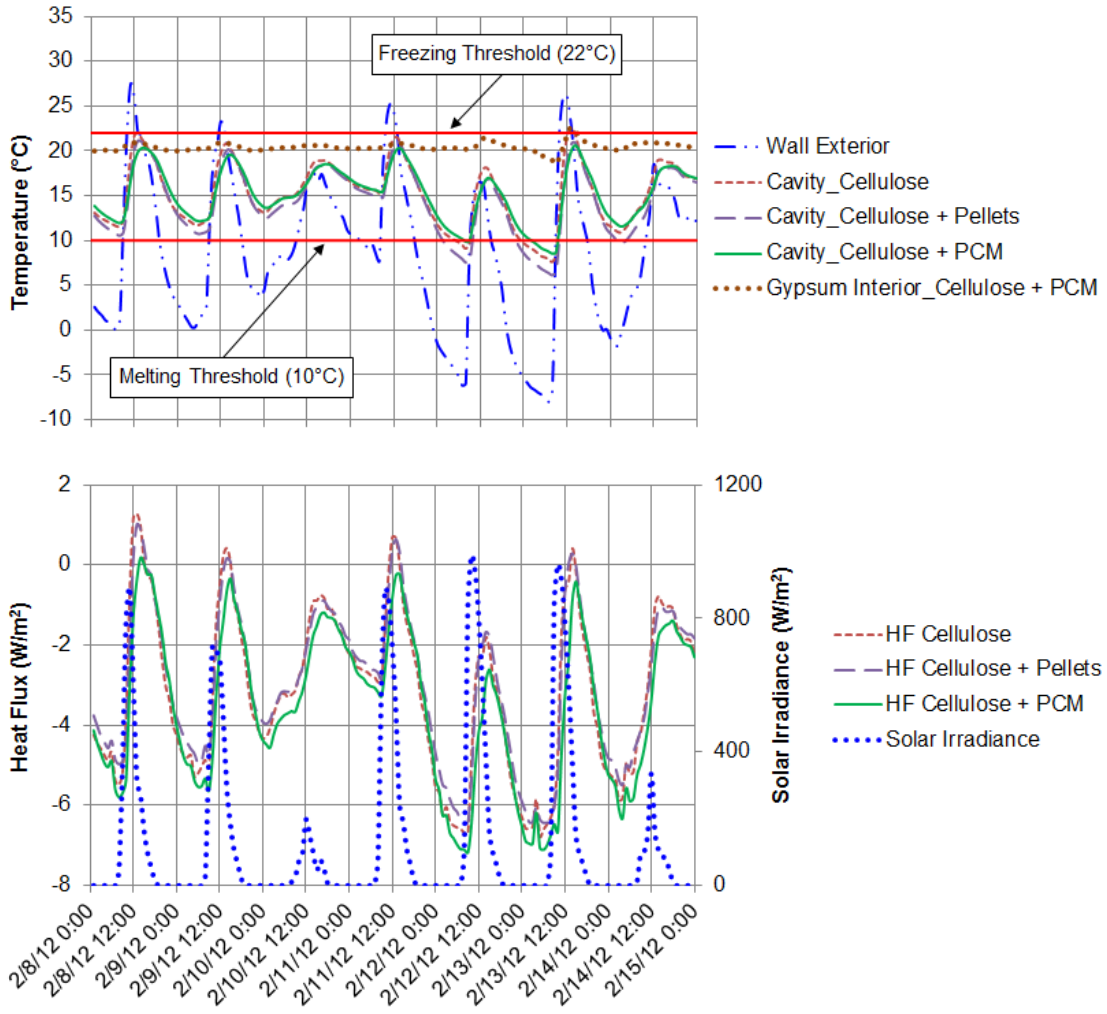

Figure 9. Temperature and heat flux variation for a week during the phase 1 winter period.

To examine whether any phase change was occurring in the PCM section, the threshold temperatures for initiation of melting and freezing have also been included. Melting threshold is the temperature at which the fully frozen PCM will start melting, and at freezing threshold a fully molten PCM will start freezing. The PCM phase change data were obtained using differential scanning calorimetry (DSC) in which the PCM sample were heated or cooled at 1°C per minute. Further, the DSC measurements revealed that, during heating, the PCM was fully melted at about 38°C. Thus, even during the coldest weather, the PCM was expected to undergo phase change as the PCM cavity and gypsum interior temperatures were always within the phase change temperature range. It should be noted, however, that the DSC heating/cooling rate of 1°C per minute is too high for characterizing PCMs for building applications as

the temperature changes in real building envelopes occur at a much slower rate. A different heating/cooling rate can appreciably alter the observed melting and freezing temperature thresholds and ranges [3].

Figure 9 also shows the heat flux variations through the different sections and the south wall solar irradiance (right axis). The heat flux transducers (HFTs) are attached to the exterior surface of the gypsum board (facing the cavity). The sign convention of heat flux is such that heat flow through the gypsum board into the building interior (heat gain) is positive, while heat flow out of the building into the wall cavities (heat loss) is negative. As expected during winter, the heat flow was predominantly out of the building. There was a strong correlation between the daytime heat flux and the solar irradiance. The PCM section showed almost no heat gain during the day and the highest heat loss at night, indicating a negative energy impact during this winter week. The heat fluxes through the 'Cellulose + Pellets' and 'Cellulose' sections were very similar.

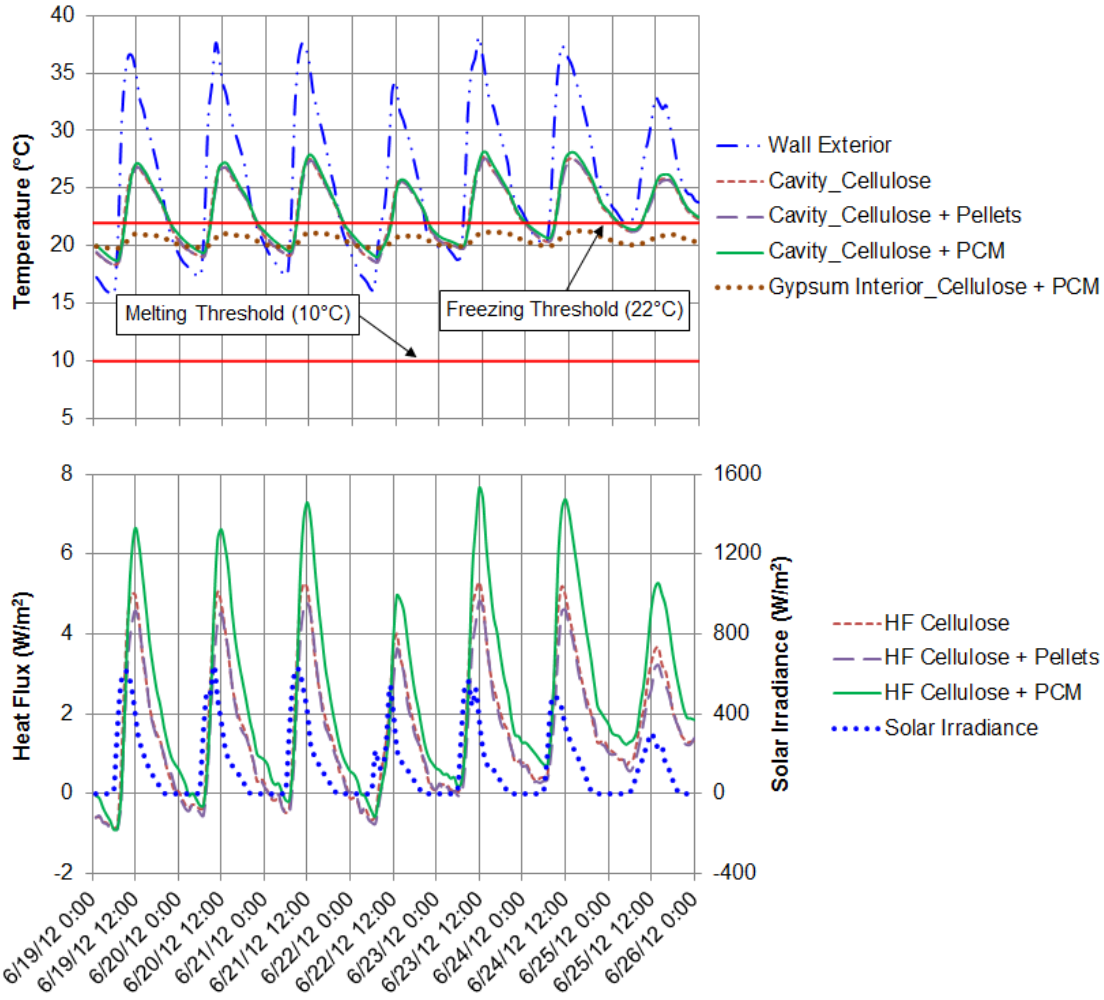

Figure 10. Temperature and heat flux variation for a week during the phase 1 summer period.

Figure 10 shows the cavity center and heat flux comparisons during a phase summer week, with the hottest ambient conditions during phase 1. There were no discernible differences between the cavity

center temperatures of the different sections. The cavity center temperatures indicated that the PCM may not be freezing during this period. The heat flux data showed substantially higher heat gains through the cellulose-PCM section, again indicating a negative energy impact compared to cellulose-only insulation. Interestingly, the cellulose-pellets section allowed the lowest peak heat gains.

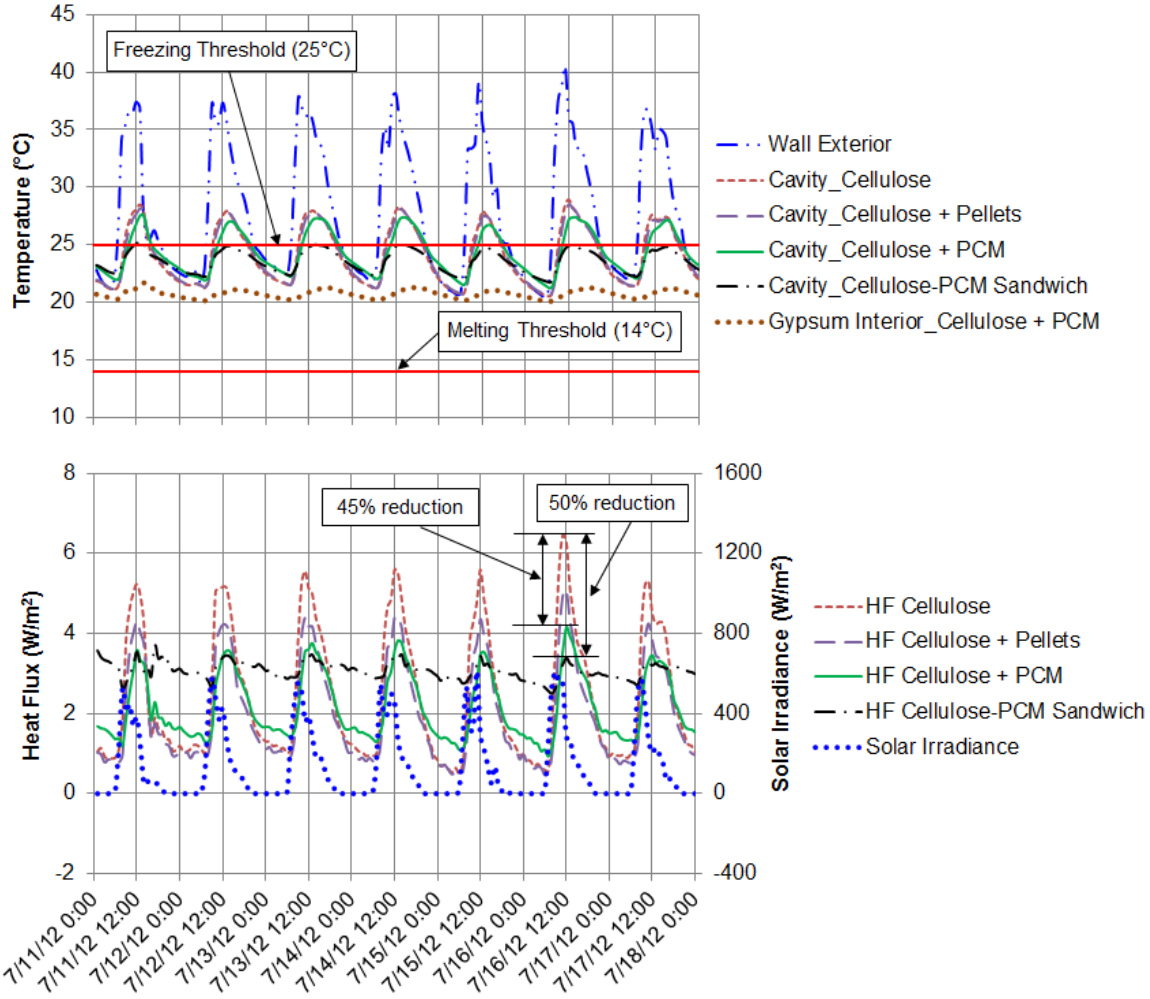

Figure 11. Temperature and heat flux variation for a week during the phase 2 summer period.

On June 27, 2012, the test wall was modified to test another PCM with different phase change characteristics, higher melting and freezing thresholds than the phase 1 PCM. Figure 11 shows the temperature and heat flux data from the four sections during a summer week, when the hottest ambient conditions for the phase 2 period were observed. Again, the cavity center temperatures are relatively high, but with a higher freezing threshold, some phase change can be expected in the cellulose-PCM cavity. The cellulose-PCM sandwich section showed the least fluctuations in the cavity center temperature. With the new PCM, there was a substantial reduction in the peak heat gains, up to 45 and 50% in the cellulose-PCM and cellulose-PCM sandwich sections, respectively, compared to the cellulose-only section. The heat flows were always into the building for all sections, but cellulose and cellulose-pellet sections had lower heat gains during the nights. This indicates some cooling energy penalty for the PCM containing sections, especially the cellulose-PCM sandwich section.

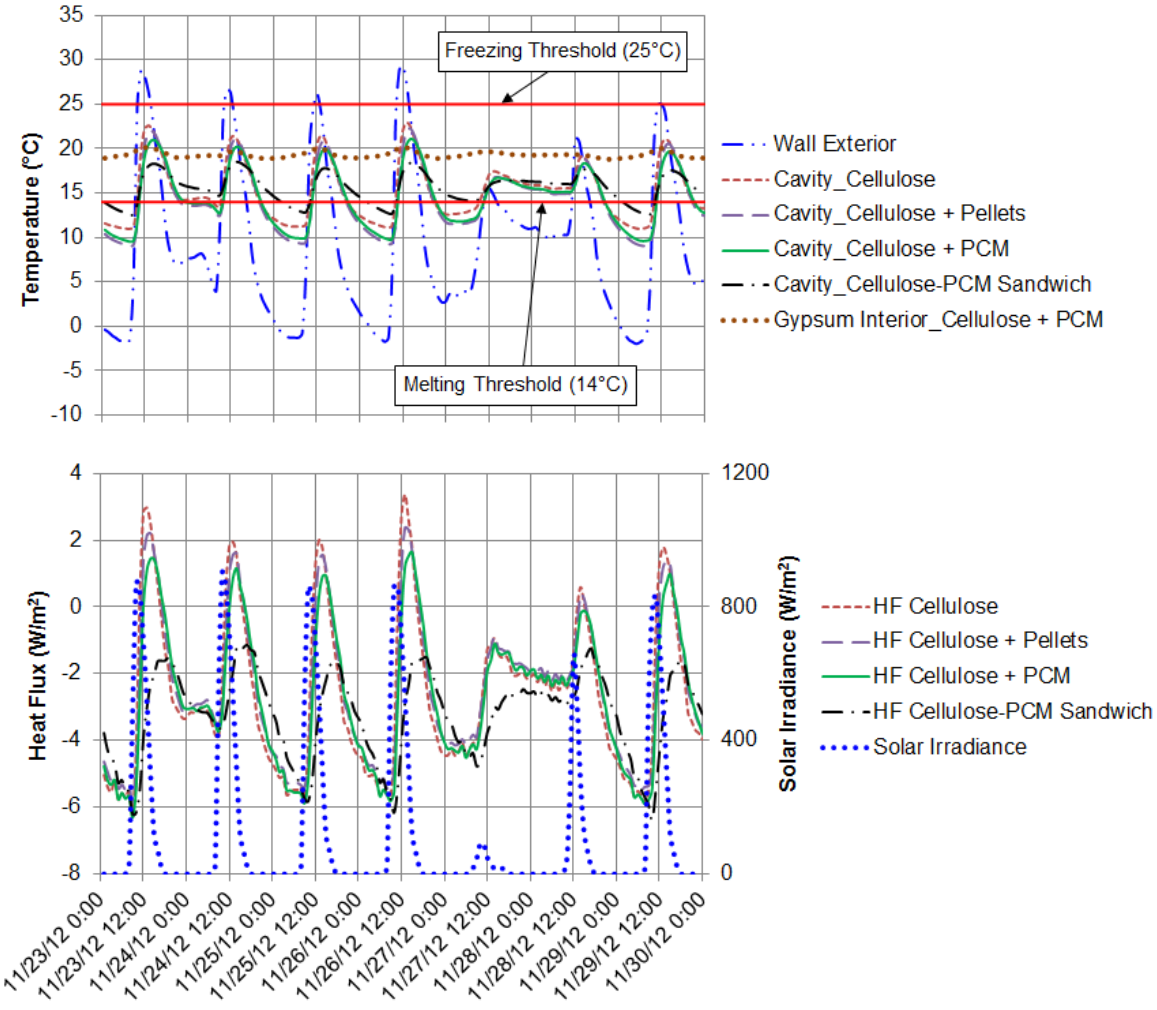

Figure 12. Temperature and heat flux variation for a week during the phase 2 winter period.

Figure 12 shows the temperatures and heat fluxes during a winter week of phase 2. During the week of November 23-30, 2012, the coldest weather for phase 2 was observed. The heat flows were primarily out of the building during this week. There was some daytime heat gain through all sections, except the cellulose-PCM sandwich section. The nighttime losses were similar through all sections. The lower daytime heat gains through the cellulose-PCM section and no heat gains at all through the cellulose-PCM sandwich section indicate heating penalties compared to cellulose-only insulation. It is noted that the coldest period of winter could still be forthcoming and the data collection till end of December will allow better winter performance analysis for the current PCM.

To further investigate the impact of the PCM wall sections, the heat flux data were integrated over 30-day winter and summer periods to determine the total heat gains and losses through the different sections. The integration was performed by a simple application of the trapezoidal rule:

$$Total\ Integrated\ Heat\ Flow\ [\frac{kJ}{m^2}] = \sum_{n=0}^{m} .5 * \Delta X_n * (Y_n + Y_{n+1}) \qquad (1)$$

Where Y_n and Y_{n+1} correspond to the current and future time step, ΔX_n is the time step (one hour in this case), and the subscript m denotes the final point in the series which varies depending on the summer or winter data sets. Keep in mind that this integration represents a summation of the area under the curve of the heat flux. The positive and negative heat fluxes were integrated separately to determine the heat gains and losses for each section. The integrated or total heat gains and losses and the net heat transfer during phase 1 (January – June, 2012) are shown in Table 3 and during phase 2 (June – December, 2012) in

Table 4. The net heat transfer for each period was obtained by integrating the positive and negative heat fluxes together. Also shown in Table 3 and

Table 4 are the percent reductions with respect to the section with only cellulose insulation. The periods considered are listed in the tables, and these were selected based on maximum and minimum 30-day average outside temperatures for the corresponding summer and winter periods, respectively.

During phase 1, the cellulose-PCM section showed a substantial reduction in the heat gained during the winter 30-day period, but showed an increase in the heat lost. Overall, the net transfer was negative for all sections, but the PCM section showed higher losses. During summer, the PCM section showed a large increase in the net heat gain compared to the cellulose-only section. Thus, for the ambient and building conditions, the PCM used during phase 1 had negative energy impacts during both the heating and cooling seasons. The cellulose-pellet section resulted in reduced net heat transfers during both the heating and cooling seasons, compared to the cellulose-only section.

Table 3. Integrated heat flow into and out of the conditioned space through the different cavities during Jan-Jun, 2012.

Cavity	Heat Gain (kJ/m^2)	% Reduction	Heat Loss (kJ/m^2)	% Reduction	Net (kJ/m^2)	% Reduction
Winter 30-day period (Phase 1) (Jan 28 - Feb 26, 2012)						
Cellulose	482.26		-5675.54		-5193.29	
Cellulose + Pellets	387.89	19.57	-5353.36	5.68	-4965.47	4.39
Cellulose + PCM	270.77	43.85	-6180.60	-8.90	-5909.83	-13.80
Summer 30-day period (Phase 1) (May 27 - Jun 25, 2012)						
Cellulose	3635.75		-249.16		3386.59	
Cellulose + Pellets	3265.68	10.18	-262.77	-5.46	3002.91	11.33
Cellulose + PCM	5153.54	-41.75	-171.73	31.07	4981.80	-47.10

During the phase 2 summer period, the cellulose-PCM section reduced the heat gains compared to the cellulose-only section by 12%. While the cellulose-PCM sandwich section was very effective in reducing the peak heat gains (Figure 11), it allowed higher total heat gain compared to the cellulose-only section. During the winter period, the cellulose-PCM section reduced the total heat loss by 4.28%, but also reduced the heat gains by almost 50% compared to the cellulose-only section. The heating penalty due to reduced daytime gains is reflected by a small increase (1.69%) in the net heat loss through the cellulose-PCM compared to the cellulose-only section. The cellulose-PCM sandwich section performed poorly during the winter period, with almost 25% higher total heat loss compared to the cellulose-only section.

With the added thermal mass, the cellulose-pellets section actually performed better than all other wall sections by reducing both heat gains and losses during the summer and winter periods.

Table 4. Integrated heat flow into and out of the conditioned space through the different cavities during Jun-Dec, 2012.

Cavity	Heat Gain (kJ/m^2)	% Reduction	Heat Loss (kJ/m^2)	% Reduction	Net (kJ/m^2)	% Reduction
Summer 30-day period (Phase 2) (Jun 29 - Jul 28, 2012)						
Cellulose	7068.52		0.00		7068.52	
Cellulose + Pellets	5744.47	18.73	0.00		5744.47	18.73
Cellulose + PCM	6218.95	12.02	0.00		6218.95	12.02
Cellulose-PCM Sandwich	8438.94	-19.39	0.00		8438.94	-19.39
Winter 30-day period (Phase 2) (Nov 1 - 30, 2012)						
Cellulose	708.58		-5997.34		-5288.76	
Cellulose + Pellets	535.09	24.48	-5539.69	7.63	-5004.59	5.37
Cellulose + PCM	361.96	48.92	-5740.36	4.28	-5378.40	-1.69
Cellulose-PCM Sandwich	23.22	96.72	-6613.95	-10.28	-6590.73	-24.62

It should be noted that the heat fluxes were local, center-of-cavity values and did not necessarily reflect the energy-savings impact, or lack thereof, of the PCM-enhanced cellulose insulation. Also, the settling of insulation and the stratification of the PCM-containing HDPE pellets added further uncertainty to the local heat flux data (as explained below). It should also be noted that, during phase 1, the cellulose-PCM cavity spanned the entire height of the wall, while the cellulose-only and cellulose-HPDE mix sections were less than half the wall height. There is a potential for uneven settling and density differences in the wall sections, which could potentially impact the heat flows through the center of each section. The local heat flux data are not sufficient to accurately determine the energy-saving impact of the tested PCMs. Detailed energy modeling is required that captures all the building envelope features and indoor and ambient conditions to calculate the annual energy usage to estimate the energy benefits of the cellulose-PCM insulation.

Finally, one source of uncertainties in the measurements needs to be acknowledged. The cellulose-PCM and cellulose-pellets mixing and loading method was such that it was difficult to obtain a uniform distribution of the PCM pellets within the cellulose insulation. Figure 13 shows how the PCM pellets were concentrated in certain regions within the cavities. How the PCM pellets were distributed with respected to the sensors can have an impact on the sensor readings. Figure 14 shows the temperatures measured by three thermistors located mid-depth in the cellulose-PCM cavity along the vertical centerline. The measured temperatures varied by about 5°C (9ºF). depending on the location. Such variability in distribution could also impact the measured heat flows through the sections containing PCM pellets.

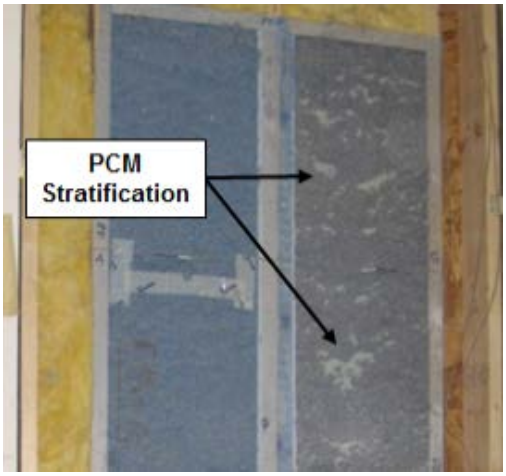

Figure 13. PCM stratification in the cellulose-PCM mixture.

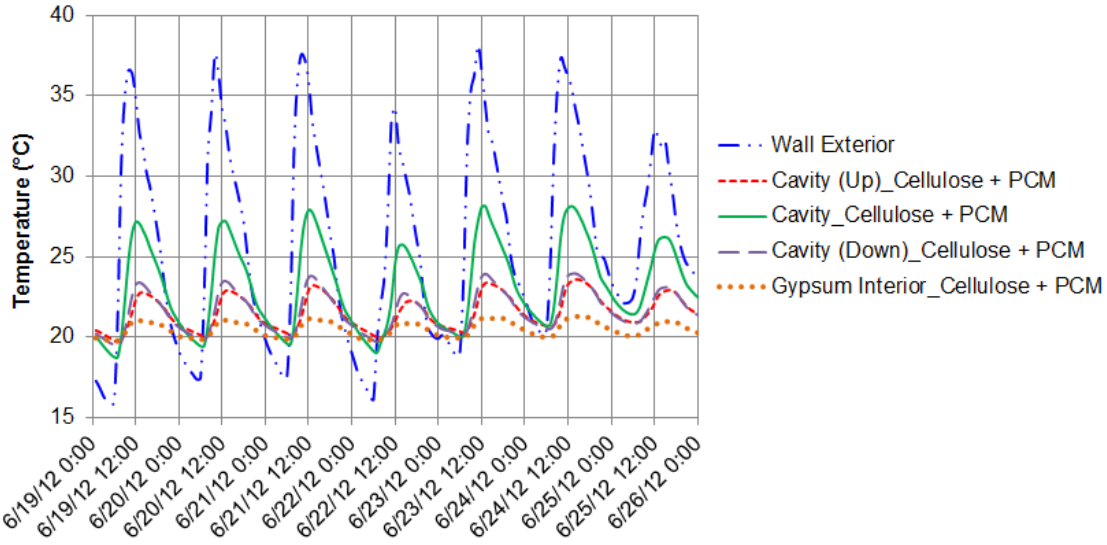

Figure 14. Temperature variation within the PCM containing cavity during phase 1; 'Up' and 'Down' represent locations about 45.7 cm (18 inch) above and below the vertical mid-point of the cavity, and at the centerline along the cavity depth.

Relative Humidity

ASHRAE standard 160 [2] lists the following criteria for minimizing mold growth on the surfaces of building envelope components:

- 30-day running average surface RH < 80% when the 30-day running average surface temperature is between 5°C (41°F) and 37.8°C (100°F)
- 7-day running average surface RH < 98% when the 7-day running average surface temperature is between 5°C (41°F) and 37.8°C (100°F)
- 24-hour running average surface RH < 100% when the 24-hour running average surface temperature is between 5°C (41°F) and 37.8°C (100°F)

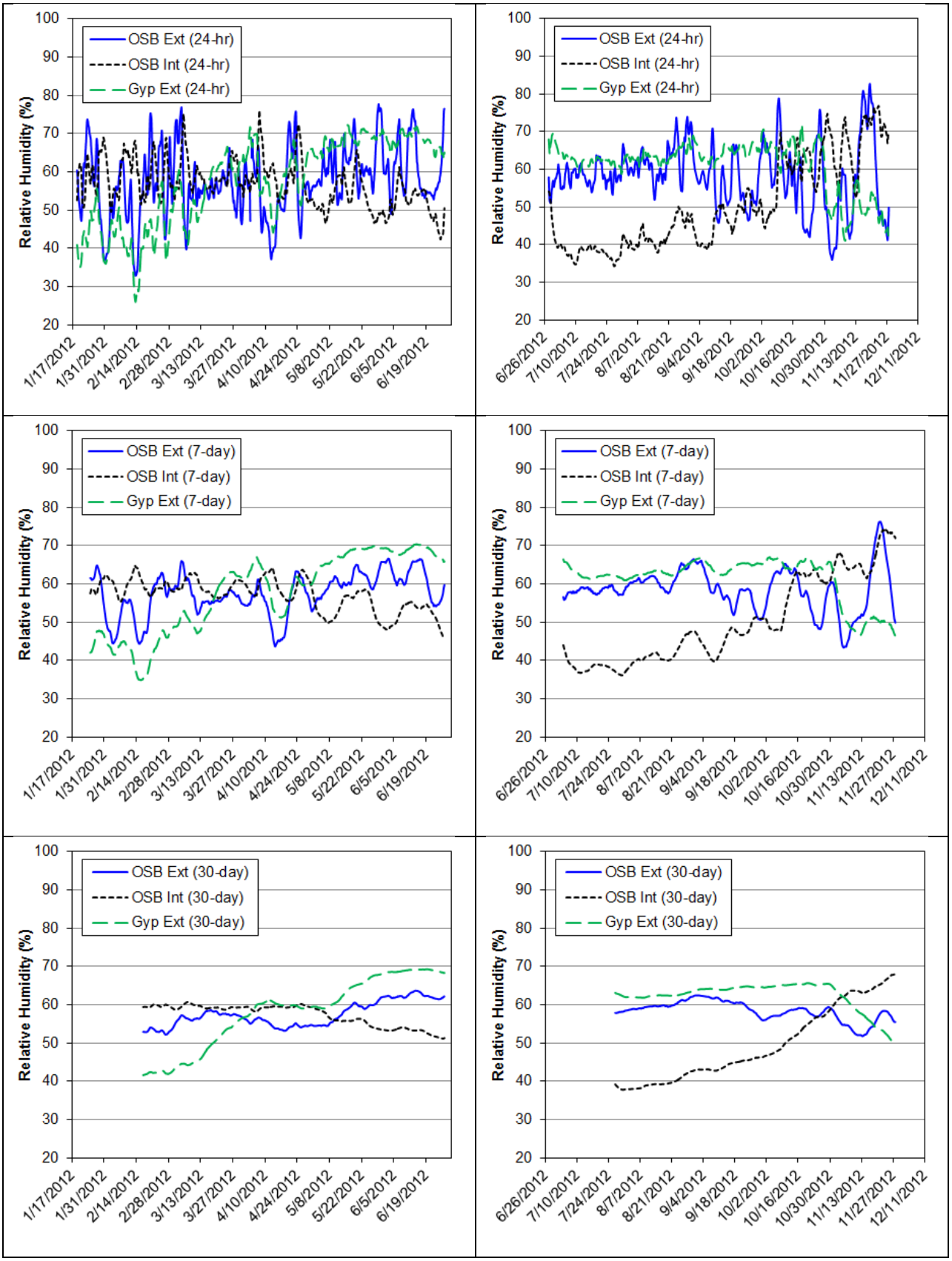

Figure 15. Running averages of relative humidity in different locations on the test wall.

Figure 15 shows the 24-hour, 7-day and 30-day running averages of the surface relative humidity at different locations within the test wall. Each cavity contained a pair of RH sensors, one on the interior face of the OSB ('OSB Int') and the exterior face of the gypsum board ('Gyp Ext'). However, the measurements were nearly identical for the corresponding locations within each cavity. Therefore, for the sake of clarity, only one pair of OSB interior and gypsum exterior RH measurements is shown. The surface temperatures were usually within the 5-37.8°C range, or lower (which would mean lower specific humidity and moisture content). It is evident from Figure 15 that none of the surfaces were ever close to the conditions needed for mold growth.

4.2. Thermal Conductivity Measurements

At the request of the sponsor, in addition to the field test, small test boxes were built and filled with cellulose insulation with and without PCM pellets to test in a heat flow meter apparatus (HFMA) (http://www.lasercomp.com/product/fox6xx.php) according to ASTM C 518 standard test method [4]. A brief description of the HFMA is provided here. The apparatus consists of two plates, upper and lower, which sandwich the test specimen. Each plate is outfitted with solid state heating/cooling systems, and the two specimen surface temperatures can be independently controlled to induce heat flow in either upward or downward direction through the specimen. Thin film heat flux transducers (HFTs) are permanently bonded to the upper and lower plate surfaces. The HFTs are of integrating type, with a 20.3 x 20.3 cm^2 (8 x 8 $inch^2$) active area in the center of each plate. In the center of the each transducer, a thermocouple is bonded near its surface, close to the test specimen. These thermocouples accurately measure the specimen surface temperatures and are also used to control the plate temperatures. Figure 16 shows the apparatus used for the thermal conductivity measurements.

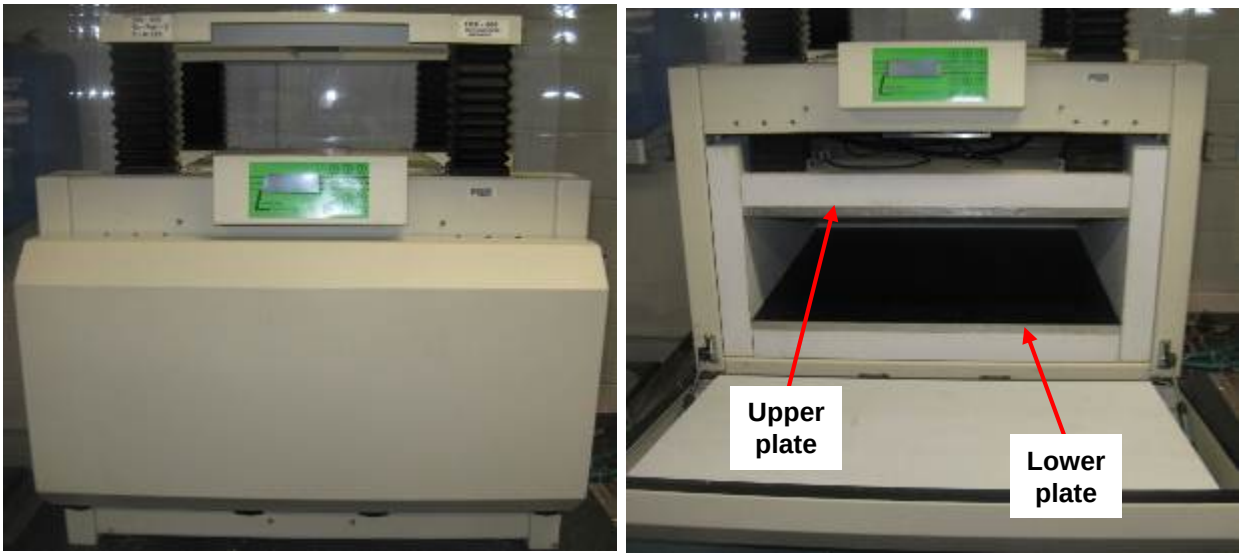

Figure 16. Heat flow meter apparatus.

During tests, a set of data is taken once every 0.7 seconds. Each set of data includes the upper and lower plate temperatures and heat flux transducer outputs. 512 consecutive sets of data are organized in one block and are averaged to yield the mean plate temperatures and heat fluxes. The following three equilibrium criteria were used to determine the completion of the tests:

1. Temperature equilibrium: The block average temperature of each plate must be within 0.2ºC of the previous block.
2. Semi-equilibrium: The average heat flux transducer output of a block must be within 70 microvolts (μV) of the previous block's average.
3. Percent-equilibrium: The average block heat flux transducer output of a block must be within a 2% of the previous block's average.

An additional criterion for test completion is the absence of any monotonic trends in the test data. Once a certain number of consecutive blocks, minimum of 30 for the present tests, satisfied all equilibrium criteria, the test for a given temperature set point is completed. With the measured sample thickness, upper and lower plate temperatures and heat fluxes, the thermal conductivity of the test specimen can be calculated. For calculating the result, the last 5 blocks out of the consecutive blocks that satisfied the equilibrium criteria were used.

Figure 17 shows the test box that was filled with cellulose mixed with 20% by weight PCM (phase 1). The cellulose and PCM were from the same batches that were used in the Charleston test wall. The filling mixing and filling mechanism was also the same as the Charleston test walls. The interior box dimensions were 55.9 x 56.5 x 14.0 cm^3 (22 x 22.3 x 5.5 $inch^3$) and the resulting density of the cellulose-PCM mix was 56.6 kg/m^3 (3.5 lb/ft^3) after filling. The test box contained an OSB on one side and a net on the other, to contain the insulation. This box was tested twice, once after two days and then after another month. During this time, the test box was placed in an un-insulated test attic at ORNL to allow the PCM to undergo several phase change cycles. Before both tests, it was observed that the top of the test box showed a gap due to settling of the insulation, similar to the Charleston test wall. It needed to be filled with insulation to prevent convection cells forming in the air gap while being tested in the HFMA. With the added insulation, the resulting densities were 62.5 kg/m^3 (3.9 lb/ft^3) and 70.4 kg/m^3 (4.4 lb/ft^3). The test box was tested with the OSB resting on the lower plate.

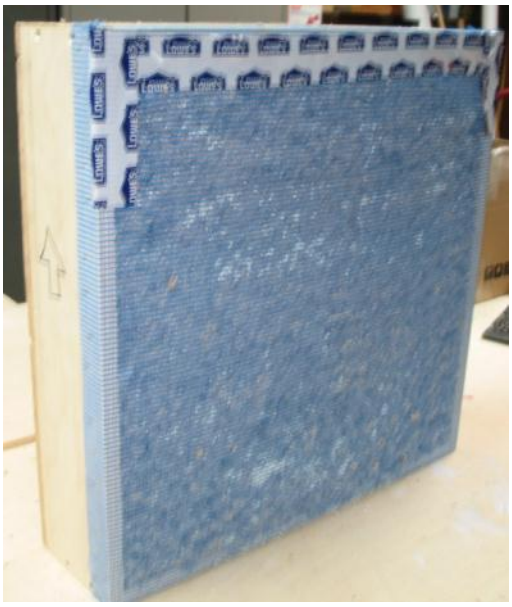

Figure 17. Test box used for the thermal conductivity measurements.

For reference, a second test box was built and filled with only cellulose insulation. The box cavity dimensions were 55.6 x 55.6 x 14.0 cm^3 (21.9 x 21.9 x 5.5 $inch^3$) and the filled density of cellulose was 42.4 kg/m^3 (1.5 lb/ft^3). The test box samples were tested at two different sets of HFMA plate temperatures, 0 and 15°C and 40 and 55°C. Given the temperature limits of the HFMA, the temperatures were chosen so that they were above and below the PCM phase change temperature range to the extent possible. Table 5 summarizes the measured thermal conductivities of the test boxes. The 'unaged' PCM refers to the test conducted 2 days after preparing the sample and 'aged' refers to the test conducted after 30-plus days.

Table 5. Summary of thermal conductivity measurements.

	Upper Temp (ºC)	Lower Temp (ºC)	Mean Temp (ºC)	Upper Cond (W/mK)	Lower Cond (W/mK)	Average Cond (W/mK)
Cellulose only	0.01	15.01	7.51	0.04416	0.03576	0.03996
	40.02	55.02	47.52	0.04796	0.04979	0.04887
Unaged PCM + Cellulose	0.01	15.01	7.51	0.04827	0.03122	0.03974
	40.02	55.02	47.52	0.04715	0.05782	0.05248
Aged PCM + Cellulose	0.01	15.01	7.51	0.04734	0.04091	0.04413
	40.03	55.02	47.52	0.04552	0.05824	0.05188

As indicated by the difference in the upper and lower conductivities (determined using the HFTs in the upper and lower plates, respectively), especially at the lower temperature range, there were two-dimensional heat transfer effects present (i.e. edge losses through the framing of the test boxes). There are additional uncertainties in the test data due to the settling of cellulose and stratification of the PCM in the box with the PCM-cellulose mix. According to the HFMA specifications, the instrument has an accuracy better than 1%, with 0.2% repeatability and 0.5% reproducibility. The tests were set to continue for a minimum number of 30 block (~180 minutes) once all equilibrium criteria were met, with the final 5 blocks used for calculating the thermal conductivities. The PCM-cellulose tests ran for a minimum of 16 hours, while the cellulose-only tests ran for a minimum of 8 hours.

5. SUMMARY

A field test of a low-cost PCM is currently ongoing in a natural exposure test facility in Charleston, SC. Temperature and heat flow data from the test wall sections with different combinations of cellulose-PCM-HDPE pellets were analyzed and the main findings are presented in this report. The PCM installed in the test walls showed potential for energy savings, compared to conventional cellulose insulation. The data have been provided to the sponsor for further analysis and energy modeling, which are needed to quantify the actual energy savings with the PCM-enhanced insulation for different building and climate types. Interestingly, the addition of HDPE pellets (without PCM) also showed improved thermal performance compared to cellulose-only insulation.

6. REFERENCES

1. Kosny, J., Yarbrough, D. W., Miller, W. A., 2007. “Use of PCM Enhanced Insulation in the Building Envelope,” Oak Ridge National Laboratory, Oak Ridge, TN.

2. ANSI/ASHRAE Standard 160-2009, Criteria for Moisture-Control Design Analysis in Buildings, 2009.

3. Kosny, J., Biswas, K., Miller, W., Kriner, S., 2012. “Field Thermal Performance of Naturally Ventilated Solar Roof with PCM Heat Sink,” Solar Energy, v 86, n 9, p 2504-2514.

4. ASTM C518-04: Standard Test Method for Steady-State Thermal Transmission Properties by Means of the Heat Flow Meter Apparatus.

A2. Franunhofer Report - Evaluation

Dynamic Phase-Change Property Characterization of Synpar

In this project, we characterized phase change properties of following three physical forms of Syntroleum PCM product called Synpar:

1) Dusted pellets – a fine powder of calcium silicate is sprinkled with the pellets to improve the flowability of the pellets
2) Undusted pellets – pellets without addition of any powder
3) Sheet – Synpar rolled in thin sheets of ~1 mm thickness

Following two measurement methods were employed for property determination:

1) Differential Scanning Calorimeter (DSC)

Majority of characterization carried out in this project has been conducted on dusted Synpar PCM and unless otherwise stated, dusted PCM will be referred to as Synpar. DSC tests have been performed using two different modes: ramp and step methods. In ramp method, sample is subjected to a constant heating or cooling rate, and heat flow through the sample is measured. It is important to note that due to finite thermal mass of the sample, thermal response of the DSC may lag behind the ramp input, resulting in a ramp rate dependent heat capacity data. In step method, sample temperature is changed in increments or steps, and heat flow during the step change is measured. Step method gives very accurate measurement of PCM enthalpy as a function of temperature, provided that sufficient time is given during each temperature step change ensuring negligible head flow at the end of the of each measurement.

2) Dynamic Heat Flow Meter Apparatus (DHFMA)

DHFMA follows the same principle as the step method but is applicable for large-scale samples such as building components. DHFMA test method utilizes temperature and heat flux information from a conventional HFMA to determine the dynamic thermal properties of PCM-enhanced components.

Results

Small samples of 20-30 g were prepared for DSC measurement. Figure 1 shows DSC results on Synpar sample during melting phase-change. Ramp rates of 0.2, 1, 5 and 10°C/min were used. We observe that the enthalpy curve shifts to left and approaches closer to the step method results as the ramp rate is slowed. Results for ramp of 0.2°C/min is found to be close to the step mode results with peaks of the two curves offset by ~0.5°C, which is within the resolution of 0.5°C used for the step mode. The enthalpy change during phase change is determined to be ~120 J/g.[1]

[1] Defining phase change regime for a real PCM appears to be arbitrary in scientific literature. This is because in the

Figure 2 shows DSC results during solidification process. Here we notice enthalpy profiles are quite different for ramps of 0.2, 1, 5 and 10°C/min. The slowest ramp of 0.2°C/min exhibits multiple peaks in the enthalpy curve with the first and the highest peaks occurring at ~24.5°C and 23°C, respectively. On the other hand, step mode gives three peaks in the enthalpy profile with both the first and the highest peak occurring at ~25°C. The enthalpy change during solidification is measured to be ~95 J/g. Table 1 compiles phase-change data for Syntroleum products and octadecane.

Table 1: Phase change properties of octadecane, and Synpar in dusted, undusted and sheet forms. A DSC system in step mode has been used to determine the phase change properties.

Properties		Octadecane	Dusted Synpar	Undusted Synpar	Synpar Sheet
Enthalpy change (J/g)	Melting	224	119	124	123
	Solidification	212	94	95	95
Peak Temperature (°C)	Melting	27	26	26	26
	Solidification	25.5	25	25	25
Sub-cooling (°C)		1.5	1	1	1

Figure 3 and 4 compare dusted, undusted and sheet samples during melting and solidification, respectively. We observe that DSC enthalpy curves for the three samples are very similar, suggesting composition remains same in all three forms. This also indicates that dusting has little effect on the phase change properties.

DHFMA data for sheet sample is slightly off than the step data. There could be several reasons for this:

1) DSC and DHFMA resolutions are 0.5 and 0.75°C, respectively

2) Four sheets were stacked and tested. After first melting test, sheets were found to fuse together. This may cause a change in the volume of the sample, hence, in the final result.

solid phase, the heat capacity increases more or less linearly with the temperature unlike in the liquid phase where it remains constant with the temperature. This fact introduces uncertainty regarding selection of onset of melting or end of solidification process. In our analysis in this report, we assumed, phase change starts/ends (for melting/freezing) once deviation in heat capacity linear trend is more than 10%.

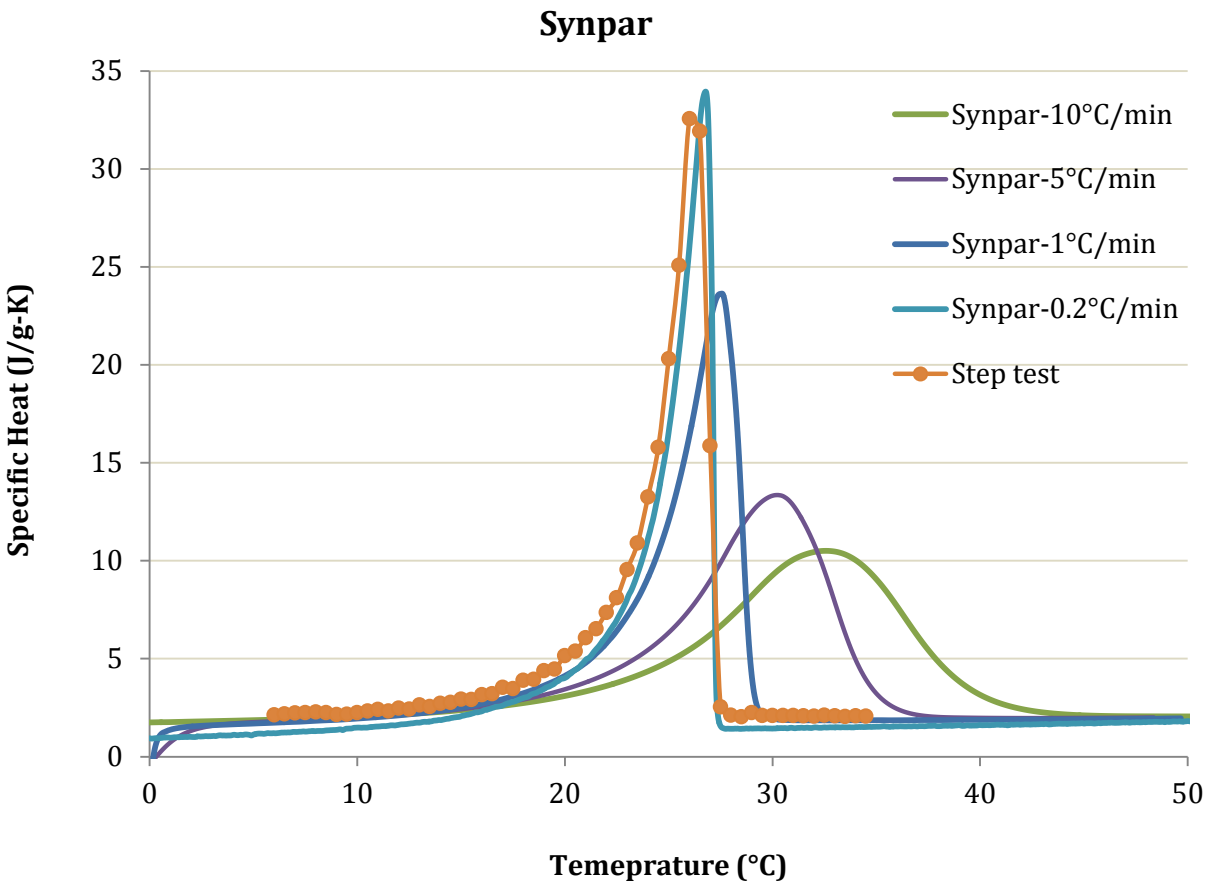

Figure 1: Specific heat during melting for dusted Synpar pellets using DSC method. DSC is run in ramp and step modes to obtain the data. Ramp rate seems to have a profound effect on the profile of the curve. As ramp is decreased, data tend to approach step mode data.

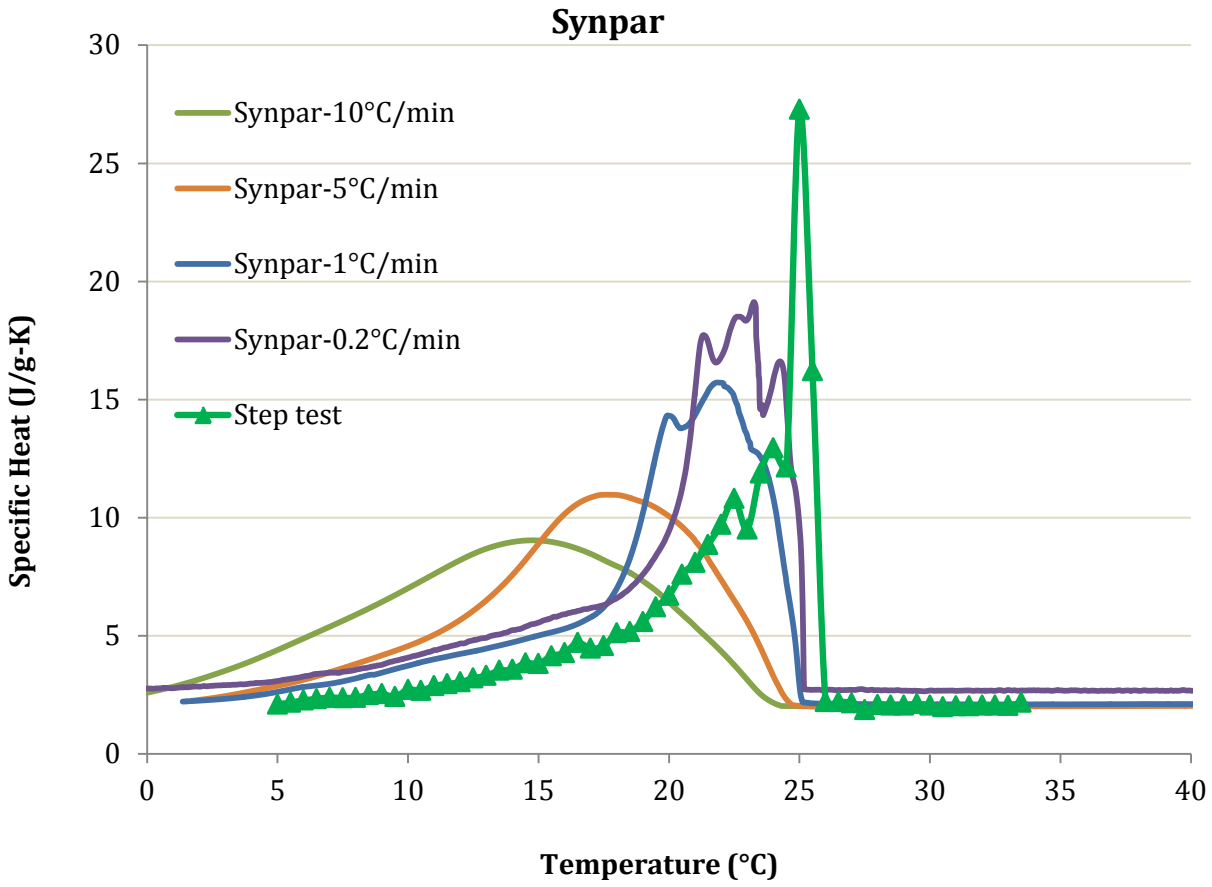

Figure 2: Specific heat during solidification for dusted Synpar pellets using DSC method. DSC is run in ramp and step modes to obtain the data. Ramp rate seems to have a profound effect on the profile of the curve. As ramp is decreased, data tend to approach step mode data.

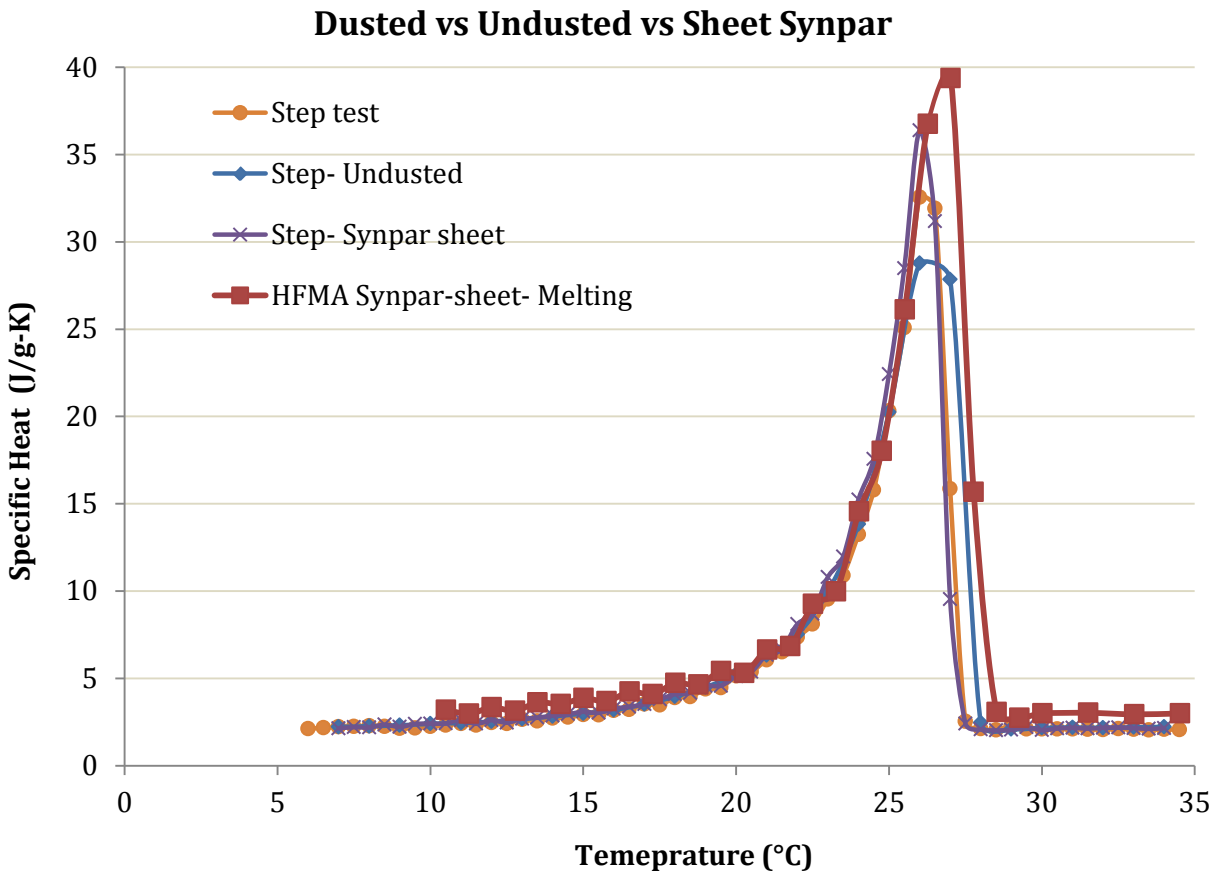

Figure 3: Comparison of specific heat data for dusted, undusted and sheet samples during melting. DSC in step mode has been used to generate data for the three forms of Synpar studied in this project, while DHFMA method has been employed to obtain data on an 8”x8” sized sheet sample.

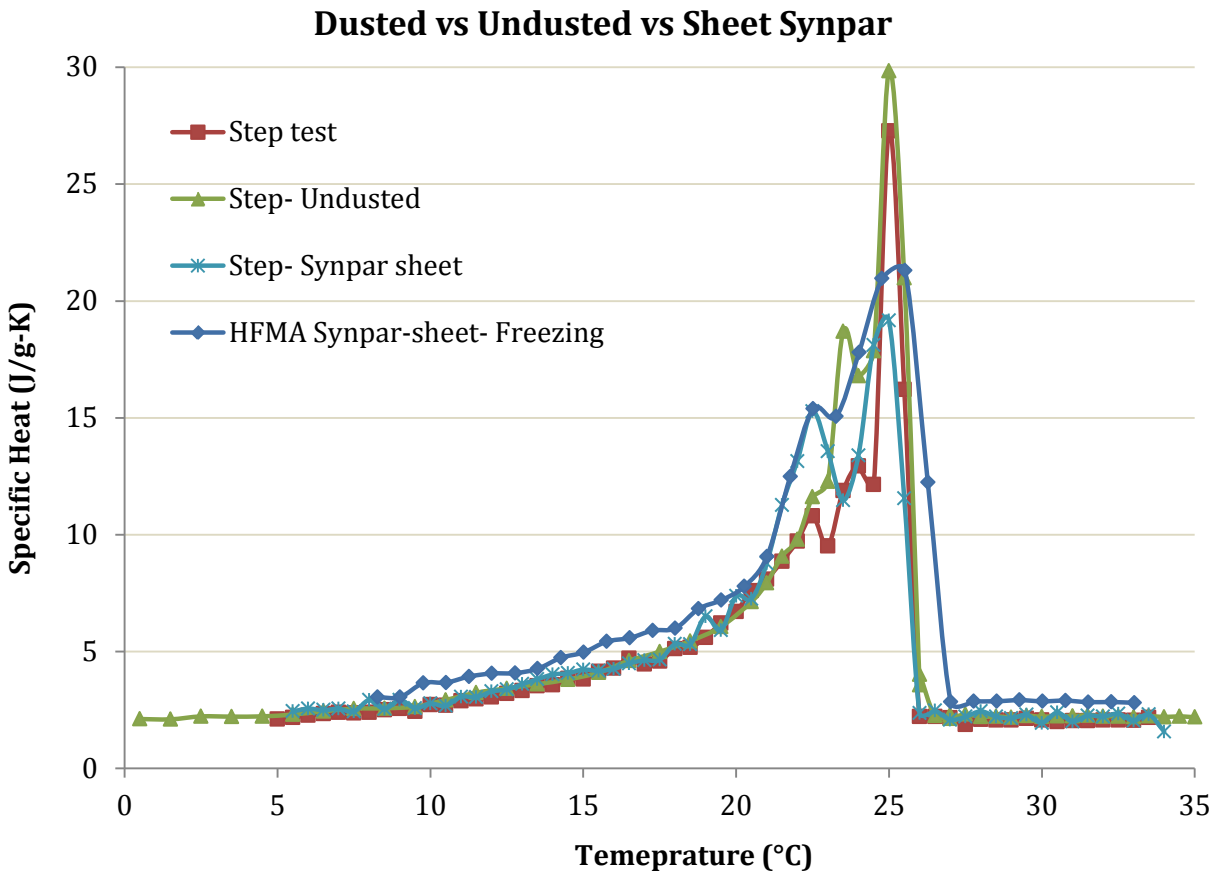

Figure 4: Comparison of specific heat data for dusted, undusted and sheet samples during solidification. DSC in step mode has been used to generate data for the three forms of Synpar studied in this project, while DHFMA method has been employed to obtain data on an 8”x8” sized sheet sample.

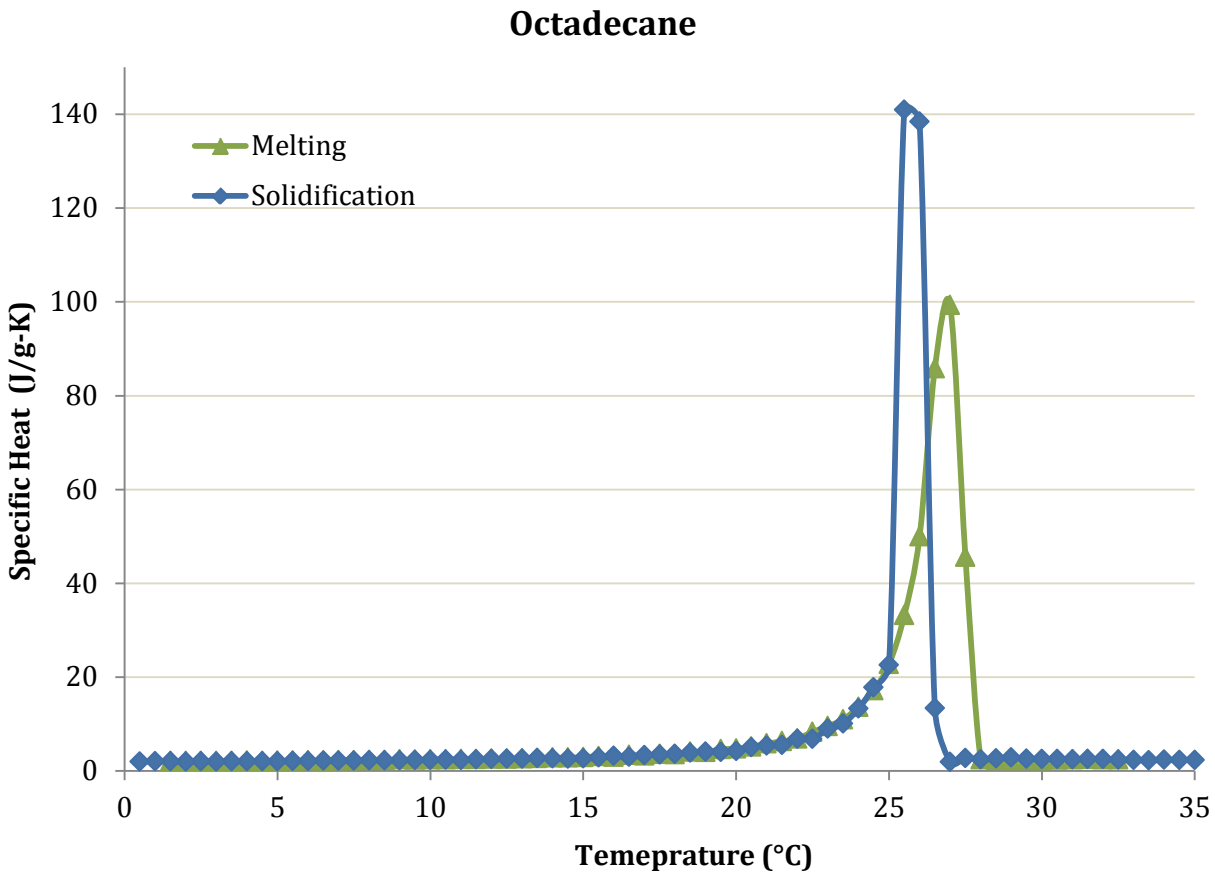

Figure 5: Specific heat for octadecane sample during melting and solidification. A DSC in step mode has been used to generate the data.

PCM-enhanced Cellulose Samples

As a first step towards integrating Synpar PCM with building materials, it was decided to mix Synpar with cellulose insulation. Blown cellulose samples were prepared at Advanced Fiber Technology, Inc. (AFT) facility. In 2011, an ORNL experimental study performed in Charleston, SC showed that a 30% blend of Synpar pellets with cellulose insulation is possible without causing segregation of the two materials. An identical composition mixture of 30% by weight of Synpar in cellulose was prepared for this study. A batch of blown cellulose sample was also prepared as a control sample.

C518 thermal testing was performed on control cellulose and Synpar enhanced cellulose samples, and results are shown in Table 2. We found that thermal conductivity for both samples increased with temperature. Addition of PCM to cellulose causes a slight increase in the thermal conductivity of the mixture.

Dynamic HFMA testing was performed on cellulose-PCM mixture to evaluate phase change properties including latent heat of the mixture. Volumetric heat capacity of the mixture as a function of temperature is given in Figure 6. Melting peak occurs at ~26.75°C, which is close to melting peak data observed with pure Synpar. Freezing data shows saturation near peak range,

suggesting more testing time is needed at temperature steps near peak range to ensure no heat is flowing at the end of the step.

Table 1: Thermal conductivity of cellulose and Synpar-blended cellulose insulations

Sample	Density, Kg/m^3 (lb/ft^3)	Thermal Conductivity, W/m.K	
		T=12.5°C	T=45°C
Cellulose	42.4 (2.65)	0.0375	0.0420
Synpar-enhanced Cellulose	55.1 (3.44)	0.0403 (Solid PCM)	0.0446 (Liquid PCM)

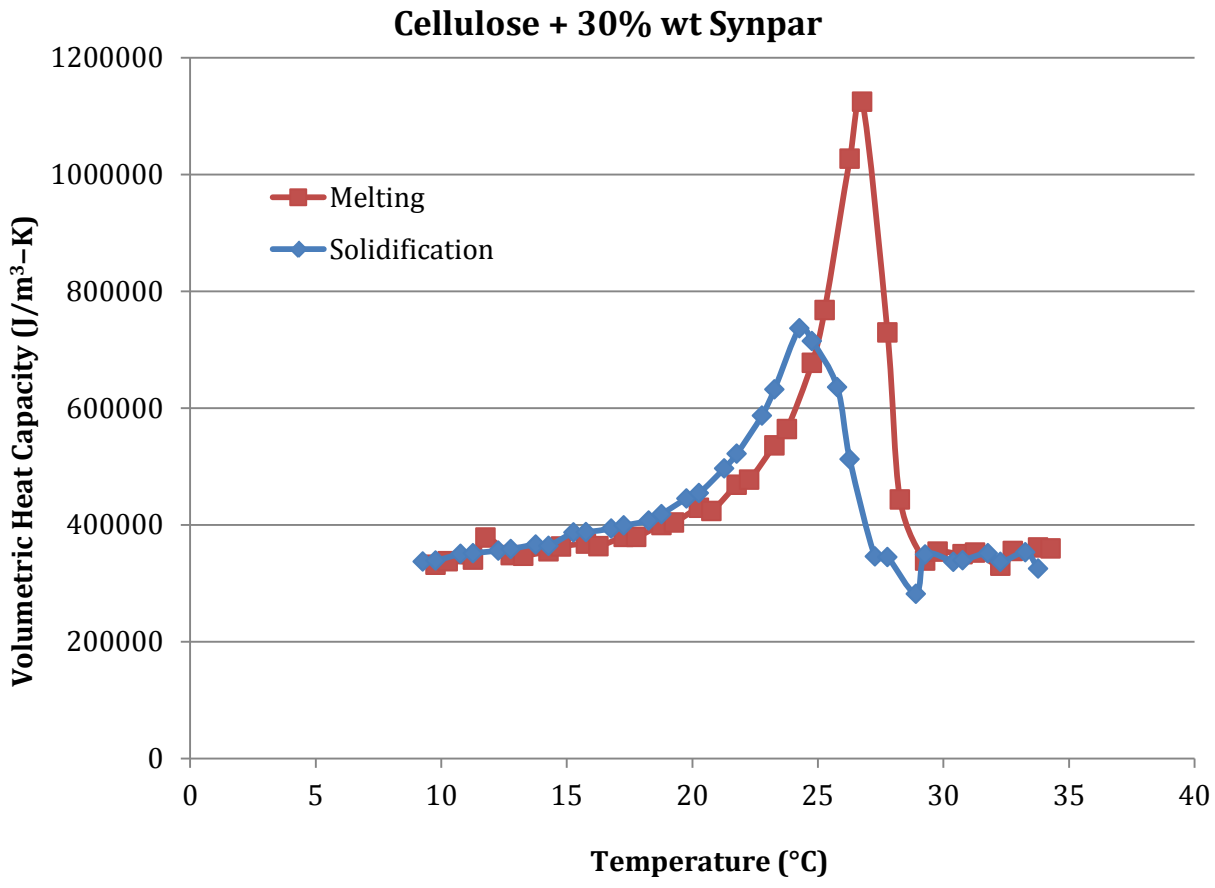

Figure 6: Volumetric heat capacity for Synpar enhanced cellulose insulation sample. DHFMA method was used to generate the data.

Fire Testing

Fire resistance properties of PCM enhanced cellulose samples were evaluated using two methods- ASTM C1485 Critical Radiant Flux method and ASTM C739 Smolder Resistance method. Two different compositions of Synpar were used in the Fire Resistance study: Dusted Synpar (white colored) and Synpar mixed with graphite (dark colored).

ASTM C1485 Standard Test Method for Critical Radiant Flux of Exposed Attic Floor Insulation Using an Electric Radiant Heat Energy Source

This test involves exposing a uniformly and horizontally placed specimen to the heat from an electric radiant heat energy panel located above and inclined at 30° to the specimen. The specimen is preheated, and then a flame is ignited on the highest radiant flux point (i.e. farthest end) of the specimen. In the calibrated radiant heat panel test apparatus used, if the flame extinguished before reaching 40 cm length mark, the specimen was considered to pass the test. The test apparatus and specimen tray are shown in Figure 7.

Three configurations of cellulose PCM were prepared and tested:

1. 30 wt% graphite-PCM dispersed evenly with cellulose (2" thick layer) – FAILED
   Once the flame was ignited, it continued to spread and passed the 40 cm mark. Flame stopped at ~50 cm length mark and sustained for a long period of time of ~25-30 minutes, suggesting PCM acted as a heat and fire source (See Figure 8a). A closer examination also revealed that fire spread all the way along the depth of the sample as well.
2. Cellulose (1" thick top layer) + 40 wt% graphite-PCM mixed evenly with cellulose (1" thick bottom layer) – PASSED
   Once the flame was ignited, it continued to spread but stopped at ~39 cm mark (See Figure 8b).
3. 30 wt% graphite-PCM dispersed evenly with Fire Shield cellulose (2" thick layer) – PASSED
   AFT FIRE SHIELD™ is a new cellulose product that contains higher levels of flame retardant than the regular insulations available in the market. Once the flame was ignited, it sustained for almost ~20 minutes, but burn length was found to only 31.5 cm (See Figure 8c).

(a) (b)

Figure 7: ASTM C1485 Standard Test Method (a) Radiant Heat Flux apparatus, (b) cellulose insulation placed inside sample tray.

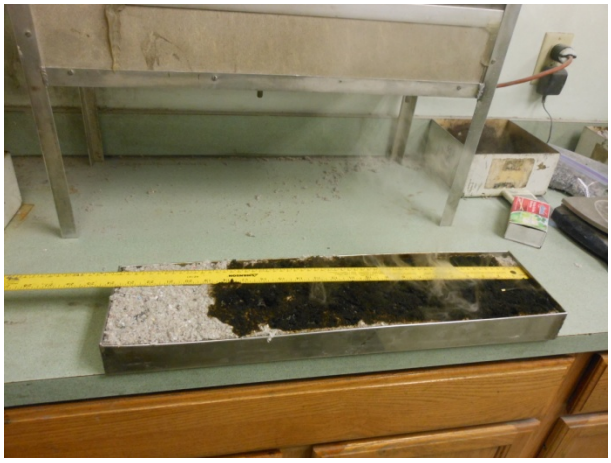

(a)

(b)

(c)

Figure 8: Flame spread on (a) 30 wt% graphite-PCM dispersed evenly with cellulose (2” thick layer), (b) Cellulose (1” thick top layer) + 40 wt% graphite-PCM mixed evenly with cellulose (1” thick bottom layer), (c) 30 wt% graphite-PCM dispersed evenly with Fire Shield cellulose (2” thick layer)

ASTM C739 Section 14 Smoldering Combustion Test

In this test, a well-lighted unfiltered cigarette is vertically inserted into the center of specimen. The cigarette is allowed to burn undisturbed in the test area for at least 2 h or until the smoldering is no longer progressing, whichever period is longer. Percent mass loss of the original specimen is determined and evidence of flaming is reported. We prepared a test sample by evenly dispersing 30 wt% graphite-PCM into cellulose insulation. A mass loss of 0% was observed for the specimen and no evidence of burning was found (See Figure 9). The specimen passed the Smoldering Test.

Figure 9: ASTM C793 Sec 14 Smoldering Combustion Test on (30 wt% graphite-PCM + cellulose insulation) sample.

A3. Franunhofer Report – Whole-Building Simulation

Fraunhofer USA

Fraunhofer Center for Sustainable Energy Systems

ENERGY PERFORMANCE AND COST ANALYSIS OF ENCAPSULATED PHASE CHANGE MATERIAL PRODUCED BY SYNTROLEUM CORPORATION

FINAL DRAFT REPORT TO SYNTROLEUM (FOR INTERNAL USE ONLY)

March 2013

by Ali Fallahi, Jan Kosny & Nitin Shukla

Ali Fallahi, Ph.D., Building Enclosures Group
afallahi@fraunhofer.org 617-575-7259

Jan Kosny, Ph.D., Building Enclosures Group
jkosny@fraunhofer.org 617-714-6525

Nitin Shukla, Ph.D., Building Enclosures Group
nshukla@fraunhofer.org 617-575-7250 x 169

Energy Model

A series of whole-building energy simulations were performed to assess the energy performance of PCM manufactured by Syntroleum. Savings due to the addition of PCM in the attic of residential houses were calculated. This report documents and summarizes the modeling work.

The report is divided into three parts. The first part compares the whole building energy performance of dispersed and condensed PCMs installed in an attic of a residential building in south US climate, and finds which of the two yields higher energy savings. The second part of the report compares energy savings of condensed PCM located at different depths across cellulose insulation. Finally, the third part calculates the payback time period required after installation of condensed PCM in four US climates.

1.1 Model Description

A single family ranch-style house[2] in Phoenix, Arizona was modeled using the ESP-r[3] computer program. ESP-r is a whole-building energy software with a built-in capability to model PCM sub-cooling effects with two different specific heat profiles (melting and solidification).

The dimensions of the house are 16.8 m * 8.4 m * 2.4m for the conditioned space and the height of the attic is 1.6m. The house was modeled as two zones representing the conditioned space and the attic space (see Figure 1). Outside boundary conditions were specified by ASHRAE IWEC weather files, while the interior conditioned space followed an HVAC set point temperature. The infiltration rate through the walls and the ventilation rate between the attic and the outside are listed in Table 1 below.

One "Base Case" model was developed to represent the energy load of the existing house with 25.4cm (10in) cellulose insulation in the attic. Four variations of the "Base Case" model (configurations: 1-A, 2-A, 2B and 2C) were developed, which represent different ways of applying PCM to the attic insulation (see Table 1 and Figure 2). The cellulose insulation used in the simulation has a density of 40 kg/m^3, a conductivity of 0.042 W/kg.K, and a specific heat of 1380 J/kg. The parameters for the "Base Case" and the four modeled cases are listed in Table 1.

[2] The same single story house was used for development of Model Energy Code (Council of American Building Officials, 1995 and Huang, 1996) and ASHRAE 90.2 (ASHRARE 2007).

[3] ESP-r is an advanced whole-building energy modeling software, extensively used by researchers to model multi-zone thermal, air, HVAC, and other building-domain related phenomena. The software allows a detailed parametric study of the factors which influence the energy and environmental performance of buildings. ESP-r uses a finite volume conservation approach, which translates geometry, construction, operation, etc. into a set of conservation equations for energy, mass, and momentum. The conservation equations are integrated at successive time-steps to determine the response of the building to climate, occupant, and control system influences.

2 Modeled Configurations

2.1 Condensed vs. Dispersed PCM

Configurations (1-A & 2-A) were modeled to compare annual energy load savings due to applying condensed and dispersed PCM in the attic. In configurations 1-A, PCM is blended homogenously into 254mm (10in) cellulose insulation of the attic. The amount of PCM is equal to 30% weight of cellulose (approximately 3 kg/m2). In configuration 2-A, PCM is applied in layers of pure PCM with a total thickness of 71mm (0.28in) on the attic floor. Configurations 1-A and 2-A have the same amount of PCM by mass (approximately 3 kg/m^2).

The modeling results are listed in Table 2 both for heating and cooling periods. The modeled loads show configuration 2-A with condensed PCM having a lower cooling load than configuration 1-A with dispersed PCM. During cooling season, condensed PCM configuration yields 5.6% cooling load savings versus 3.1% for dispersed PCM configuration (both configurations are compared to the base case without any PCM). For the whole year the total annual savings show that condensed PCM with 6.2% savings performs better than dispersed PCM with 3.6% savings. The annual savings takes into account the savings for both heating and cooling loads.

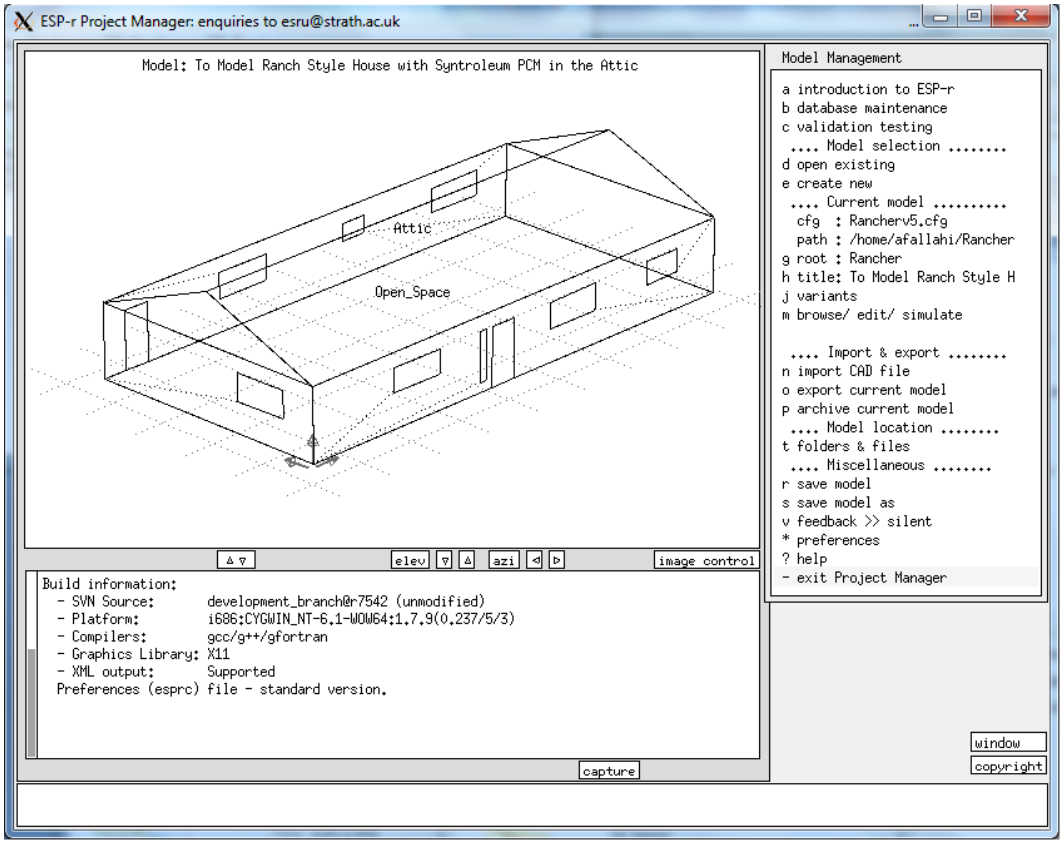

Figure 18: Geometry of "Base Case" model in ESP-r software

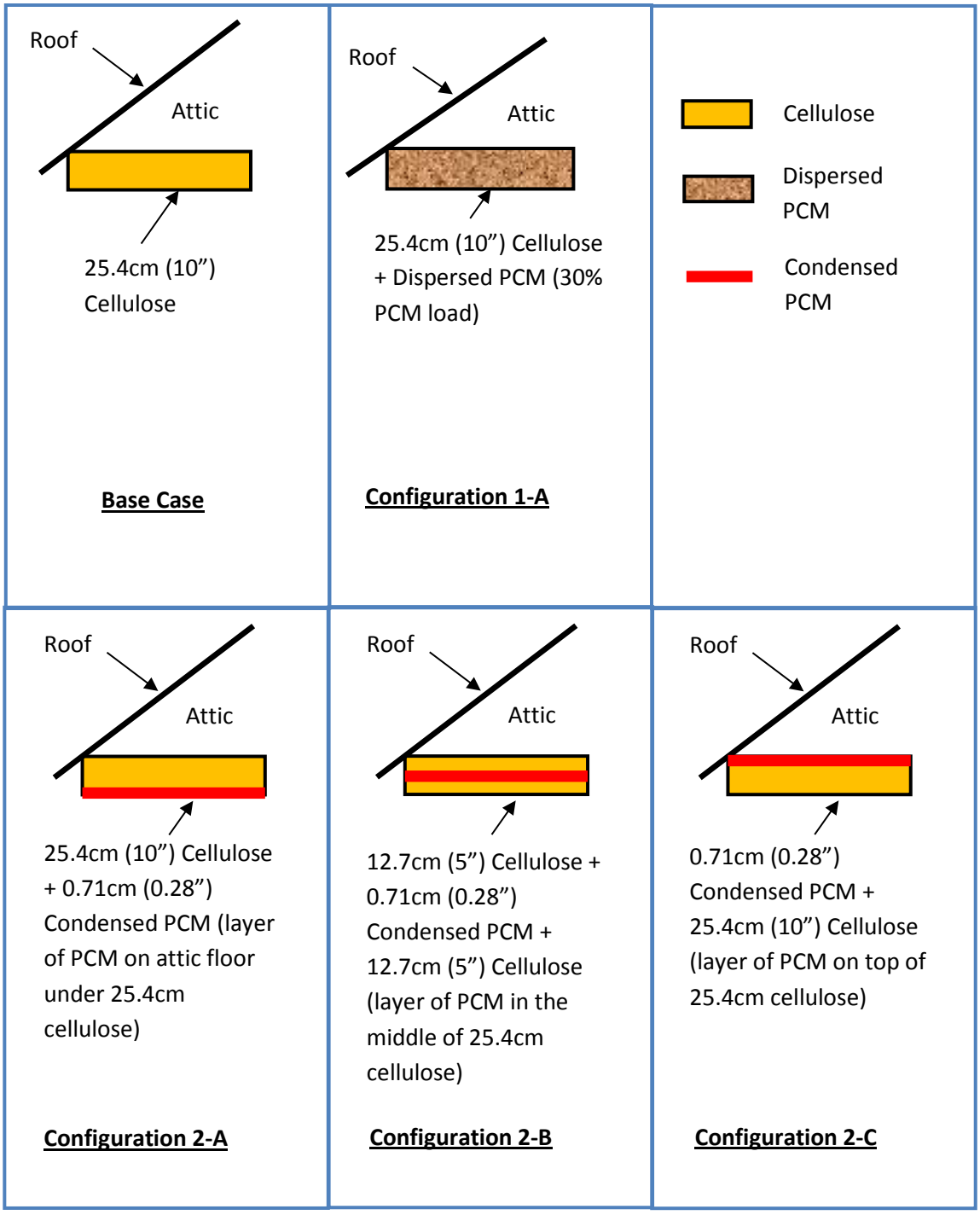

Figure 19: Modeled Configurations of PCM in the attic

Table 6: Model Parameters

		Base Case Configuration	*Configuration 1-A (dispersed PCM)*	*Configuration 2-A (condensed PCM)*	*Configuration 2-B (condensed PCM)*	*Configuration 2-C (condensed PCM)*
Construction						
	Wall (R-13 or 2.3RSI)	Siding; Plywood; 2x4 wood studs with fiberglass batt insulation; Gypsum board	Siding; Plywood; 2x4 wood studs with fiberglass batt insulation; Gypsum board	Siding; Plywood; 2x4 wood studs with fiberglass batt insulation; Gypsum board	Siding; Plywood; 2x4 wood studs with fiberglass batt insulation; Gypsum board	Siding; Plywood; 2x4 wood studs with fiberglass batt insulation; Gypsum board
	Roof	Shingle; Plywood	Shingle; Plywood	Shingle; Plywood	Shingle; Plywood	Shingle; Plywood
	Ceiling (R-34 or 6RSI)	254mm (10in) cellulose; gypsum board	254mm (10in) cellulose mixed with 30% dispersed PCM by weight; gypsum board	254mm (10in) cellulose; 71mm (0.28in) pure PCM on attic floor; gypsum board	254mm (10in) cellulose; 71mm (0.28in) pure PCM on attic floor; gypsum board	127mm (5in) cellulose; 71mm (0.28in) pure PCM; 127mm (5in) cellulose; gypsum board
	Gable	Siding; Plywood	Siding; Plywood	Siding; Plywood	Siding; Plywood	Siding; Plywood
	Floor	50.8mm (2in) Heavy concrete; 50.8mm (2in) cement screed	50.8mm (2in) Heavy concrete; 50.8mm (2in) cement screed	50.8mm (2in) Heavy concrete; 50.8mm (2in) cement screed	50.8mm (2in) Heavy concrete; 50.8mm (2in) cement screed	50.8mm (2in) Heavy concrete; 50.8mm (2in) cement screed
	Door	Oak Wood	Oak Wood	Oak Wood	Oak Wood	Oak Wood
	Window	Clear Glass Double Glazed	Clear Glass Double Glazed	Clear Glass Double Glazed	Clear Glass Double Glazed	Clear Glass Double Glazed
Set points (°C)						
	Cool	23C	23C	23C	23C	23C
	Heat	20C	20C	20C	20C	20C
Soil Temperature						

	Method of calculation	Basesimp[4]	Basesimp	Basesimp	Basesimp	Basesimp
Climate						
	Weather file	ASHRAE IWEC weather file for Phoenix, AZ	ASHRAE IWEC weather file for Phoenix, AZ	ASHRAE IWEC weather file for Phoenix, AZ	ASHRAE IWEC weather file for Phoenix, AZ	ASHRAE IWEC weather file for Phoenix, AZ
Continuous Infiltration (ACH)						
	Exterior to conditioned space	0.6	0.6	0.6	0.6	0.6
Continuous Attic Ventilation (ACH)						
	Exterior with Attic space	4	4	4	4	4
Internal Gains						
	Occupants, Lighting & Equipment	Residential Schedule	Residential Schedule	Residential Schedule	Residential Schedule	Residential Schedule

[4] BASESIMP algorithm was used to predict the heat loss and gain from the house's slab-on-grade floor. BASESIMP is a regression-based algorithm which expresses both above-grade and below-grade time dependent heat losses. BASESIMP regression algorithm was generated based on 33,000 parametric run of a computationally intensive program, performing a series of two dimensional finite-element analyses for each type of foundation (Beausoleil-Morrison, 1997).

Table 7: Modeled Load Savings in Phoenix, AZ climate

	Configuration -1A (dispersed PCM)		*Configuration 2-A (condensed PCM)*	
	Heating	***Cooling***	***Heating***	***Cooling***
Annual Load (kW.hr)	283	15252	265	14857
Base Case Annual Load (kW.hr)	384	15739	384	15739
Saving	26.0%	3.1%	31.0%	5.6%
Total Annual Savings	**3.6%**		**6.2%**	
Time Step	60min		60min	

2.2 Location of Condensed PCM

Location of condensed PCM across the attic cellulose insulation affects the amount of the house cooling and heating loads, which affects the energy savings obtainable by PCM. Three models were developed (configurations 2-A, 2-B & 2-C). Each were simulated for a southern US climate to find a location across the cellulose insulation where the load saving becomes maximum. The results were compared with the base case, and the savings were calculated (see Table 4).

Table 8: Modeled Load Savings of Condensed PCM in Phoenix, AZ climate

	Configuration 2-A		*Configuration 2-B*		*Configuration 2-C*	
	Heating	***Cooling***	***Heating***	***Cooling***	***Heating***	***Cooling***
Annual Load (kW.hr)	242	15103	277	15137	301	16126
Base Case Annual Load (kW.hr)	328	16217	328	16217	328	16217
Saving	26.2%	6.8%	15.5%	6.6%	8.2%	0.56%
Total Annual Savings	**7.3%**		**6.8%**		**0.71%**	
Time Step	1min		1min		1min	

The modeling results show that condensed PCM located on the bottom of attic cellulose insulation and

next to the attic floor (configuration 2-A) has the highest saving of the all three configurations. The total annual savings is 7.3% compared to the base case house annual load.

Configuration 2-B, where PCM is located in the middle of attic cellulose insulation, has a lower total annual savings of 6.8%. Configuration 2-C, where condensed PCM is on top of attic cellulose insulation, shows the lowest total annual savings of 0.71%.

Table 4 lists the modeled loads and savings based on one minute time step simulation. This lower time step increases the resolution and accuracy of the model, and allows for small saving difference between configurations 2-A and 2-B to be captured.

Table 9: Specification of the modeled HVAC unit for heating and cooling

Cooling			**Heating**	
Type	Air Source Heat Pump		Type	Furnace
Capacity	2.5 kW		Fuel Type	Natural gas
Total Steady State COP*	1.5		Capacity	2.5 kW
Flow Rate	1 m3/s		Total Steady State efficiency	85%
Circulation Fan Power	300 W			
Sensible Heat ratio	0.75			

*the COP includes the air leakage through the ducts.

2.3 Payback Period

This part of report compares the payback periods in four different US climates. In order to find the payback period at each considered climate, the electricity and gas consumptions of the condensed PCM (configuration 2-A), which had the highest energy savings, were modeled using ESP-r software. Then, the electricity and gas consumption of each case was compared against the base case house without PCM (configuration 1-A).

The savings in previous parts are cooling/heating load savings, which represent the house energy demands, do not require any HVAC modeling. However, in this part of report the HVAC system needs to be included in the numerical model to find the electricity and gas consumption of each house. For the purpose of this model, a typical HVAC unit for a retrofit house was considered. Table 4 lists the specifications of the HVAC unit.

After modeling the electrical and gas consumption, the energy cost was calculated based on a bundled utility price in the corresponding climates (Table 5). Utility prices were reported by Edison Electric Institute, 2012 and Department of Energy, 2012. Table 6 shows the energy costs and savings in the four considered climates. The HVAC system was modeled using ESP-r software with a 1min time step.

Table 10: Residential utility price based on considered climates

Climate	Elec. Price [$/kW.hr]	Gas Price [$/THERM]
Phoenix	0.13311	2.2
Houston	0.10489	1.5
San Francisco	0.2043	1.01
Miami	0.12619	2.16

Phoenix has the highest total annual utility cost savings of $106.4 followed by Miami, San Francisco, and Houston with savings of $55.2, $51.5, $49.2 respectively. This saving takes into account both heating and cooling cost. Table 6 and Figure 3 shows the total annual utility savings are due to electricity consumption rather than gas consumption, especially for southern hot climates. Therefore, the utility cost savings are higher in Southern climates like Phoenix where electricity is more expensive.

Table 7 lists the modeled payback period required to repay the total installed cost of PCM. In order to calculate the payback period, the current cost of 3.5$/lb was assumed to be the total installed cost[5] of condensed PCM (configuration 2-A) in the attic. Future cheaper prices from 3.0$/lb to 1.5$/lb were also considered. For 30% PCM load, the payback period ranges from 26.5yr for Phoenix to 56.9yr for Houston based on the current cost of 3.5$/lb. The future cheaper price of 1.5$/lb can reduce the payback period range to 19.3yr for Phoenix and 41.5yr for Houston.

ORNL earlier field experiments demonstrated similar energy performance for 22% PCM load (Kosny, 2008). If the amount of 30% PCM load be optimized to 22%[6], then the payback period decreases as well. Table 7 shows that the payback period with 22% PCM load in attic cellulose insulation has a payback period ranging from 19.3yr for Phoenix to 41.5yr for Houston with the current 3.5$/lb installed cost. The payback period decreases to less than half (ranging from 8.3yr to 17.8yr) if the future price of 1.5$/lb is considered.

Table 11: Modeled utility cost consumptions in considered climates

[5] Total installed cost includes both material and labor costs

[6] An experimental paper by ORNL reports that changes in energy consumption are minor due to the changing the PCM load from 22% to 30% (Child et al., 2012). Therefore, with 22% PCM load instead of 30%, and having the same utility cost savings, the payback period decreases.

Climate		**Electricity**		**Gas**		**Total Annual Utility Cost Savings**
		Base Case 1-A	Configuration 2-A	Base Case 1-A	Configuration 2-A	
Phoenix	Consumption [GJ]	63.8	61.1	1.4	1.1	**$106.4**[7]
	Savings	**4.2%**		**26.2%**		
Houston	Consumption [GJ]	50.1	48.7	4.8	4.1	**$49.5**
	Savings	**2.7%**		**14%**		
San Francisco	Consumption [GJ]	4.5	3.7	6.6	5.5	**$51.5**
	Savings	**16.1%**		**16.9%**		
Miami	Consumption [GJ]	79.1	77.6	0	0	**$55.2**
	Savings	**2.0%**		**0%**		

[7] The cost saving is a function of the specifications of the modeled HVAC unit (Table 4). If the specifications change the savings and the payback period will also change. If the COP in Table 4 changes from 1.5 to 2.5 the cost savings drops from $106.4 to $67.0.

Table 12: Modeled payback period in considered climates

	Payback Period with 30% PCM Load					Payback Period with 22% PCM Load				
Installed PCM Cost	3.5$/ lb	3.0$/ lb	2.5$/ lb	2.0$/ lb	1.5$/ lb	3.5$/ lb	3.0$/ lb	2.5$/ lb	2.0$/ lb	1.5$/ lb
Installed Cost of PCM for the base-case attic	$2819	$2416	$2016	$1611	$1208	$2067	$1772	$1478	$1181	$886
Phoenix	26.5yr	22.7yr	18.9yr	15.1yr	11.4yr	19.3yr	16.9yr	13.8yr	11.1yr	8.3yr
Houston	56.9yr	48.8yr	40.6yr	32.5yr	24.4yr	41.5yr	35.6yr	29.7yr	23.7yr	17.8yr
San Francisco	54.7yr	46.9yr	39.1yr	31.3yr	23.4yr	39.9yr	34.2yr	28.5yr	22.8yr	17.1yr
Miami	51.0yr	43.7yr	36.4yr	29.2yr	21.9yr	37.2yr	31.9yr	26.6yr	21.3yr	16.0yr

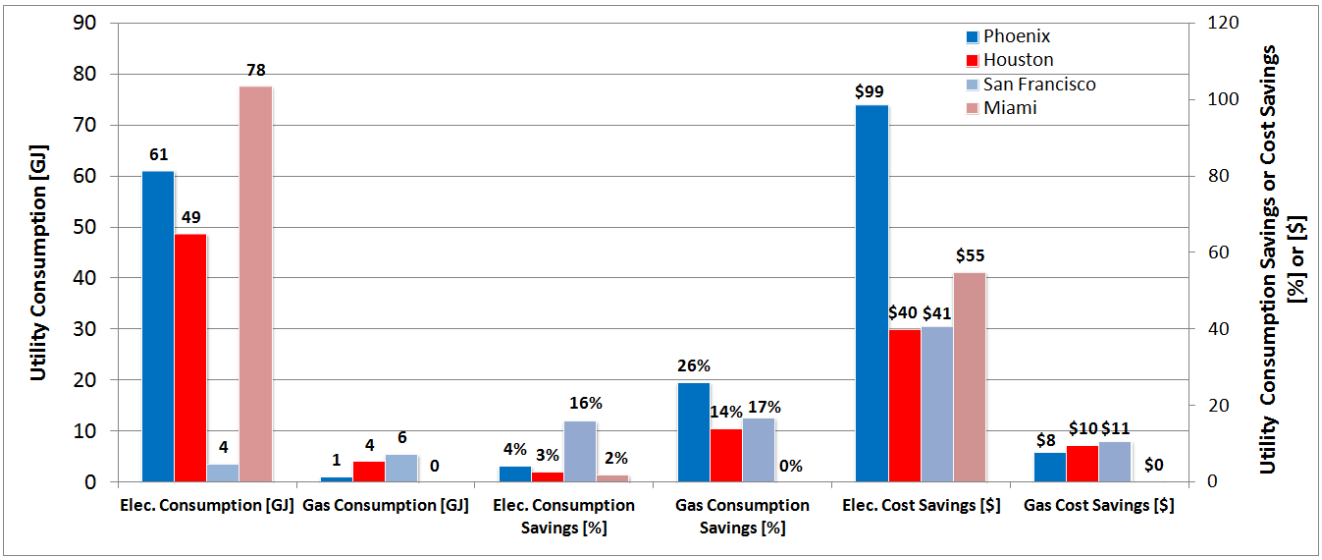

Figure 20: Modeled utility consumptions and savings. The savings are compared to the utility consumptions of the base case configuration.

3 References

ANSI/*ASHRAE 90.2*-2007: Energy Efficient Design of Low-Rise Residential Buildings

Council of American Building Officials (CABO), Model Energy Code, Falls Church, Virginia, 1995

Beausoleil-Morrison I., Mitalas G.,"BASESIMP: A Residential-Foundation Heat-Loss Algorithm for Incorporating into Whole-Building Energy-Analysis Programs', Proc. Building Simulation '97, (2) 1-8, Int. Building Performance Simulation Association, Prague Czech Republic, 1997

Child Kenneth, Stovall Therese, "Use of Phase Chang Material in a Building Envelope: A Case Study," ORNL, July 2012

Department of Energy for monthly "bundled" supply and delivery costs for July 2012 (http://www.northwesternenergy.com/ourcustomers/shared/NaturalGasRates.pdf)

Edison Electric Institute Typical Bills and Average Rates Report, July 2012 (http://www.northwesternenergy.com/ourcustomers/shared/ElectricRates.pdf)

ESRU, ESP-r, http://www.esru.strath.ac.uk/Programs/ESP-r.htm

Huang J, Hanford J and Yang F., "Residential Heating and Cooling Loads Component Analysis", LBNL 44636, 1996

Kosny Jan, "2006/07 Field Testing of Cellulose Fiber Insulation Enhanced with Phase Change Material," Oak Ridge National Laboratory report, ORNL/TM-2007/186, September 2008

A4. ORNL Field Test – Weekly Data Plots

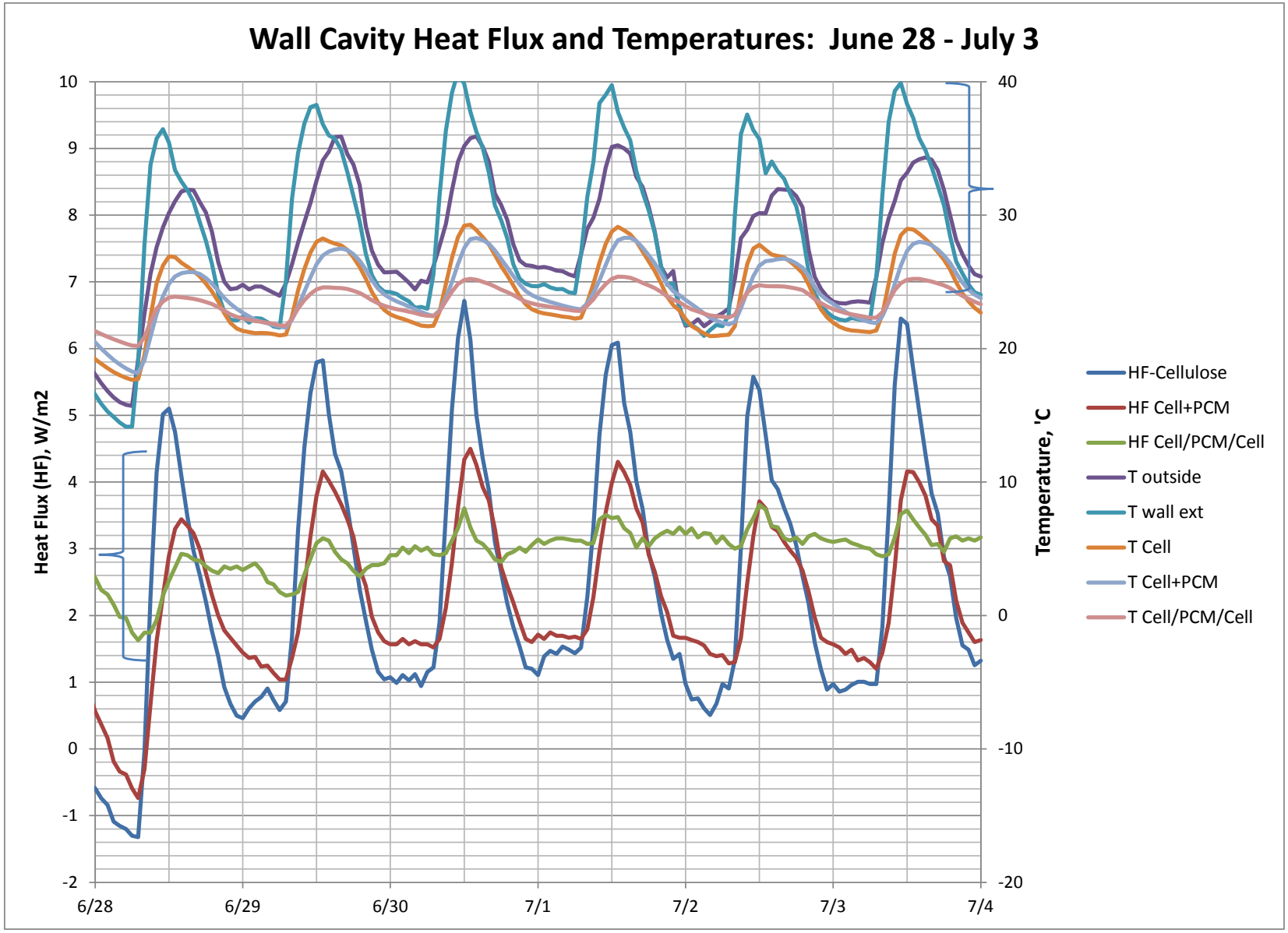
Wall Cavity Heat Flux and Temperatures: June 28 - July 3
Heat Flux (HF), W/m2
Temperature, 'C
10
9
8
7
6
5
4
3
2
1
0
-1
-2
40
30
20
10
0
-10
-20
6/28
6/29
6/30
7/1
7/2
7/3
7/4
HF-Cellulose
HF Cell+PCM
HF Cell/PCM/Cell
T outside
T wall ext
T Cell
T Cell+PCM
T Cell/PCM/Cell

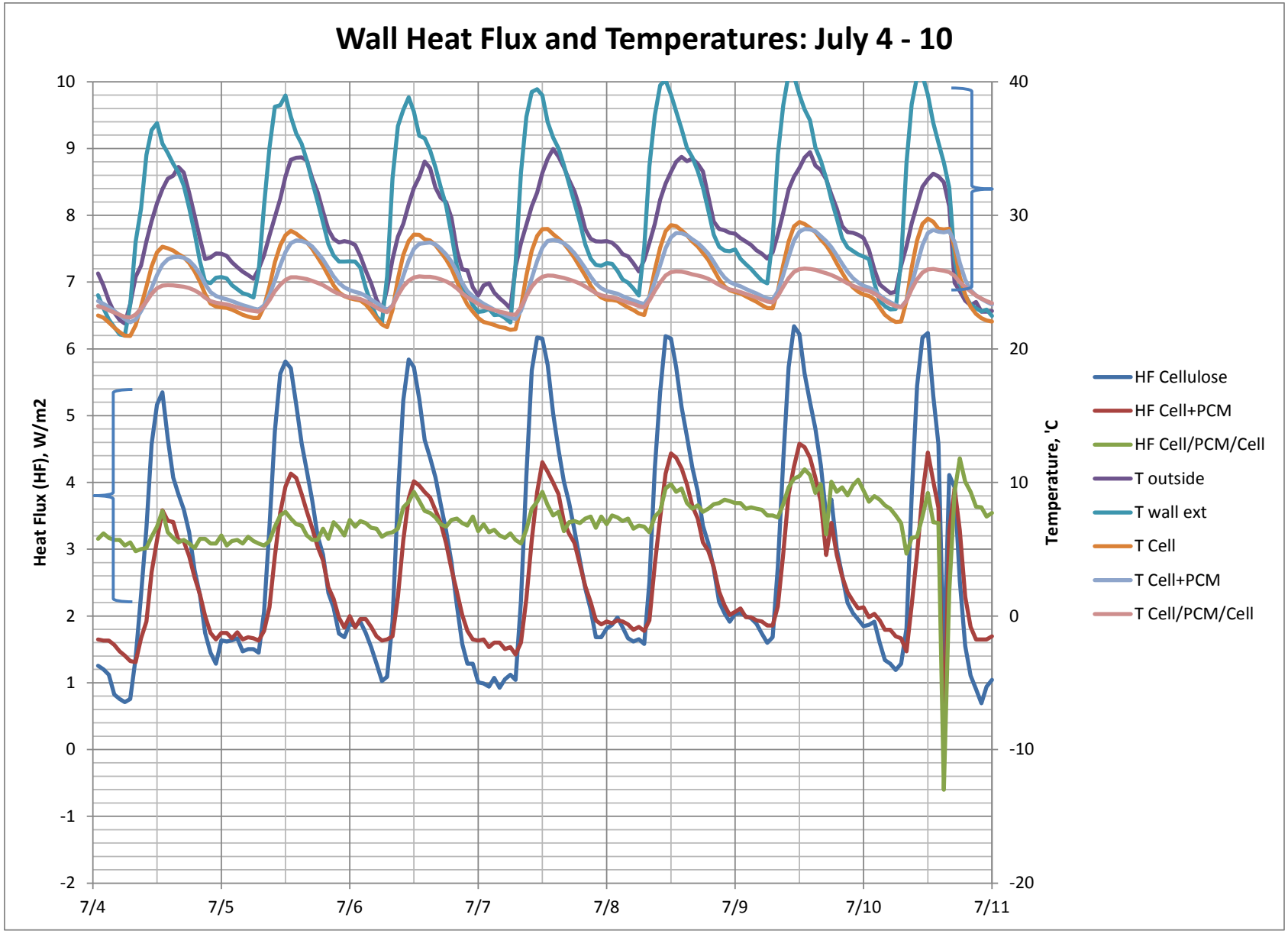
Wall Heat Flux and Temperatures: July 4 - 10
Heat Flux (HF), W/m2
Temperature, 'C
10
9
8
7
6
5
4
3
2
1
0
-1
-2
40
30
20
10
0
-10
-20
7/4
7/5
7/6
7/7
7/8
7/9
7/10
7/11
HF Cellulose
HF Cell+PCM
HF Cell/PCM/Cell
T outside
T wall ext
T Cell
T Cell+PCM
T Cell/PCM/Cell

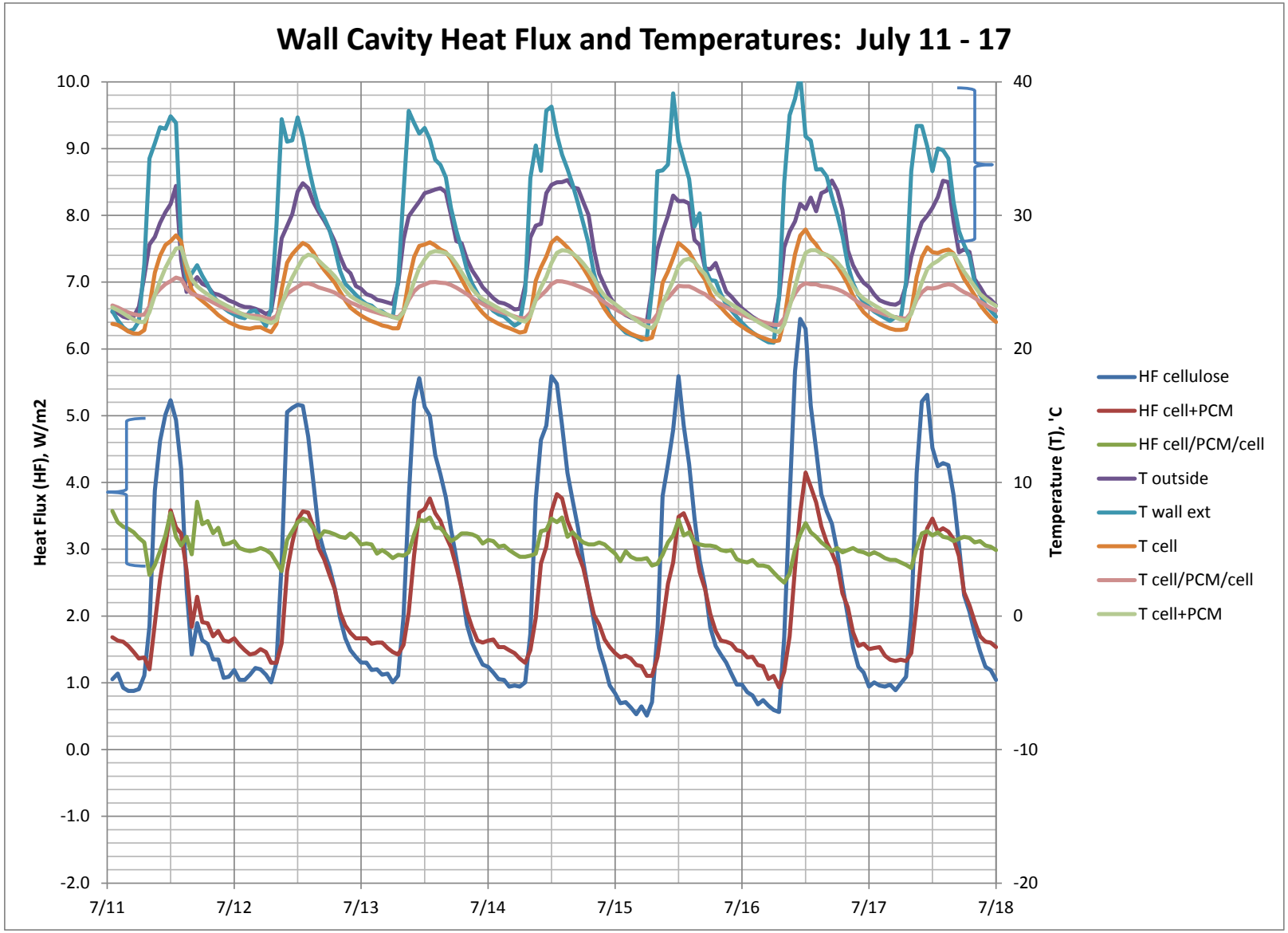
Wall Cavity Heat Flux and Temperatures: July 11 - 17
Heat Flux (HF), W/m2
Temperature (T), 'C
10.0
9.0
8.0
7.0
6.0
5.0
4.0
3.0
2.0
1.0
0.0
-1.0
-2.0
40
30
20
10
0
-10
-20
7/11
7/12
7/13
7/14
7/15
7/16
7/17
7/18
HF cellulose
HF cell+PCM
HF cell/PCM/cell
T outside
T wall ext
T cell
T cell/PCM/cell
T cell+PCM

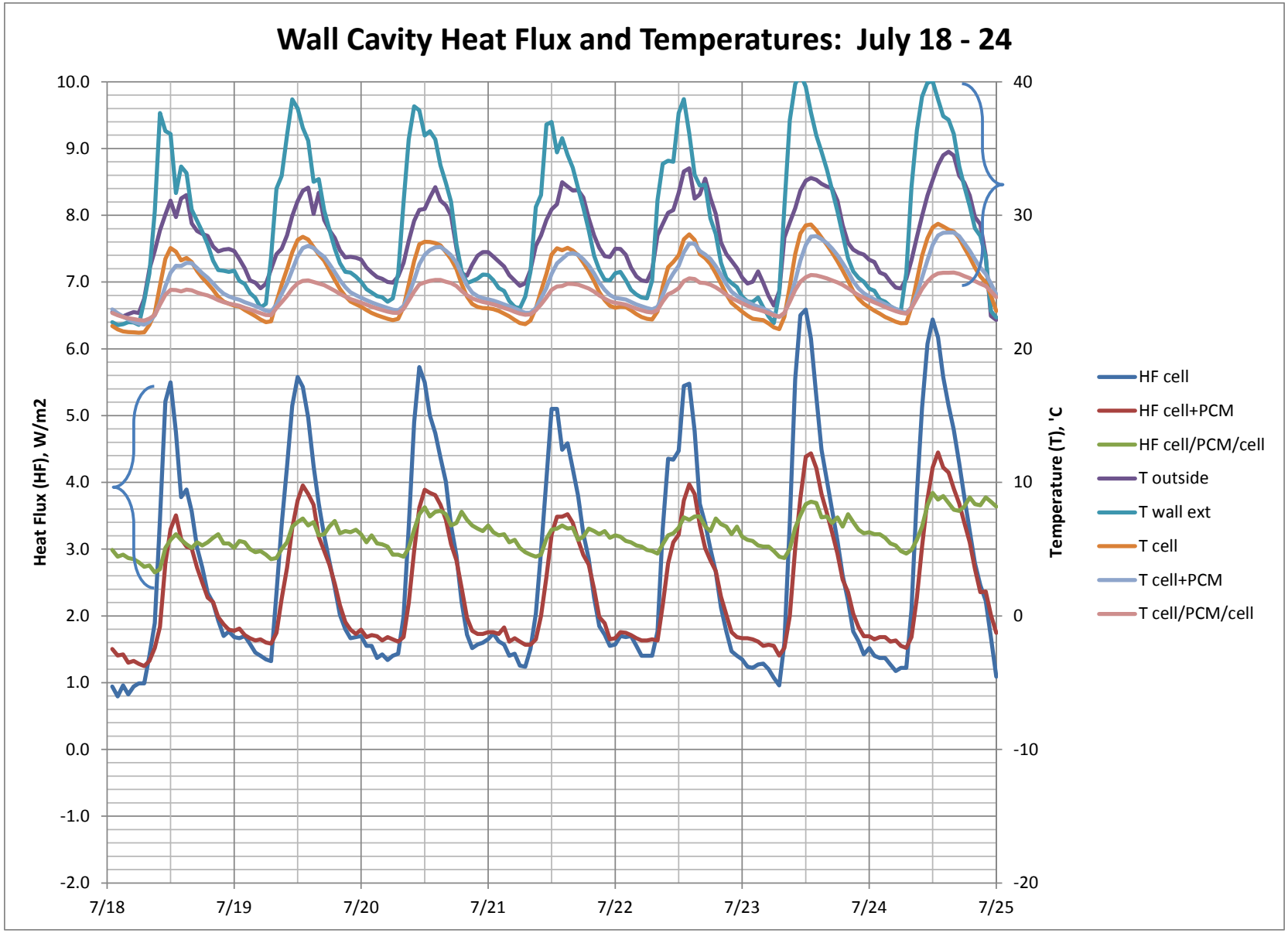
Wall Cavity Heat Flux and Temperatures: July 18 - 24
Heat Flux (HF), W/m2
Temperature (T), 'C
10.0
9.0
8.0
7.0
6.0
5.0
4.0
3.0
2.0
1.0
0.0
-1.0
-2.0
40
30
20
10
0
-10
-20
7/18
7/19
7/20
7/21
7/22
7/23
7/24
7/25
HF cell
HF cell+PCM
HF cell/PCM/cell
T outside
T wall ext
T cell
T cell+PCM
T cell/PCM/cell

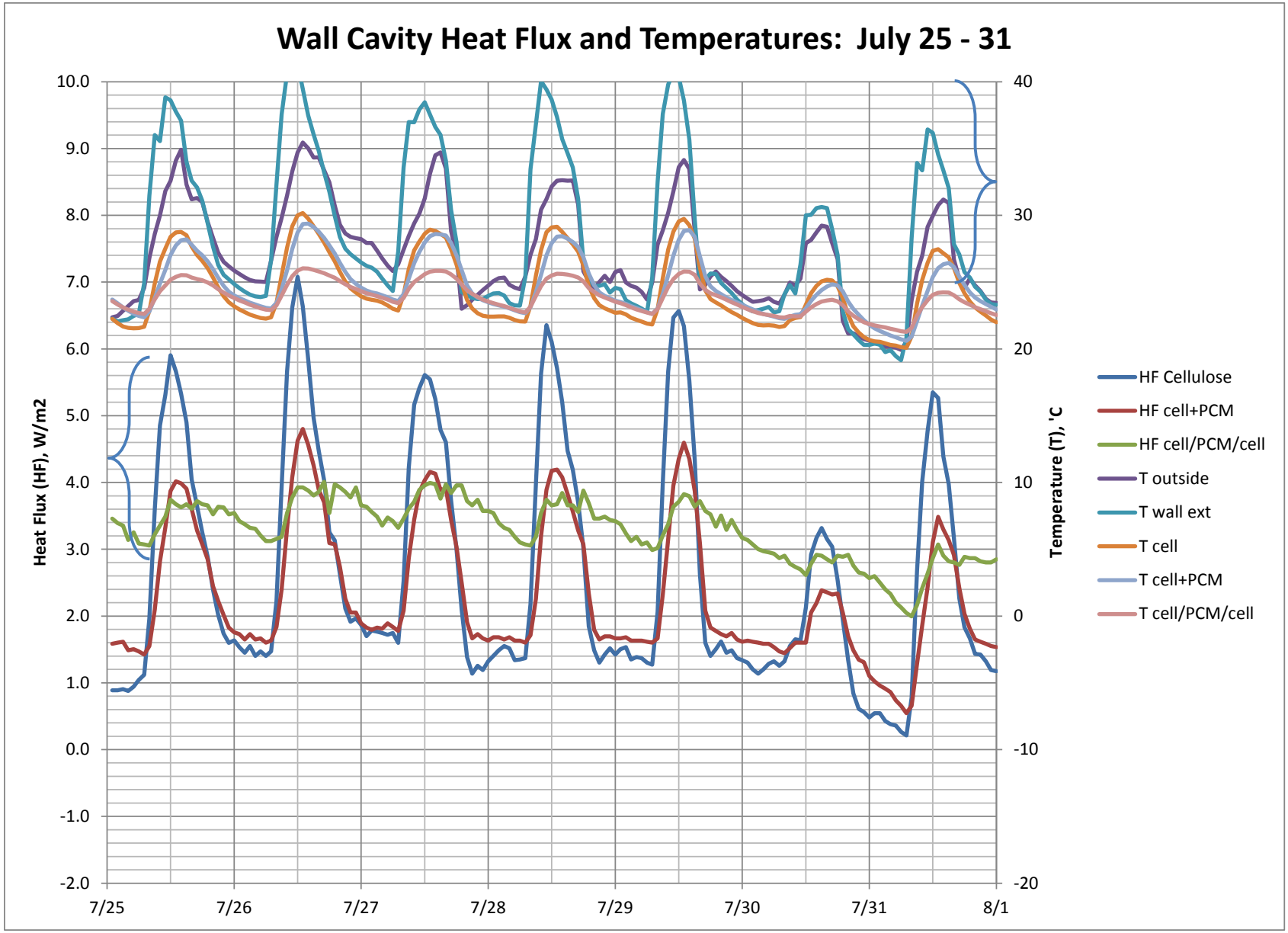
Wall Cavity Heat Flux and Temperatures: July 25 - 31
Heat Flux (HF), W/m2
Temperature (T), 'C
10.0
9.0
8.0
7.0
6.0
5.0
4.0
3.0
2.0
1.0
0.0
-1.0
-2.0
40
30
20
10
0
-10
-20
7/25
7/26
7/27
7/28
7/29
7/30
7/31
8/1
HF Cellulose
HF cell+PCM
HF cell/PCM/cell
T outside
T wall ext
T cell
T cell+PCM
T cell/PCM/cell

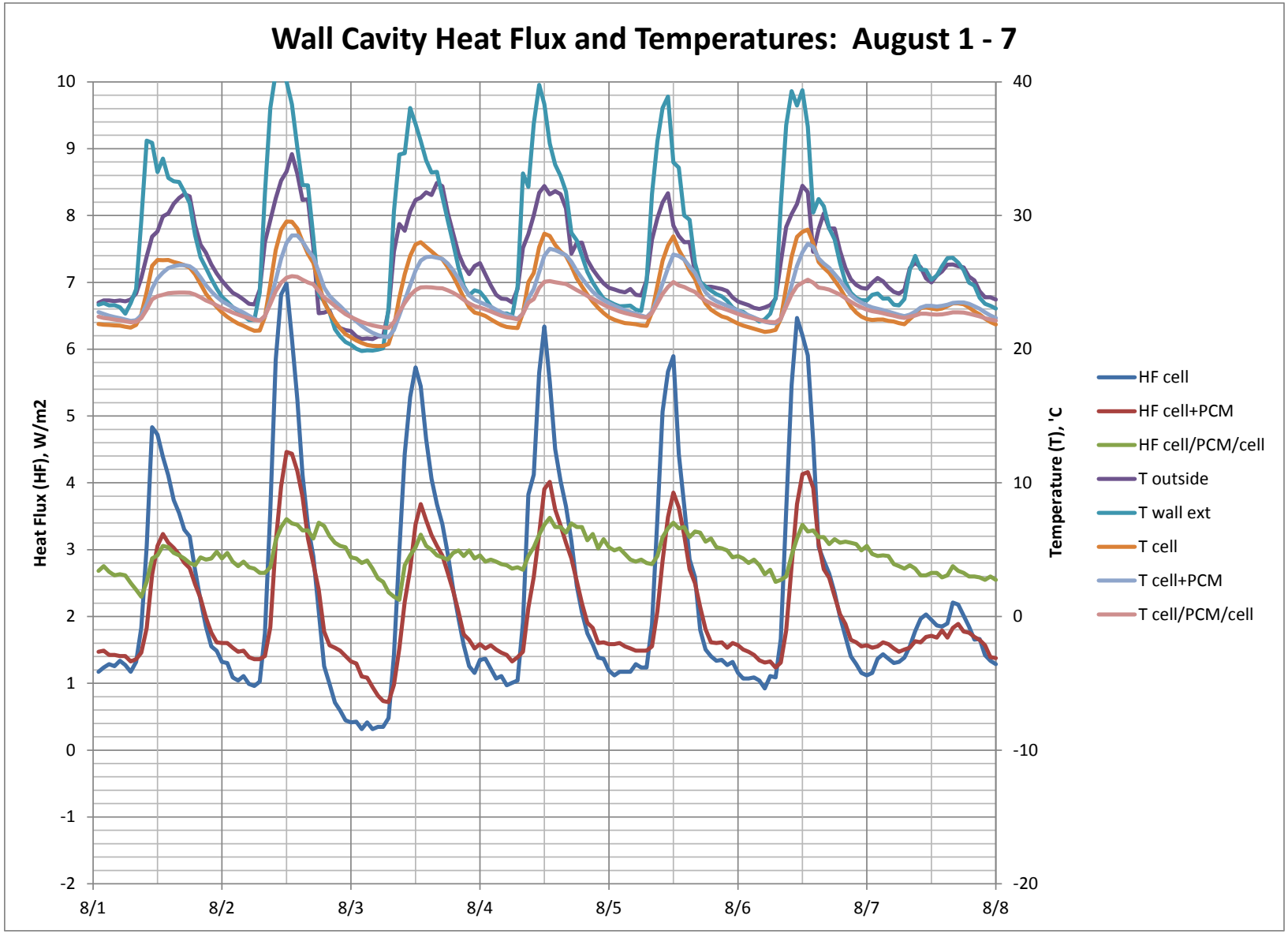
Wall Cavity Heat Flux and Temperatures: August 1 - 7
Heat Flux (HF), W/m2
Temperature (T), 'C
10
9
8
7
6
5
4
3
2
1
0
-1
-2
40
30
20
10
0
-10
-20
8/1
8/2
8/3
8/4
8/5
8/6
8/7
8/8
HF cell
HF cell+PCM
HF cell/PCM/cell
T outside
T wall ext
T cell
T cell+PCM
T cell/PCM/cell

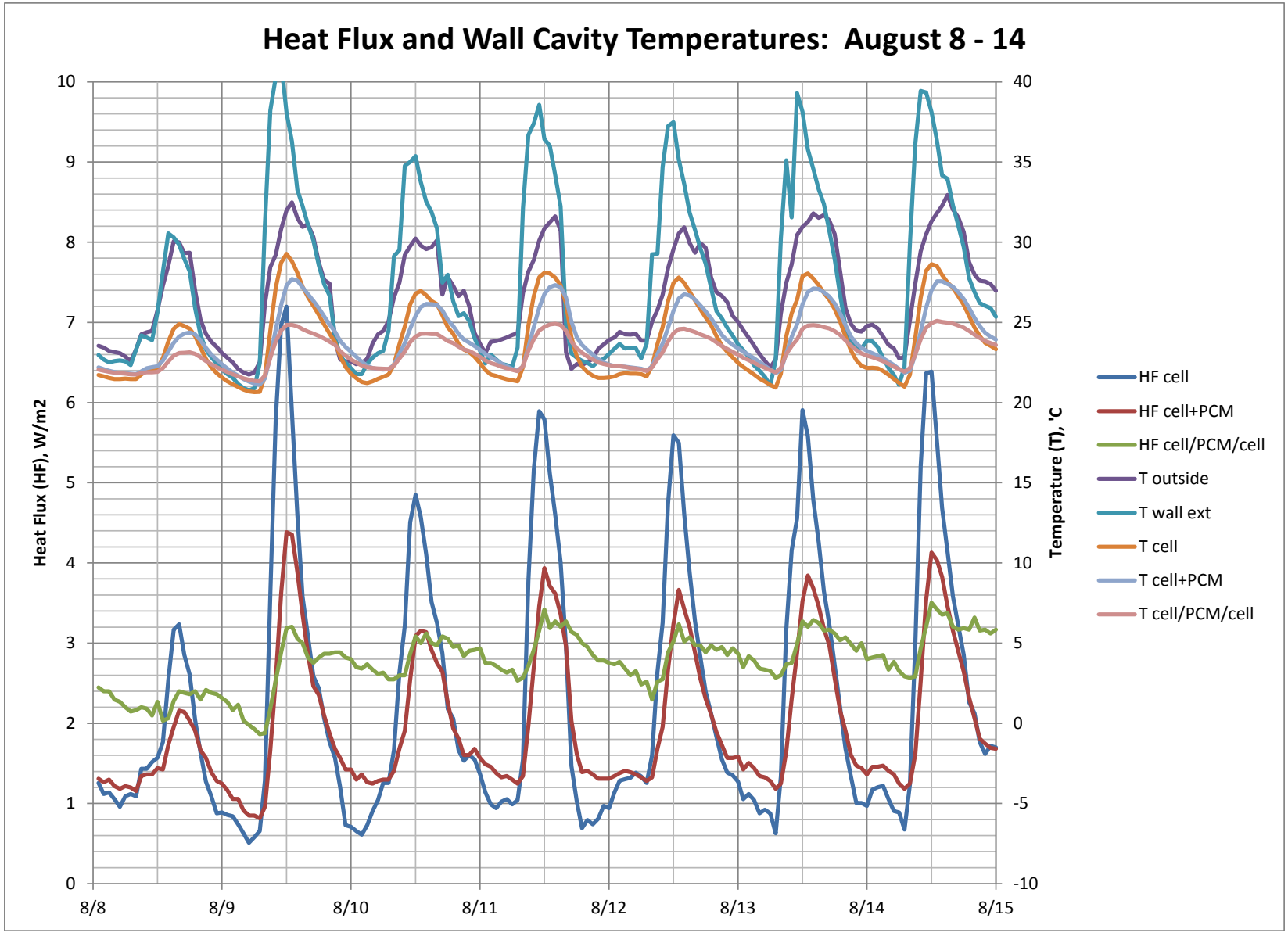
Heat Flux and Wall Cavity Temperatures: August 8 - 14
Heat Flux (HF), W/m2
Temperature (T), 'C
10
9
8
7
6
5
4
3
2
1
0
40
35
30
25
20
15
10
5
0
-5
-10
8/8
8/9
8/10
8/11
8/12
8/13
8/14
8/15
HF cell
HF cell+PCM
HF cell/PCM/cell
T outside
T wall ext
T cell
T cell+PCM
T cell/PCM/cell

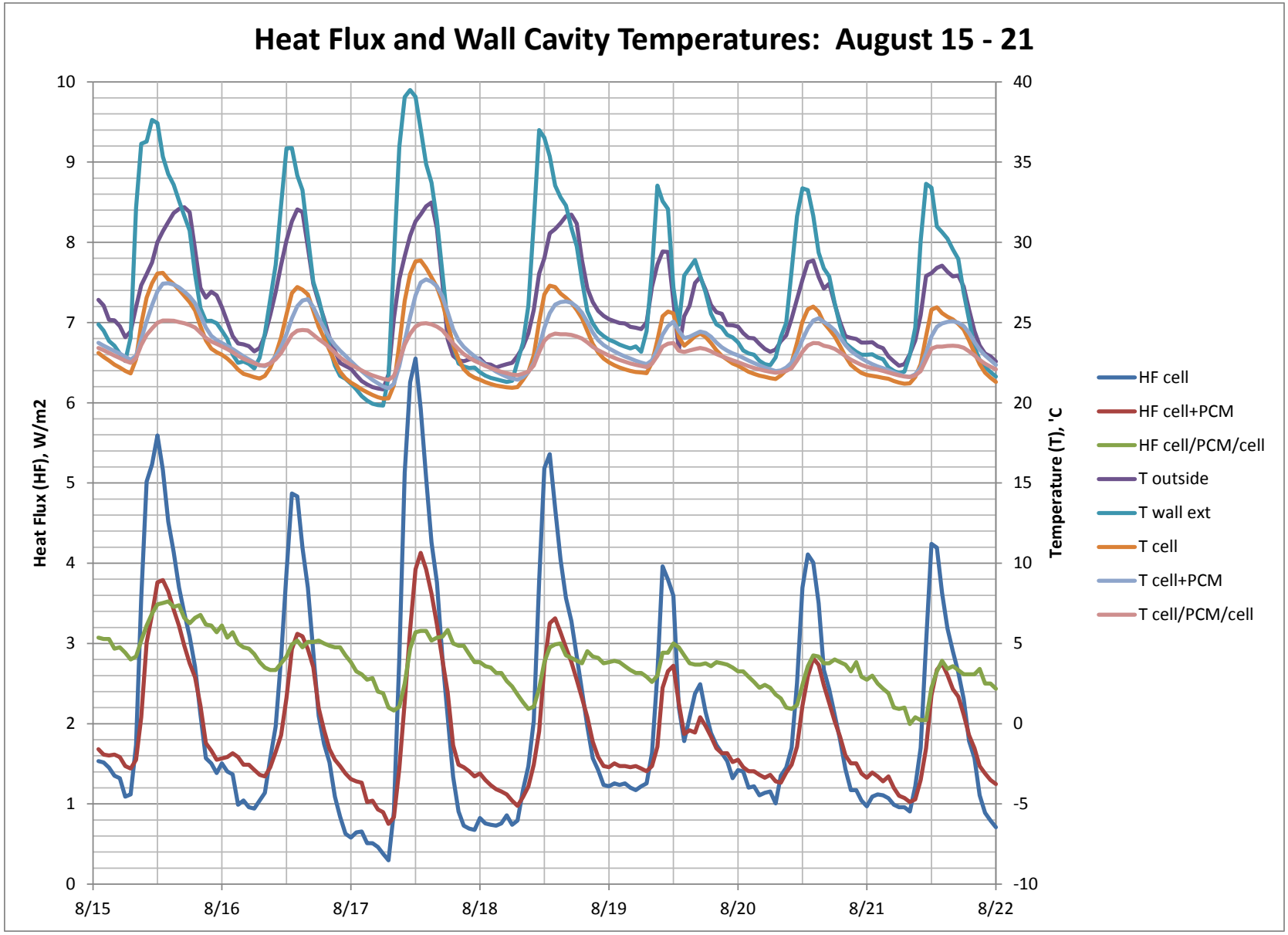
Heat Flux and Wall Cavity Temperatures: August 15 - 21
Heat Flux (HF), W/m2
Temperature (T), 'C
10
9
8
7
6
5
4
3
2
1
0
40
35
30
25
20
15
10
5
0
-5
-10
8/15
8/16
8/17
8/18
8/19
8/20
8/21
8/22
HF cell
HF cell+PCM
HF cell/PCM/cell
T outside
T wall ext
T cell
T cell+PCM
T cell/PCM/cell

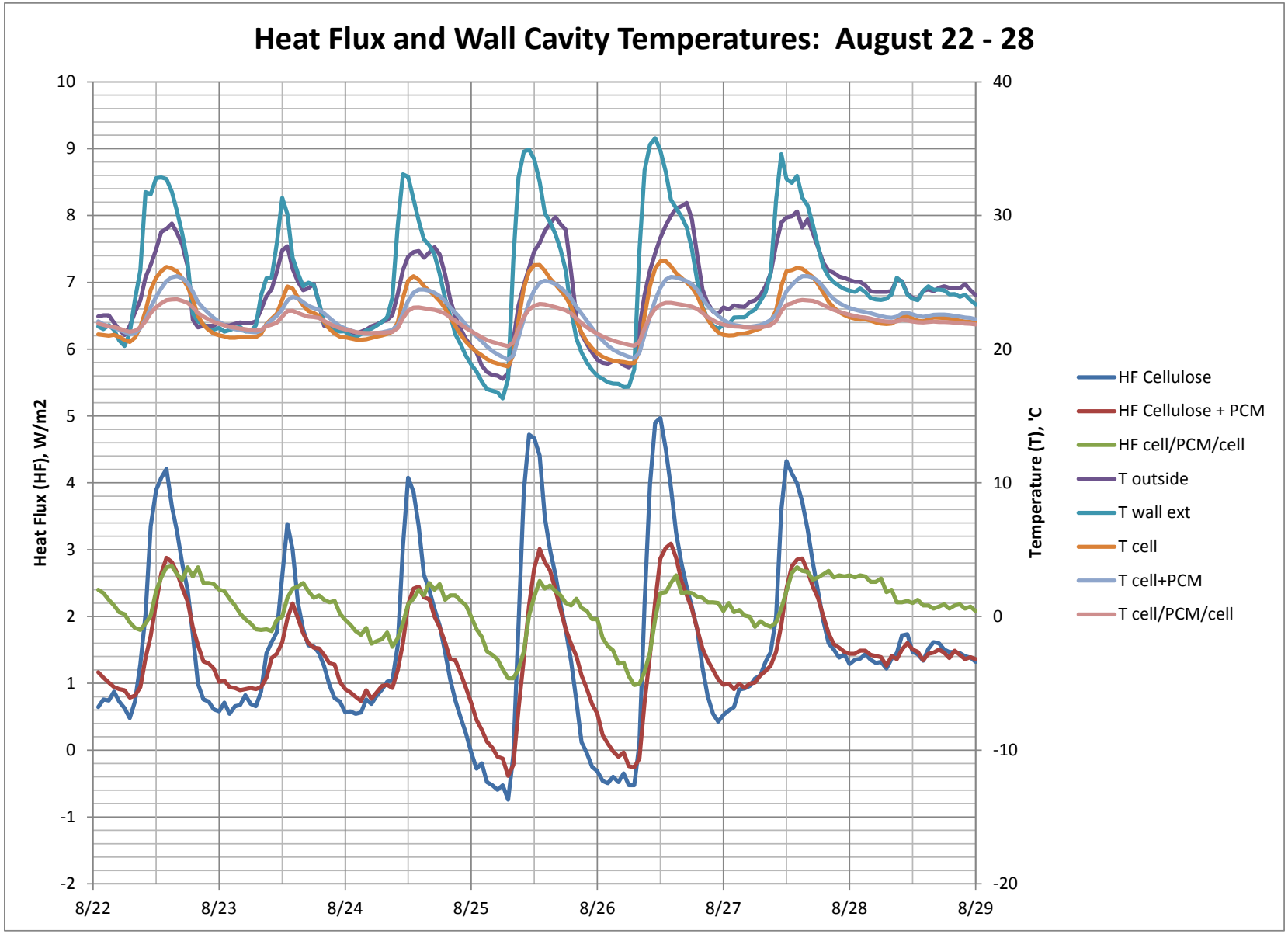
Heat Flux and Wall Cavity Temperatures: August 22 - 28
Heat Flux (HF), W/m2
Temperature (T), 'C
10
9
8
7
6
5
4
3
2
1
0
-1
-2
40
30
20
10
0
-10
-20
8/22
8/23
8/24
8/25
8/26
8/27
8/28
8/29
HF Cellulose
HF Cellulose + PCM
HF cell/PCM/cell
T outside
T wall ext
T cell
T cell+PCM
T cell/PCM/cell

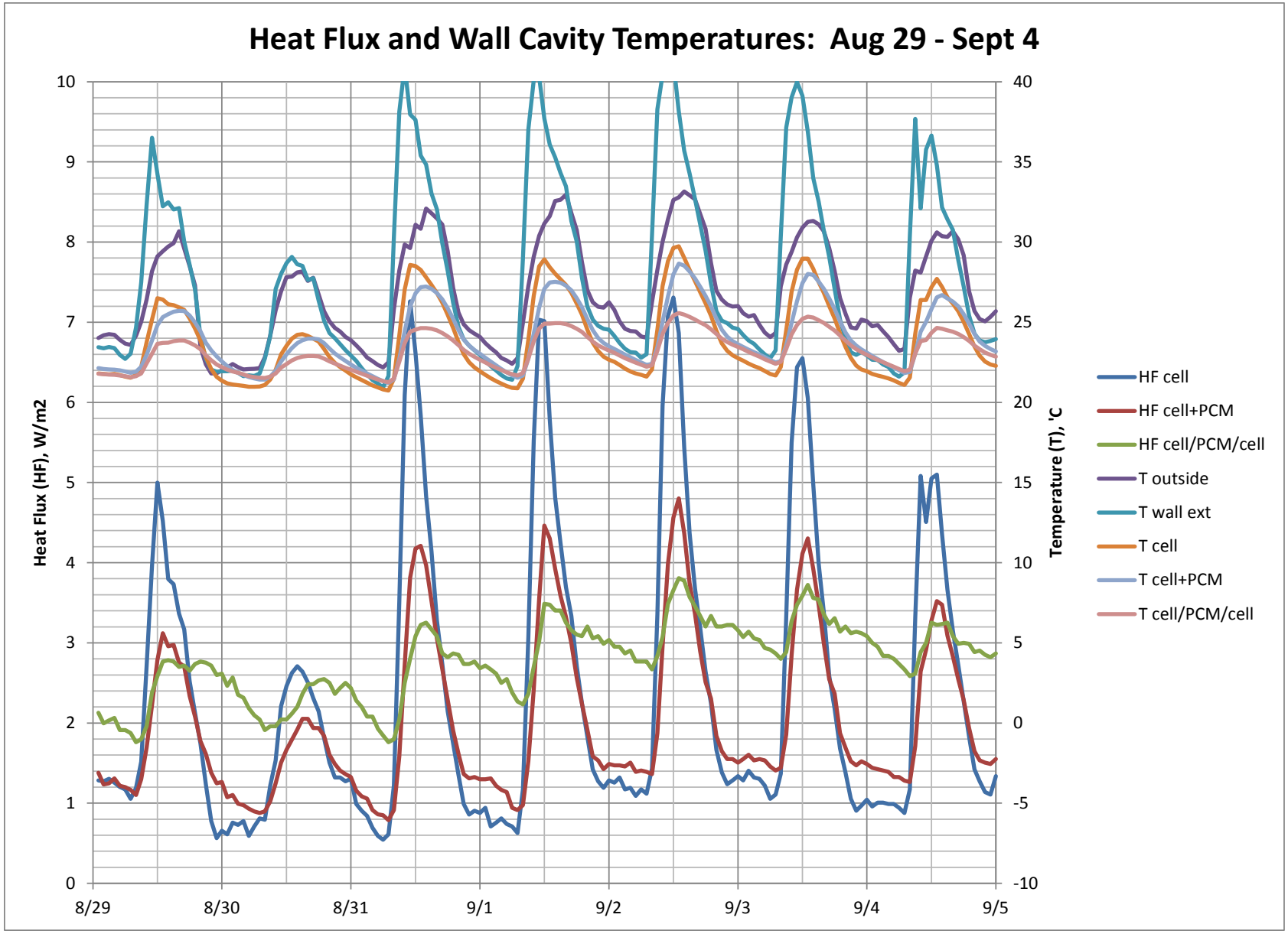
Heat Flux and Wall Cavity Temperatures: Aug 29 - Sept 4
Heat Flux (HF), W/m2
Temperature (T), 'C
10
9
8
7
6
5
4
3
2
1
0
40
35
30
25
20
15
10
5
0
-5
-10
8/29
8/30
8/31
9/1
9/2
9/3
9/4
9/5
HF cell
HF cell+PCM
HF cell/PCM/cell
T outside
T wall ext
T cell
T cell+PCM
T cell/PCM/cell

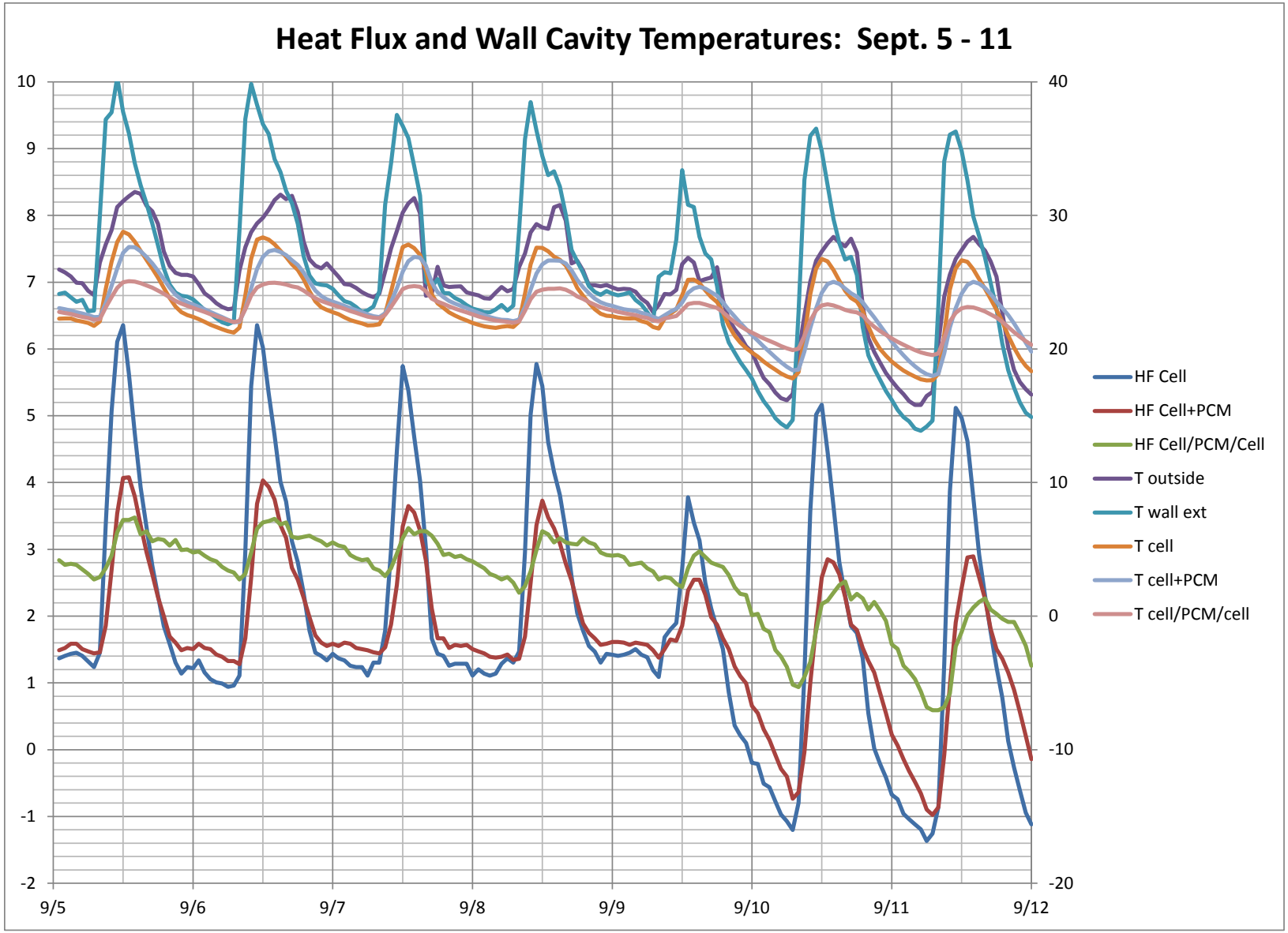
Heat Flux and Wall Cavity Temperatures: Sept. 5 - 11
10
9
8
7
6
5
4
3
2
1
0
-1
-2
40
30
20
10
0
-10
-20
9/5
9/6
9/7
9/8
9/9
9/10
9/11
9/12
HF Cell
HF Cell+PCM
HF Cell/PCM/Cell
T outside
T wall ext
T cell
T cell+PCM
T cell/PCM/cell

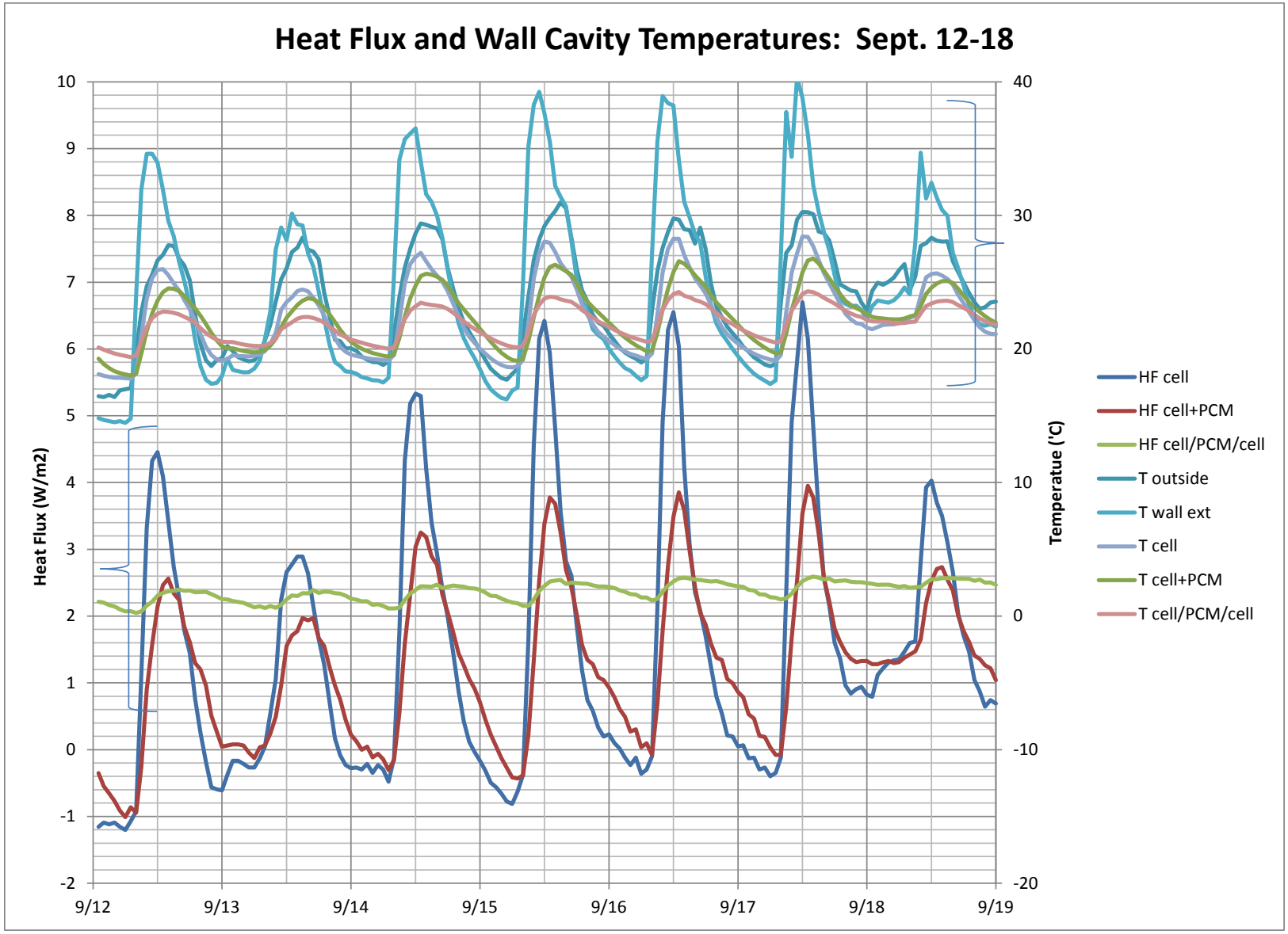

Figure 9A. Paraffin seepage from PCM pellets

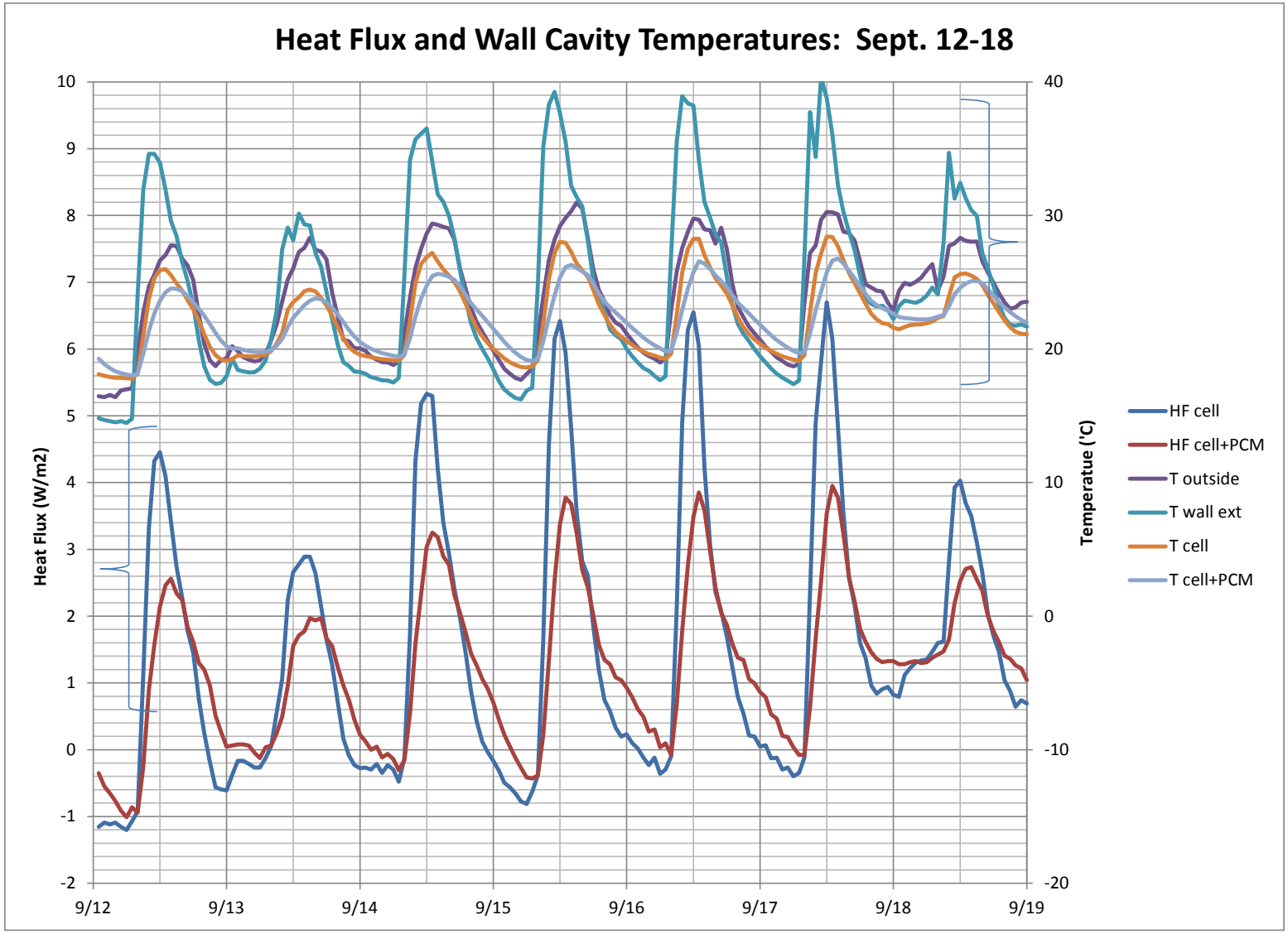

Figure 9A. Paraffin seepage from PCM pellets

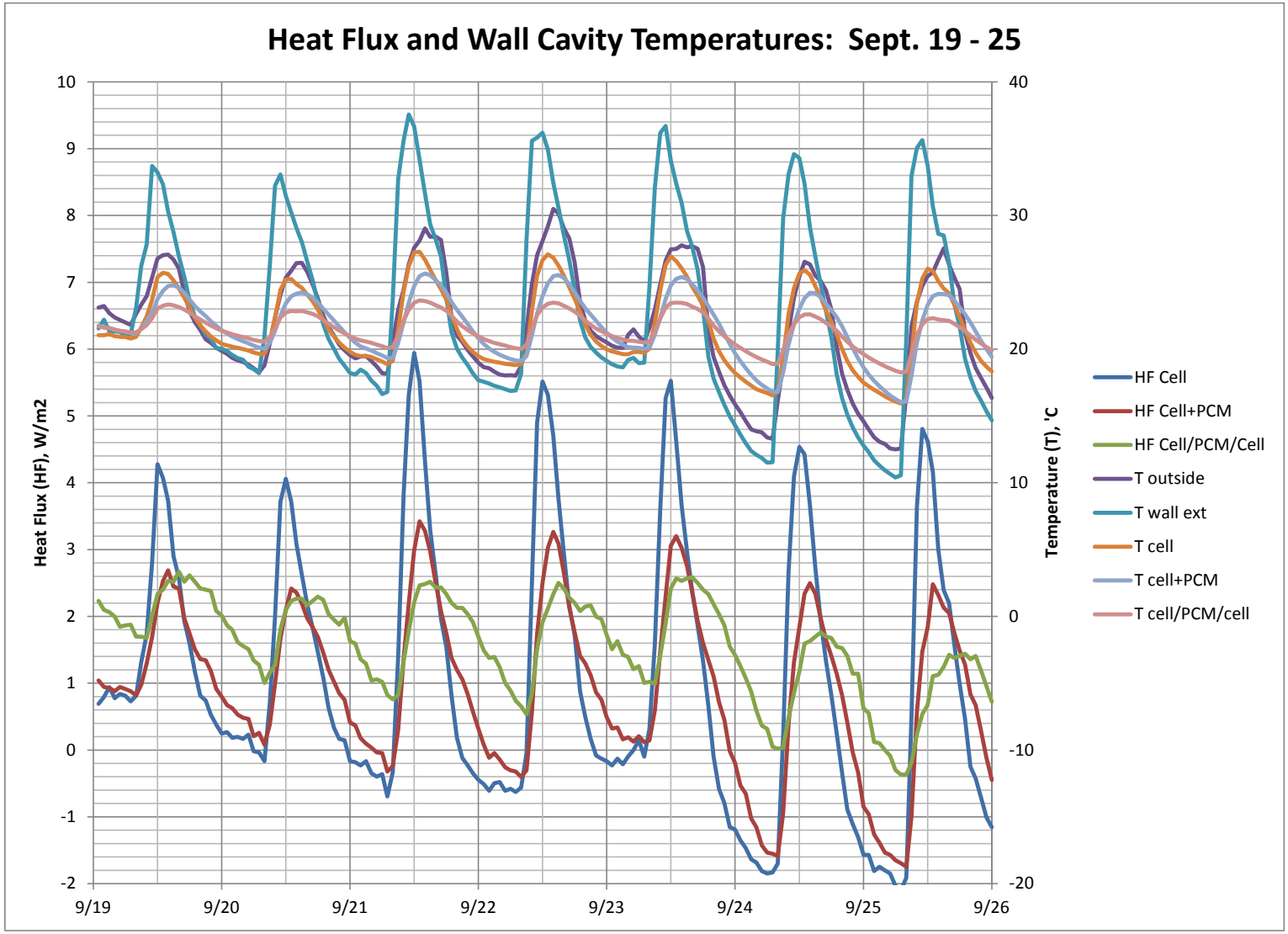

Figure 9A. Paraffin seepage from PCM pellets

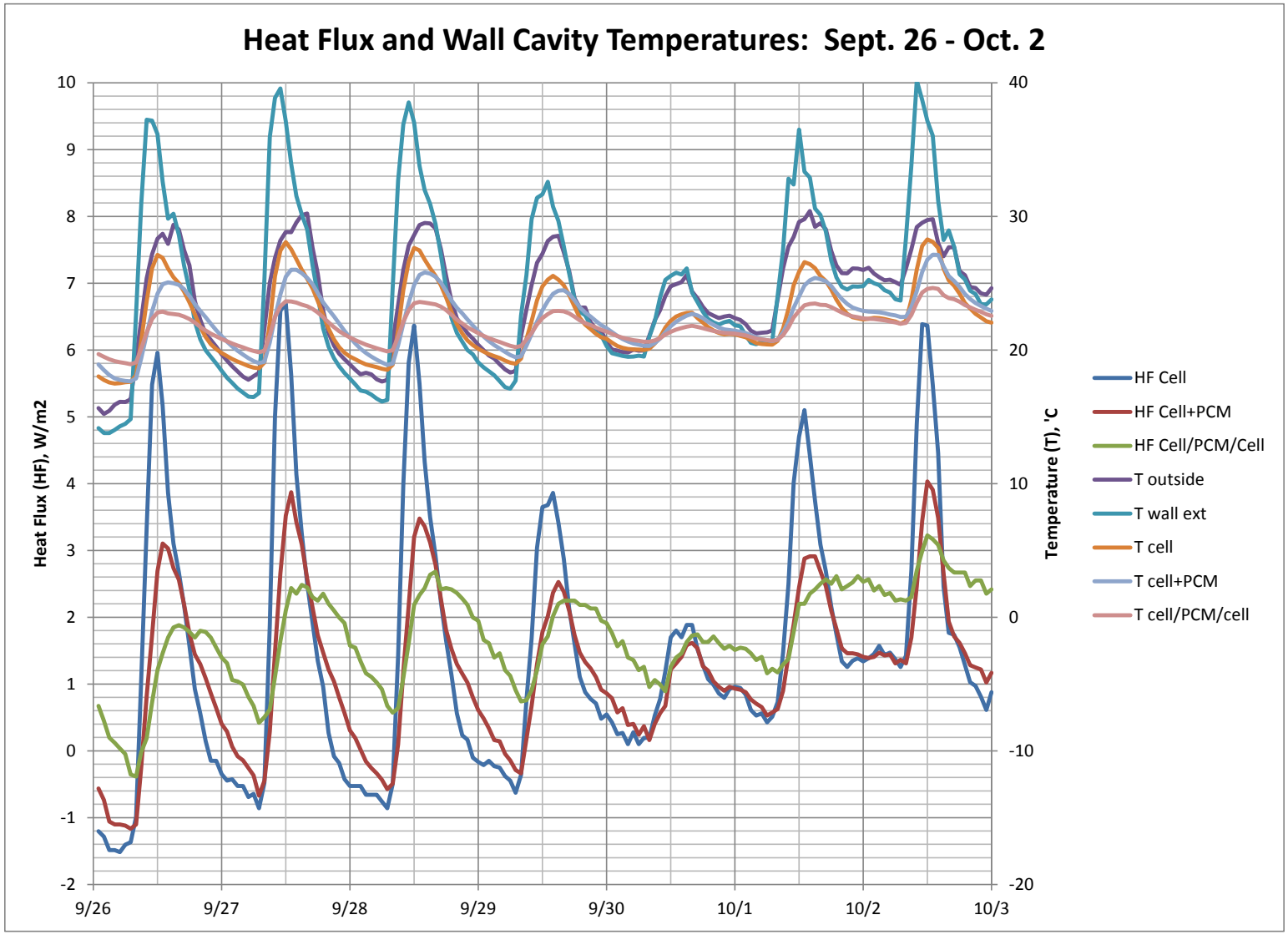
Heat Flux and Wall Cavity Temperatures: Sept. 26 - Oct. 2
Heat Flux (HF), W/m2
Temperature (T), 'C
10
9
8
7
6
5
4
3
2
1
0
-1
-2
40
30
20
10
0
-10
-20
9/26
9/27
9/28
9/29
9/30
10/1
10/2
10/3
HF Cell
HF Cell+PCM
HF Cell/PCM/Cell
T outside
T wall ext
T cell
T cell+PCM
T cell/PCM/cell